



# Mathematical modelling of Akt : Insulin signalling and glucose metabolism

**Author:**

Gray, Catheryn

**Publication Date:**

2021

**DOI:**

<https://doi.org/10.26190/unsworks/22318>

**License:**

<https://creativecommons.org/licenses/by-nc-nd/3.0/au/>

Link to license to see what you are allowed to do with this resource.

Downloaded from <http://hdl.handle.net/1959.4/70594> in <https://unsworks.unsw.edu.au> on 2024-04-29



Australia's  
Global  
University

# Thesis/Dissertation Sheet

Surname/Family Name	: <b>Gray</b>
Given Name/s	: <b>Catheryn Wilma</b>
Abbreviation for degree as give in the University calendar	: <b>PhD</b>
Faculty	: <b>Science</b>
School	: <b>Mathematics and Statistics</b>
Thesis Title	: <b>Mathematical Modelling of Akt: Insulin Signalling and Glucose Metabolism</b>

### Abstract 350 words maximum: (PLEASE TYPE)

Akt is a signalling protein that regulates many processes in the cell, such as cell growth, anti-apoptosis, and glucose metabolism.

The abnormal regulation of Akt is implicated in the development of a number of diseases, including cancer, cardiovascular disease, and type two diabetes.

Initially synthesized on the endoplasmic reticulum, Akt moves to the plasma membrane in response to insulin, where it is activated by phosphorylation. Phosphorylated Akt is found in many cellular locations, and the spatial distribution of Akt is thought to be an important determinant of downstream regulation. However, this aspect of Akt signalling has received scant treatment in the mathematical modelling literature to date.

This thesis consists of a number of mathematical models of Akt translocation and phosphorylation.

The Akt Switch model is a simple, linear, ordinary differential equation (ODE) model of Akt activation that tracks both the biochemical state and cellular location of Akt. Whilst elucidating some of the apparent anomalies of Akt signalling, it enables the differential regulation of downstream substrates via the two branches of Akt signalling (plasma membrane-bound and cytosolic), without recourse to complex feedback mechanisms.

However, the Akt Switch model has some limitations, including a noticeable discrepancy between the model output and the experimental data in the early stages of simulation. As a result, the Akt Translocation model was developed to further investigate the translocation of Akt in response to insulin in vitro.

The Akt Translocation model is a three-compartment ODE model that reproduces the salient features of Akt translocation. Analysis of the model shows that it behaves as a heavily damped harmonic oscillator with solution curves that either increase monotonically or overshoot.

Optimisation of the model to TIRF microscopy data quantified a time delay of approximately 0.4 min between the application of insulin and the Akt translocation response. In addition, the optimisation revealed that the processes regulating the size of the plasma membrane bound pool vary with the insulin level. For physiological insulin, the rate limiting step is the release of Akt to the plasma membrane. At high insulin levels, however, the down-regulation of Akt movement away from the plasma membrane is also necessary to explain the data.

The models developed in this thesis provide a framework for understanding the dynamics of this vital signalling node.

### Declaration relating to disposition of project thesis/dissertation

I hereby grant to the University of New South Wales or its agents a non-exclusive licence to archive and to make available (including to members of the public) my thesis or dissertation in whole or in part in the University libraries in all forms of media, now or here after known. I acknowledge that I retain all intellectual property rights which subsist in my thesis or dissertation, such as copyright and patent rights, subject to applicable law. I also retain the right to use all or part of my thesis or dissertation in future works (such as articles or books).

.....  
Signature

.....  
Date

The University recognises that there may be exceptional circumstances requiring restrictions on copying or conditions on use. Requests for restriction for a period of up to 2 years can be made when submitting the final copies of your thesis to the UNSW Library. Requests for a longer period of restriction may be considered in exceptional circumstances and require the approval of the Dean of Graduate Research.

## **COPYRIGHT STATEMENT**

'I hereby grant the University of New South Wales or its agents a non-exclusive licence to archive and to make available (including to members of the public) my thesis or dissertation in whole or part in the University libraries in all forms of media, now or here after known. I acknowledge that I retain all intellectual property rights which subsist in my thesis or dissertation, such as copyright and patent rights, subject to applicable law. I also retain the right to use all or part of my thesis or dissertation in future works (such as articles or books).'

'For any substantial portions of copyright material used in this thesis, written permission for use has been obtained, or the copyright material is removed from the final public version of the thesis.'

## **AUTHENTICITY STATEMENT**

'I certify that the Library deposit digital copy is a direct equivalent of the final officially approved version of my thesis.'

## INCLUSION OF PUBLICATIONS STATEMENT

UNSW is supportive of candidates publishing their research results during their candidature as detailed in the UNSW Thesis Examination Procedure.

**Publications can be used in their thesis in lieu of a Chapter if:**

- The candidate contributed greater than 50% of the content in the publication and is the “primary author”, ie. the candidate was responsible primarily for the planning, execution and preparation of the work for publication
- The candidate has approval to include the publication in their thesis in lieu of a Chapter from their supervisor and Postgraduate Coordinator.
- The publication is not subject to any obligations or contractual agreements with a third party that would constrain its inclusion in the thesis

Please indicate whether this thesis contains published material or not:

- This thesis contains no publications, either published or submitted for publication  
*(if this box is checked, you may delete all the material on page 2)*
- Some of the work described in this thesis has been published and it has been documented in the relevant Chapters with acknowledgement  
*(if this box is checked, you may delete all the material on page 2)*
- This thesis has publications (either published or submitted for publication) incorporated into it in lieu of a chapter and the details are presented below

### CANDIDATE'S DECLARATION

I declare that:

- I have complied with the UNSW Thesis Examination Procedure
- where I have used a publication in lieu of a Chapter, the listed publication(s) below meet(s) the requirements to be included in the thesis.

Candidate's Name	Signature	Date (dd/mm/yy)

# Mathematical Modelling of Akt Insulin Signalling and Glucose Metabolism

Catheryn Gray

A thesis in fulfilment of the requirements for the  
degree of  
Doctor of Philosophy



**UNSW**  
THE UNIVERSITY OF NEW SOUTH WALES

School of Mathematics and Statistics  
Faculty of Science

August 2020



## **ORIGINALITY STATEMENT**

‘I hereby declare that this submission is my own work and to the best of my knowledge it contains no materials previously published or written by another person, or substantial proportions of material which have been accepted for the award of any other degree or diploma at UNSW or any other educational institution, except where due acknowledgement is made in the thesis. Any contribution made to the research by others, with whom I have worked at UNSW or elsewhere, is explicitly acknowledged in the thesis. I also declare that the intellectual content of this thesis is the product of my own work, except to the extent that assistance from others in the project’s design and conception or in style, presentation and linguistic expression is acknowledged.’



# Abstract

Akt is a signalling protein that regulates many processes in the cell, such as cell growth, anti-apoptosis, and glucose metabolism. The abnormal regulation of Akt is implicated in the development of a number of diseases, including cancer, cardiovascular disease, and type two diabetes.

Initially synthesized on the endoplasmic reticulum, Akt moves to the plasma membrane in response to insulin, where it is activated by phosphorylation. Phosphorylated Akt is found in many cellular locations, and the spatial distribution of Akt is thought to be an important determinant of downstream regulation. However, this aspect of Akt signalling has received scant treatment in the mathematical modelling literature to date.

This thesis consists of a number of mathematical models of Akt translocation and phosphorylation. The Akt Switch model is a simple, linear, ordinary differential equation (ODE) model of Akt activation that tracks both the biochemical state and cellular location of Akt. Whilst elucidating some of the apparent anomalies of Akt signalling, it enables the differential regulation of downstream substrates via the two branches of Akt signalling (plasma membrane-bound and cytosolic), without recourse to complex feedback mechanisms.

However, the Akt Switch model has some limitations, including a noticeable discrepancy between the model output and the experimental data in the early stages of simulation. As a result, the Akt Translocation model was developed to further investigate the translocation of Akt in response to insulin *in vitro*.

The Akt Translocation model is a three-compartment ODE model that reproduces the salient features of Akt translocation. Analysis of the model shows that it behaves as a heavily damped harmonic oscillator with solution curves that either increase monotonically or overshoot.

Optimisation of the model to TIRF microscopy data quantified a time delay of approximately 0.4 min between the application of insulin and the Akt translocation response. In addition, the optimisation revealed that the processes regulating the size of the plasma membrane bound pool vary with the insulin level. For physiological insulin, the rate limiting step is the release of Akt to the plasma membrane. At high insulin levels, however, the down-regulation of Akt movement away from the plasma membrane is also necessary to explain the data.

The models developed in this thesis provide a framework for understanding the dynamics of this vital signalling node.

# Publications and Conference Presentations

## Publications

*The following is a list of publications associated with this thesis. These publications were published with my supervisor, Adelle Coster. The substantive work was my own, under her advice.*

- (1) CW Gray and ACF Coster. A receptor state space model of the insulin signalling system in glucose transport. *Mathematical Medicine and Biology: A Journal of the IMA*, 32(4):457–473, 2015.
- (2) CW Gray and ACF Coster. The Akt switch model: Is location sufficient? *Journal of Theoretical Biology*, 398:103–111, 2016.
- (3) CW Gray and ACF Coster. Crosstalk in transition: The translocation of Akt. *Journal of Mathematical Biology*, pages 919–942, 2019.
- (4) CW Gray and ACF Coster. Models of membrane-mediated processes: Cascades and cycles in insulin action. In Wolkenhauer & Voit (Eds.), *Systems Medicine: Integrative, Qualitative and Computational Approaches*, Academic Press. To appear September 2020.
- (5) CW Gray and ACF Coster. From insulin to Akt: Time delays and dominant processes. *Journal of Theoretical Biology*. Online 19 August 2020. <https://doi.org/10.1016/j.jtbi.2020.110454>

## Conference Presentations

- (1) CW Gray and ACF Coster. A streamlined model of the insulin receptor system for glucose transport. *The 37th Annual Conference of the Australian Society for Biophysics*, RMIT University, Melbourne, Australia, 24–27 November 2013.
- (2) CW Gray. Modelling the insulin receptor system for glucose transport. *The 50th Australian and New Zealand Industrial and Applied Mathematics Conference*, Rotorua, New Zealand, 2–6 February 2014.
- (3) CW Gray. Insulin signalling in metabolism: The Akt switch. *The 8th Australia-New Zealand Mathematics Convention*, University of Melbourne, Australia, 8–12 December 2014.
- (4) CW Gray. It's not just what you do, it's where you do it: Signalling through Akt. *The 51st Australian and New Zealand Industrial and Applied Mathematics Conference*, Surfers' Paradise, Australia, 1–5 February 2015.
- (5) CW Gray. From insulin to the Akt switch. *The 2015 Annual Meeting of the Society for Mathematical Biology*, Georgia State University, United States, 30 June–3 July 2015.
- (6) CW Gray. The Akt translocation model. *The 39th Annual Conference of the Australian Society for Biophysics*, University of New England, Armidale, Australia, 22–25 November 2015.
- (7) CW Gray. Akt translocation in mammalian fat cells. *The 52nd Australian and New Zealand Industrial and Applied Mathematics Conference*, Canberra, Australia, 7–11 February 2016.
- (8) CW Gray. Akt translocation in response to insulin: Quantifying the known unknowns. *The 2016 Annual Meeting of the Society for Mathematical Biology and European Conference for Mathematical and Theoretical Biology*, University of Nottingham, United Kingdom, 11–15 July 2016.

- (9) CW Gray. Akt translocation under increasing insulin stimulation. *The 2016 Annual Conference of the Australian Society for Biophysics*, University of South Australia, Adelaide, Australia, 4–7 December 2016.
- (10) CW Gray and ACF Coster. Getting ready to jump. *The 53rd Australian and New Zealand Industrial and Applied Mathematics Conference*, Hahndorf, Australia, 5–9 February 2017.
- (11) CW Gray. Akt translocation as a controller of metabolic activity. *The 2017 Annual Meeting of the Australian Society for Biophysics*, University of Technology Sydney, Sydney, Australia, 27–29 November 2017.
- (12) CW Gray. Akt translocation as a harmonic oscillator. *The 61st Annual Meeting of the Australian Mathematical Society*, Macquarie University, Sydney, Australia, 12–15 December 2017.
- (13) CW Gray. Tracking the location of metabolic controllers: Akt as a harmonic oscillator. *The 54th Australian and New Zealand Industrial and Applied Mathematics Conference*, Hobart, Australia, 4–8 February 2018.
- (14) CW Gray. The downstream signalling motifs of Akt. *Asian Biophysics Association Symposium in conjunction with the 2018 Annual Meeting of the Australian Society for Biophysics*, RMIT University, Melbourne, Australia, 2–6 December 2018.
- (15) CW Gray. Hysteresis and the drift to depletion: Akt under repeated insulin stimulation. *The 55th Australian and New Zealand Industrial and Applied Mathematics Conference*, Nelson, New Zealand, 3–7 February 2019.
- (16) CW Gray. Dynamic relocation of Akt in response to insulin. *Joint meeting of The Australian Physiological Society and The Australian Society for Biophysics*, Australian National University, Canberra, Australia, 1–4 December 2019.



# Acknowledgements

Foremost, I would like express my gratitude to my supervisor, Adelle Coster, for her continued guidance. From initially suggesting an appropriate thesis topic, to the final stages of proof reading, she has supported, advised, guided, occasionally criticised, but above all encouraged me in the writing of this thesis.

I would also like to thank my co-supervisor, Bruce Henry, for his advice, support, and encouragement.

Finally I am grateful to my family—my husband, Azhar, and my children, Rafid and Tariq—for their personal support, without which this thesis would not have been possible.



# Contents

Abstract	i
Publications and Conference Presentations	iii
Acknowledgements	vii
<b>I Overview and Background</b>	<b>1</b>
<b>1 Overview</b>	<b>3</b>
<b>2 Biological Context</b>	<b>5</b>
2.1 Introduction . . . . .	5
2.2 The Insulin Signalling Pathway . . . . .	5
2.3 Summary . . . . .	13
<b>3 Mathematical Models of the Insulin Signalling Pathway</b>	<b>15</b>
3.1 Introduction . . . . .	15
3.2 Signalling Network Models . . . . .	16
3.3 Models of the Insulin Receptor System . . . . .	20
3.4 Models of Akt Activation . . . . .	22
3.5 Summary . . . . .	29
<b>4 Mathematical Modelling Philosophy and Techniques</b>	<b>31</b>
4.1 Modelling Approach . . . . .	31
4.2 Model Development . . . . .	33
4.3 Model Analysis . . . . .	37
4.4 Parameter Optimisation . . . . .	38
4.5 Parametric Sensitivity Analysis . . . . .	40
4.6 Summary . . . . .	41

---

<b>II</b>	<b>Mathematical Models of Akt Translocation and Phosphorylation</b>	<b>43</b>
<b>5</b>	<b>Preliminary Study on the Insulin Signalling Network</b>	<b>45</b>
5.1	Introduction . . . . .	45
5.2	Methods . . . . .	46
5.3	Results . . . . .	53
5.4	Discussion . . . . .	58
5.5	Summary . . . . .	59
<b>6</b>	<b>The Akt Switch Model</b>	<b>61</b>
6.1	Introduction . . . . .	61
6.2	Method . . . . .	63
6.3	Results . . . . .	71
6.4	Discussion . . . . .	82
6.5	Summary . . . . .	87
<b>7</b>	<b>The Akt Translocation Model</b>	<b>89</b>
7.1	Introduction . . . . .	89
7.2	Method . . . . .	90
7.3	Results . . . . .	94
7.4	Discussion . . . . .	114
7.5	Summary . . . . .	118
<b>8</b>	<b>Time Delays and Dominant Processes</b>	<b>121</b>
8.1	Introduction . . . . .	121
8.2	Method . . . . .	122
8.3	Results . . . . .	131
8.4	Discussion . . . . .	146
8.5	Summary . . . . .	151
<b>III</b>	<b>Discussion, Conclusion, Future Work</b>	<b>153</b>
<b>9</b>	<b>Discussion</b>	<b>155</b>
<b>10</b>	<b>Future Work</b>	<b>161</b>
<b>11</b>	<b>Conclusion</b>	<b>169</b>

---

<b>Appendices</b>	<b>171</b>
<b>A MATLAB</b>	<b>173</b>
A.1 Receptor State Space Model . . . . .	173
A.2 Akt Switch Model . . . . .	176
A.3 Akt Translocation Model . . . . .	177
A.4 Akt Activation Model . . . . .	179
<b>Bibliography</b>	<b>181</b>



# Part I

## Overview and Background



# Chapter 1

## Overview

Akt is a key signalling protein of mammalian cells that is involved in many cellular processes, including glucose metabolism, cell growth, cell survival, and proliferation. Located at the juncture of multiple signal transduction networks, Akt functions as a nutrient sensor that coordinates resource intensive mitogenic processes—such as cell growth and survival—with metabolism. As a result, the dysregulation of Akt is implicated in a variety of disorders, from diabetes to cancer.

The mathematical modelling of Akt activation, and particularly its role in insulin signalling, constitutes the major theme of this thesis. Firstly, an outline of the biological context is given. Next, the previous mathematical modelling of this important signalling pathway is reviewed. This is followed by a brief discussion of the rationale that underpins the choice of mathematical models and techniques employed in the current work. With this groundwork laid, a preliminary study of the insulin signalling network is presented in Chapter 5.

The three studies of Akt activation and translocation in Part II (Chapters 6–8) compose the backbone of the thesis. The three major studies presented in Part II, along with the preliminary study from Part I (Chapter 5), are based on articles that have already been published in the peer-reviewed literature.

As a consequence, these chapters follow the conventional “IMRAD” (introduction, method, results and discussion) format of a scientific paper. There is a short summary concluding each chapter.

The first major study is the Akt Switch model described in Chapter 6. This four-compartment model explicitly depicts both the translocation and phosphorylation subprocesses of Akt activation. It demonstrates that some of the enigmas of Akt signalling can be explained by a model that allows for two processes and two cellular locations—cytosol and plasma membrane.

The Akt translocation process then becomes the subject of more detailed study in Chapters 7 and 8. The Akt Translocation model is first defined in Chapter 7. Mathematical analysis yields substantial insight into both the transient and steady state behaviour of the model, and reveals an inherent hysteresis in the system. The model is then optimised to experimental data in Chapter 8. This also leads to greater insight into potential regulatory mechanisms of the underlying biological system. The interplay between these three studies is discussed further in Chapter 9, and some directions for future work are outlined in Chapter 10. The major results of the thesis are summarized in Chapter 11.

# Chapter 2

## Biological Context

### 2.1 Introduction

This chapter consists of an overview of insulin signalling events between the pancreatic release of insulin and the translocation of glucose transporter 4 (GLUT4) to the plasma membrane. A particular focus will be given to the signalling component Akt (also known as protein kinase B or PKB), as the mathematical modelling of Akt activation constitutes a major theme of this thesis. Furthermore, although insulin possesses a plethora of biological functions, the current work will take a predominantly “glucose centric” view of insulin signalling. That is to say, the focus is on the regulation of glucose metabolism by insulin, and how this is effected by the components of the insulin signalling pathway.

### 2.2 The Insulin Signalling Pathway

Insulin plays a pivotal role in the maintenance of glucose homeostasis in the body. The major targets of insulin signalling are fat cells (adipocytes),

skeletal muscle cells (myocytes) and liver cells (hepatocytes). Adipocytes and myocytes respond to insulin stimulation with the translocation of GLUT4 to the plasma membrane, enabling the clearance of glucose from the blood. In addition, insulin stimulates the synthesis of glycogen, fat, and protein in insulin sensitive cells and suppresses the break down of glycogen, fat, and protein in the liver [1]. These actions combine to promote the metabolism and storage of glucose circulating in the bloodstream, which is the predominant metabolic effect of insulin. Defects in this process can give rise to insulin resistance, diabetes, and vascular disease [2].

### **2.2.1 Insulin**

Proinsulin (the nascent, inactive form of insulin) is synthesized and stored within the  $\beta$ -cells of the pancreas. Following a rise in blood sugar, proinsulin undergoes irreversible proteolytic cleavage and is released as insulin and C-peptide into the bloodstream [3].

Insulin secretion from the pancreas is periodic, with oscillations that occur on several different timescales: rapid (5-15 minutes); ultradian (1-2 hours); or circadian (24 hours) [4]. Interestingly, the insulin signal is predominantly amplitude, rather than frequency, modulated. The  $\beta$ -cells continually secrete small pulses of insulin into the blood with a period of 5–10 minutes [4–6], even in the fasted state. However, the amplitude of these pulses increases dramatically within a few minutes of a rise in blood sugar. Once secreted, the insulin circulates in the bloodstream until it either binds to an insulin receptor or is degraded by the liver. The half-life of insulin in the blood is 5 minutes [4], approximately the same as the period of pancreatic insulin release.

In addition to its effect on glucose metabolism, insulin also manifests profound mitogenic effects on cellular growth, proliferation, and anti-apoptosis. This explains why dysregulation of the insulin signalling pathway is implicated in the development of cancer. Interestingly, the mitogenic actions of

insulin occur on a time frame of hours to days, in contrast to the metabolic effects, which occur within a matter of minutes. How the cell regulates processes on such different time scales using the same signal transduction machinery is an area of active research: see for instance [7–10].

### 2.2.2 The Upstream Signalling Pathway

The insulin receptor is a transmembrane protein composed of two parallel half-receptors [11] found on insulin sensitive cells. When insulin binds to the extracellular subunits of the receptor, the intracellular subunits undergo transphosphorylation. The phosphorylated intracellular subunits then interact with a number of signalling intermediaries, such as insulin substrates 1, 2, and 3 (IRS-1, IRS-2 and IRS-3). In this fashion, the insulin signal is relayed from the bloodstream to the internal environment of the cell. A simplified diagram of the insulin signalling pathway is given in Figure 2.1.

Numerous substrates of the insulin receptor have been identified [1], and at least six eponymous substrates (IRS-1–6) are known [12]. There is considerable redundancy and complementarity in the functions of this family of proteins, but the IRS-1 and IRS-2 isoforms play a central role in the metabolic action of insulin signalling. Ordinarily, IRS-1 is phosphorylated on tyrosine residues by the activated insulin receptor. This in turn recruits phosphatidylinositol 3-kinase (PI3K) to the plasma membrane, resulting in the forward propagation of the insulin signal.

PI3K is a scaffold protein of major importance in a number of signalling pathways. It controls vital cellular functions such as membrane trafficking, signal transduction and exocytosis [13]. In the insulin signalling pathway, PI3K catalyses the formation of phosphatidylinositol 3,4,5-trisphosphate (PIP<sub>3</sub>) [14]. PIP<sub>3</sub> functions as a docking site at the plasma membrane for the protein kinase Akt, which is activated at the plasma membrane through phosphorylation by phosphoinositide-dependent kinase-1 (PDK1) and mammalian target of rapamycin complex-2 (mTORC2) [15].

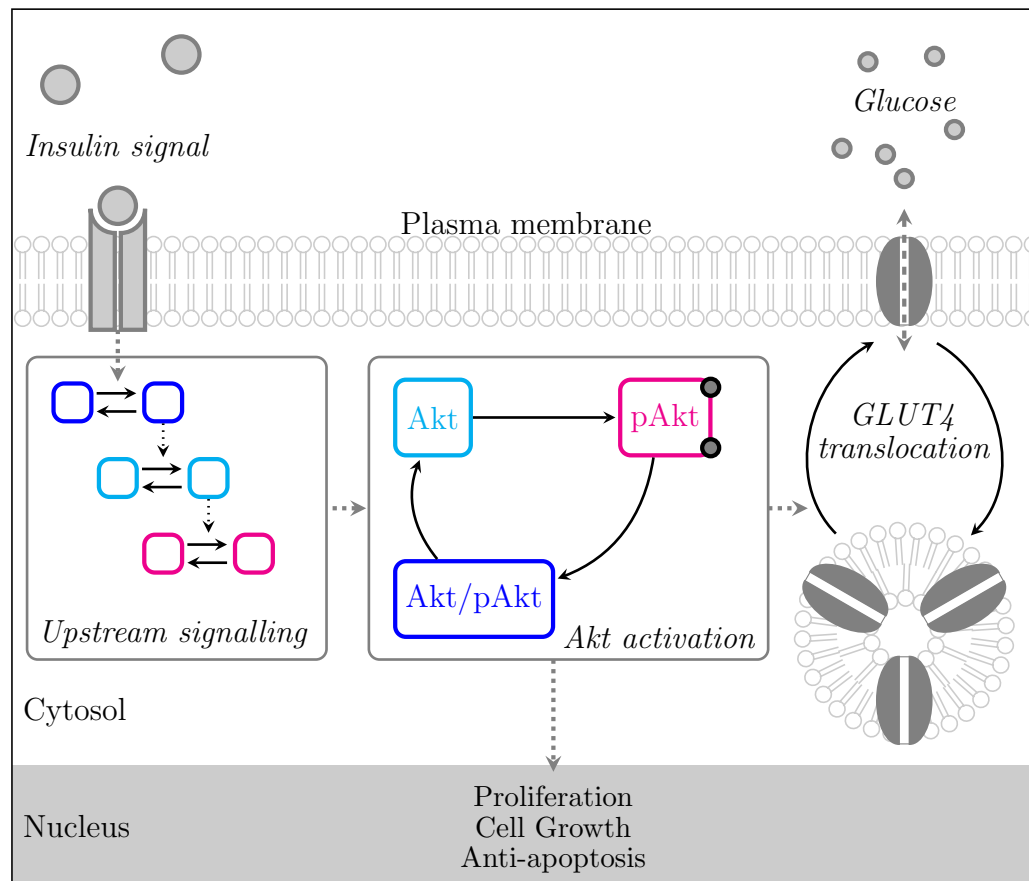


Figure 2.1: An overview of the insulin signaling pathway. Insulin in the bloodstream binds to the insulin receptor, generating the insulin signal. This signal propagates through the upstream signalling pathway to Akt, and then through the downstream signalling pathway to the GLUT4 translocation machinery.

### **2.2.3 Akt as a Key Crosstalk Node**

Akt is a key regulator of diverse cellular processes, such as survival, growth, metabolism and proliferation. As with many components of signal transduction pathways, Akt derives signalling specificity from both its intracellular location and its phosphorylation state [16–18]. Like most cellular proteins, Akt is synthesized on the endoplasmic reticulum in the inert state. It is then activated by phosphorylation, which only occurs on the inner leaflet of the plasma membrane. Consequently, the translocation of Akt from the cytosol to the plasma membrane is a crucial, albeit poorly understood, step in the activation process [19–21]. As Akt dysregulation is implicated in a wide array of disorders—from diabetes to cancer [22–24]—a deeper understanding of the Akt translocation and activation processes would be invaluable.

Akt activation is both necessary and sufficient for GLUT4 translocation. The inhibition of Akt substantially decreases GLUT4 expression at the plasma membrane [16, 25–27]. Conversely, the activation of only a small percentage of the Akt pool results in maximal GLUT4 translocation, even in the absence of an upstream insulin signal [15, 28, 29]. Thus Akt functions as an extremely low-threshold switch amplifying and transmitting the insulin signal to its downstream substrates.

In mammals there are three Akt isoforms, which exhibit distinct functions and tissue distributions [15]. Akt1 is widely expressed in many cell types and plays a role in cell proliferation and growth; Akt2 is found in skeletal muscle and fat cells where it is involved in glucose metabolism; Akt3 is found predominantly in the brain and testes [24]. The primary focus of this thesis is Akt2 and its role in glucose metabolism. Consequently, subsequent references to “Akt” should be understood as denoting the Akt2 isoform, unless stated otherwise.

Figure 2.2 shows a schematic diagram of the Akt activation process. After synthesis on the endoplasmic reticulum, Akt forms a pre-activation complex

with 3-phosphoinositide dependent protein kinase-1 (PDK1), which is widely available in the cytosol [15, 30]. In response to insulin, this pre-activation complex is recruited to the plasma membrane, where it binds to a docking site on PIP<sub>3</sub> [15, 31]. Once docked at the plasma membrane, full activation is contingent upon double phosphorylation: once on Threonine-308 (Thr308) by PDK1; and once on Serine-473 (Ser473) by the mammalian target of rapamycin (mTOR)/rapamycin-insensitive companion of mTOR (RICTOR) complex [32–34]. It is known that the catalytic activity of doubly-phosphorylated Akt (pAkt) is at least one order of magnitude higher than that of Akt phosphorylated on Thr308 alone [35], and recent work suggests that Thr308 phosphorylation precedes Ser473 phosphorylation [36].

Following activation, some of the pAkt leaves the plasma membrane to activate substrates in a variety of cellular locations, such as the mitochondrial membrane and the cell nucleus. A fraction also remains at the plasma membrane to propagate the insulin signal downstream [19, 31, 37]. The presence of activated Akt in the nucleus has been widely reported, however details concerning the nuclear transport of pAkt are disputed [19]. It is known that pAkt first appears at the plasma membrane within minutes of insulin stimulation but takes approximately 30 minutes to appear in the nucleus [38].

Akt has many downstream substrates that are found in both the cytosol and the nucleus [19, 31, 37]. These substrates can be broadly classified as either metabolic or mitogenic effectors [24], although the distinction between the two classes is not entirely clear cut. Consequently, Akt functions as an important crosstalk node between metabolic and mitogenic signalling pathways in the cell. It is clear that Akt fulfils the three criteria of a ‘critical node’ in the insulin signalling pathway as outlined by Taniguchi and co-workers: it is essential for the propagation of the insulin signal; it is tightly regulated; and it constitutes a major crosstalk node with other signalling systems in the cell [12].

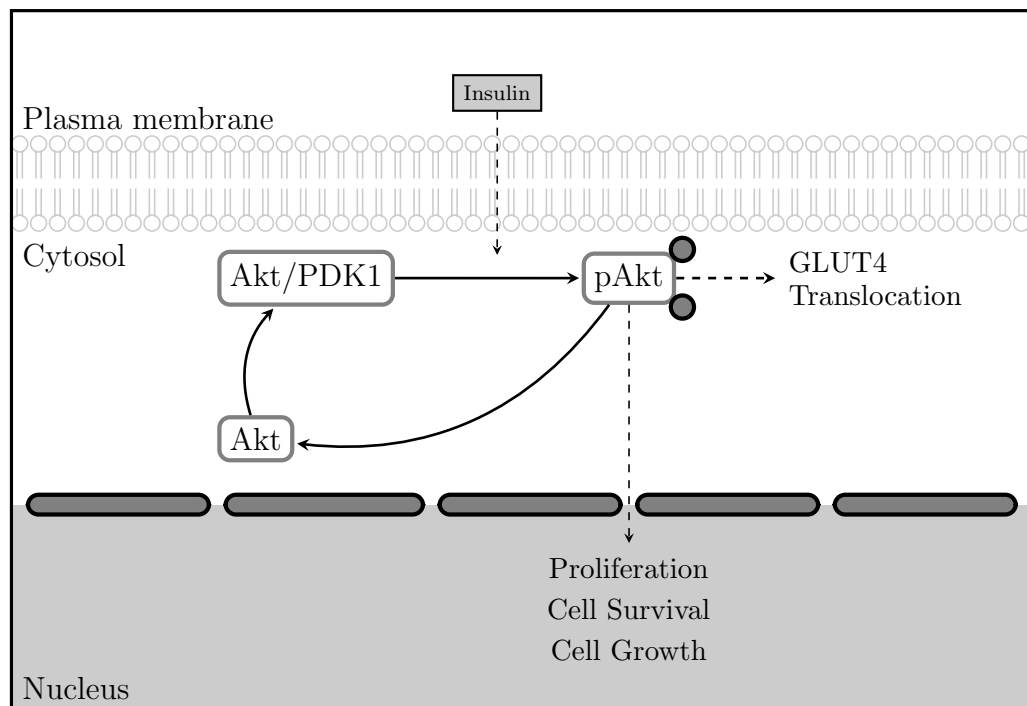


Figure 2.2: Akt in the cell. Akt is synthesized in the un-activated state near the nucleus. It forms a pre-activation complex with PDK1 in the cytosol. Under the influence of insulin, the pre-activation complex travels to the inner leaflet of the plasma membrane, where it is doubly-phosphorylated to become activated Akt (pAkt).

### 2.2.4 GLUT4 Translocation

Glucose transport into the cell is widely considered to be the rate-limiting step of glucose metabolism [15, 39]. Ordinarily, glucose cannot diffuse across the plasma membrane in the absence of a glucose transporter molecule. The glucose transporters constitute a family of membrane embedded proteins which selectively facilitate the passive transport of glucose down its concentration gradient into or out of cells. GLUT4 is the insulin-responsive member of the glucose transporter family and is predominantly found in insulin sensitive cells.

Glucose transport into insulin sensitive cells is controlled by the spatial distribution of GLUT4. In the basal (non-insulin stimulated state) over 95% of GLUT4 is embedded in membranes inside the cell, reducing the leakage of glucose to the exterior, as, *in vivo*, a basal state would generally be associated with low blood glucose concentrations. In response to insulin, up to 40% of the entire GLUT4 complement is redistributed to the plasma membrane in a dose dependent manner [40, 41]. This permits the influx of glucose from the bloodstream into the cell.

GLUT4 trafficking involves at least six steps, all of which are potential targets for regulation by insulin [42–44]. The six steps are:

- retention inside the cell under basal conditions within membrane structures such as vesicles and endosomes;
- release of GLUT4 containing vesicles from retention in response to insulin;
- movement of GLUT4 vesicles toward the plasma membrane;
- tethering, docking and fusion of vesicles at the plasma membrane;
- endocytosis from the plasma membrane back into internal membranes;
- sorting and redistribution of the internalized GLUT4.

---

The regulation of these processes remains incompletely understood and somewhat contentious. Nonetheless, GLUT4 expression at the plasma membrane constitutes a readily measured output of insulin signalling. At its simplest, the insulin signalling pathway in adipocytes can be considered a single input, single output system where the input is insulin and the output is GLUT4 expression at the plasma membrane.

## **2.3 Summary**

Although the chain of events between the release of insulin from the pancreas to the translocation of GLUT4 in adipocytes is known in broad outline, many of the details remain obscure. In general, intracellular events more distal from the insulin receptor are less well understood. Much has been discovered regarding the role of Akt in the mammalian cell, however, much also remains to be elucidated concerning its regulation, activation, and downstream signalling modalities. In order to understand the dysregulation of Akt in pathological states, it is necessary to first establish a thorough working knowledge of its function in the healthy state.



# Chapter 3

## Mathematical Models of the Insulin Signalling Pathway

### 3.1 Introduction

This chapter is a review of work done by others to model different aspects of the insulin signalling network. It begins with a discussion of the best known and most extensive model of insulin signalling to date, the Sedaghat model [45]. The Sedaghat model is discussed in some detail, as is some of the more recent work derived from it. Next, the focus shifts to components of the insulin signalling network, in particular, the insulin receptor subsystem and the Akt cycle. There are numerous studies of these components, with the great majority employing some form of deterministic ordinary differential equation (ODE) model. As the number of studies is large, only brief overviews can be given, however, it is important to note the contrast in treatments of the two components. Thus far, the insulin receptor subsystem has been modelled extensively, and with a high degree of mathematical sophistication. In comparison, the treatment of the Akt cycle in the mathematical modelling literature is far sketchier. Unquestionably this is due to

the fact that less is known about the insulin signalling network the further one moves down the cascade: it is inherently much easier to study structures like the insulin receptor that are located on the cell exterior. However, the sheer number and variety of mathematical models featuring Akt activation attest to both the biological significance of this signalling component, and the degree of interest in its role as a crosstalk node.

## **3.2 Signalling Network Models**

### **3.2.1 The Sedaghat Model**

There are few mathematical models of the insulin signalling pathway that detail all major steps between the binding of insulin to the insulin receptor and the translocation of GLUT4 to the plasma membrane [46]. The Sedaghat, Sherman and Quon model (Sedaghat model) is one such model [45]. It is widely considered to be the most comprehensive model of insulin signalling to date, and is still regularly cited, despite the passage of over fifteen years since its publication [47].

The Sedaghat model is composed of twenty deterministic, non-linear ODEs involving twenty-one state variables. While the number of equations is large, the individual equations are relatively straightforward, being generally first or second order polynomials in the state variables. (A model that embodied all chemical species and cellular subprocesses known to be involved in insulin signalling would have in excess of one hundred state variables [48].) There is also a version of the model that incorporates a number of feedback loops. A schematic diagram of the simpler open-loop system is given in Figure 3.1. In this diagram, the state variables are represented by nodes and chemical reactions by edges labelled with the appropriate rate constants and other factors that modulate these reactions. Nodes lying on the left side of

the diagram represent chemical species that are located at the plasma membrane. The model can be divided, somewhat arbitrarily, into a number of different subsystems. In this diagram, the insulin receptor subsystem has been distinguished from the downstream subsystem, with the division lying immediately above IRS-1. The parameter values used in the model are predominantly drawn from a variety of data sets found in the literature. For a full description of the Sedaghat model, including equations, initial conditions and parameter values, please consult [45].

In the Sedaghat model, insulin signalling commences when extracellular insulin ( $x_1$ ) binds to free insulin receptors on the plasma membrane ( $x_2$ ). The singly-bound receptors ( $x_3$ ) then undergo autophosphorylation ( $x_5$ ). Following this, the receptors either bind a second insulin molecule ( $x_4$ ) or dissociate from the first, thus returning to the free surface insulin receptor pool ( $x_2$ ). The binding of a second insulin molecule does not affect the phosphorylation state of the receptor, but dissociation causes almost instantaneous dephosphorylation. The insulin signal is propagated down the cascade via the sum of the variables  $x_4$  and  $x_5$ .

The model explicitly includes insulin receptor recycling and degradation. Once- and twice- bound receptors are internalized in an identical manner ( $x_7$  and  $x_8$ ) and dephosphorylated. Upon dephosphorylation, the receptors return to the intracellular pool ( $x_6$ ), where they are either recycled to the plasma membrane or degraded. Synthesis of new intracellular receptors is assumed to occur at a constant, but very low, rate. These sinks and sources are noted in Figure 3.1.

The multiplicative factor PTP, representing the relative activity of protein tyrosine phosphatases in the cell, modulates the receptor dephosphorylation rate of both surface and internalized receptors. It is thought that under certain pathological conditions, protein tyrosine phosphatases contribute to the development of insulin resistance by increasing the dephosphorylation rate of insulin receptors, leading to the premature termination of signalling

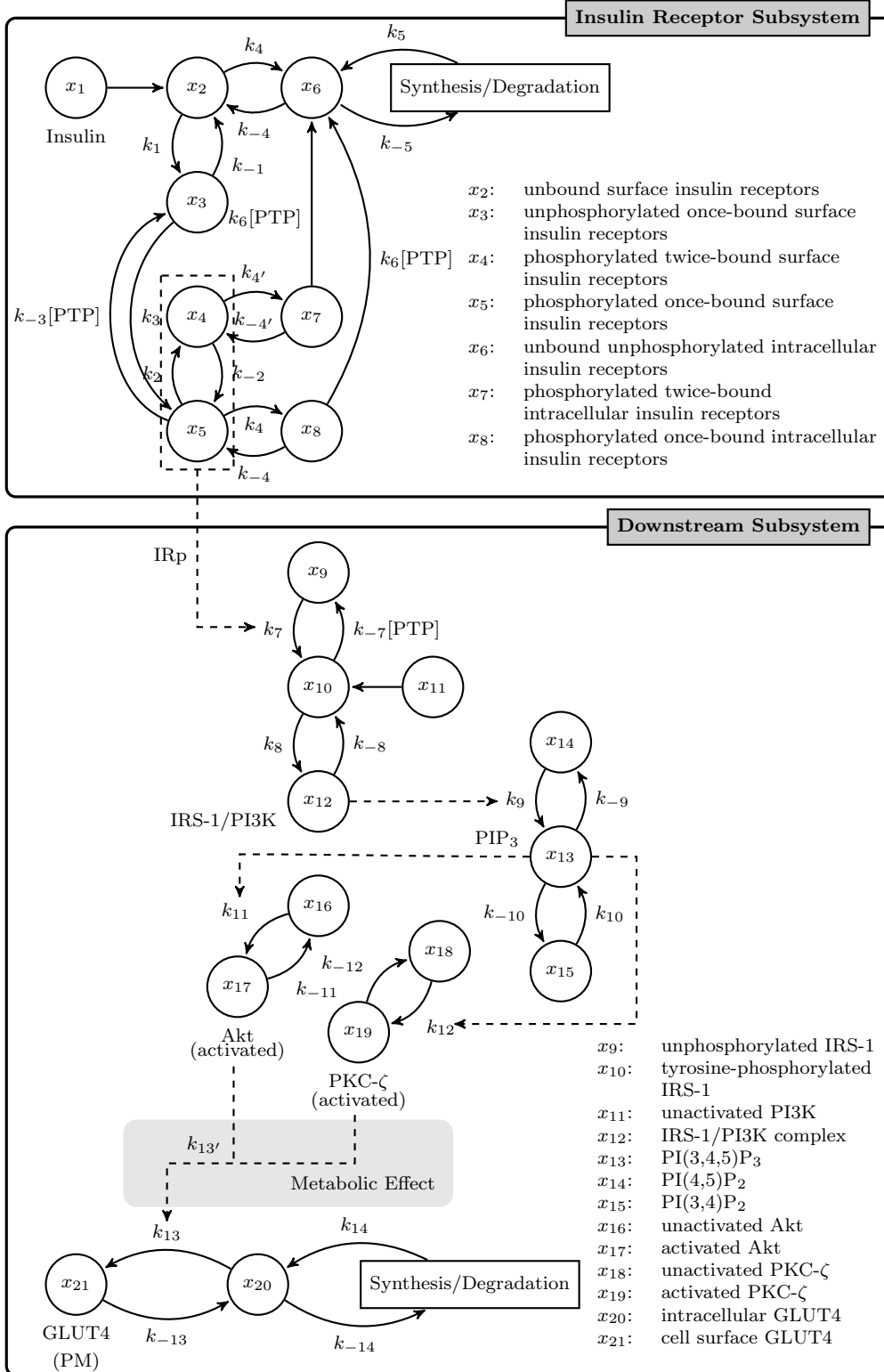


Figure 3.1: A schematic diagram of the Sedaghat model. Nodes in the diagram represent state variables; edges represent chemical reactions.

[49]. Under normal physiological conditions it is assumed that PTP equals one.

As the insulin signal is propagated downstream from the receptor subsystem, it is modulated by the factor IRp, representing the concentration of phosphorylated surface insulin receptors achieved after maximal insulin stimulation. This signal activates IRS-1 ( $x_9$  in Figure 3.1), which then binds to PI3K ( $x_{11}$ ), forming the IRS-1/PI3K complex ( $x_{12}$ ). The IRS-1/PI3K complex converts phosphatidylinositol 4,5-bisphosphate ( $x_{14}$ ) to PIP<sub>3</sub> ( $x_{13}$ ), the next major signalling component in the cascade. PIP<sub>3</sub> is also produced by the phosphorylation of phosphatidylinositol 3,4-bisphosphate ( $x_{15}$ ). It was assumed that the synthesis and degradation of these signalling molecules does not occur at an appreciable rate, and hence these processes were not included explicitly in the model.

The GLUT4 translocation machinery is located downstream from PIP<sub>3</sub>. Even under fasting conditions, GLUT4 is in a dynamic equilibrium between the internal pool ( $x_{20}$ ) and the plasma membrane pool ( $x_{21}$ ). However, the rate of exocytosis of GLUT4 is greatly increased when Akt ( $x_{16}$ ) and PKC- $\zeta$  ( $x_{18}$ ) are activated by PIP<sub>3</sub>. As a consequence, the expression of GLUT4 at the plasma membrane increases from an initial value of 4% to slightly less than 40% within 10–15 minutes of the start of insulin stimulation.

The Sedaghat model and its various subsystems have been modified, extended and reused in a number of subsequent studies. For instance, it has been used as the basis of a mathematical study of the multi-drug treatment of diabetes [47], and as the insulin signalling module of a multi-scale model of glucose metabolism and regulation [46, 50, 51]. In addition, it has been extended to include the mitogenic action of insulin on gene transcription and growth regulation [52, 53], and as one component of a systematic model of hepatic insulin signalling [54].

### 3.2.2 Limitations of the Sedaghat Model

The Sedaghat model has some significant limitations. In particular, the differential equations of the insulin receptor subsystem are stiff [50, 55], due to the widely different timescales involved. In addition, some key biochemical components in the network—most notably, insulin receptors and GLUT4 molecules—are not conserved. Furthermore, some aspects of the network, such as Akt activation, were modelled somewhat sketchily, reflecting the understanding of the biology current at the time. (For a succinct review of what was known concerning Akt activation circa 2001, please consult [56].) Akt activation in the Sedaghat model is a simple two-compartment system (activated and un-activated Akt) that does not reflect the spatial distribution of Akt within the cell.

The Sedaghat model was given a major update by Ho and colleagues in 2014 [57]. Newly elucidated components of the GLUT4 translocation machinery, such as Akt substrate of 160 kDa (AS160), were added to the original Sedaghat model. These additions are all located downstream from Akt and PKC- $\zeta$  in the signal transduction pathway, and depend upon the activation state of upstream components for their reaction rates. However, it should be noted that the Ho model retains the same simple two-pool treatment of Akt activation as the original model.

## 3.3 Models of the Insulin Receptor System

There is a long history of modelling the insulin receptor system. One of the earliest models is that of Jones, *et al.* [58], which modelled the receptor-mediated clearance and degradation of insulin. This model inspired the five-compartment model of insulin clearance of Hovorka, *et al.* [59, 60], which featured a simple two-compartment treatment of the insulin receptor system. This was followed by the models of Quon and colleagues in the nineties

[61–63], which formed the foundation for the insulin receptor subsystem of the Sedaghat model [45].

The Sedaghat insulin receptor subsystem combined previous models of insulin receptor binding kinetics with receptor internalisation and recycling dynamics. Following the model of Wanant and Quon [63], the Sedaghat model explicitly incorporated the divalent binding of the insulin receptor, in which two insulin molecules simultaneously bind a single receptor. A later, and much more detailed, treatment of this phenomenon was also given in the harmonic oscillator model of insulin receptor binding of Kiselyov and co-workers [64]. Indeed, in at least one instance, the insulin receptor model of Kiselyov, *et al.*, has been used as a replacement for the insulin receptor subsystem of the Sedaghat model in a parametric sensitivity analysis of the insulin signalling pathway [65].

Insulin receptor internalisation and recycling has also been studied by Hori and colleagues [66]. Starting with a two-compartment model of insulin receptor internalisation by Backer, *et al.* [67], they developed three further models of increasing complexity (the four-, five- and six-pool models) in order to study the effect of insulin receptor phosphorylation state and ligand dissociation on insulin receptor trafficking in FAO hepatoma cells under conditions of maximal insulin stimulation (100 nM).

Koschorreck and Gilles have also investigated the role of insulin receptor activation in rat hepatocytes on the concentration of insulin in the blood [68]. The Koschorreck model relaxes the tight connection between ligand dissociation and receptor dephosphorylation seen in the Sedaghat model. It also details some processes not included in previous models, such as renal clearance of insulin from the bloodstream.

Most of the insulin receptor models discussed thus far have been compartmental ODE models in which either the law of mass action or Michaelis-Menten kinetics has been assumed. (For a more in-depth discussion of the law of

mass action and Michaelis-Menten kinetics, see [69].) The resulting mathematical models may be large, but the individual equations are generally quite simple. A potential pitfall of this approach, however, is the generation of a large number of model parameters which must be estimated from experimental data. In many cases, the experimental data either does not exist, lacks the necessary temporal or spatial resolution, or is very noisy. Fitting models to scant or noisy data can result in many unidentifiable parameters.

The Cedersund group have taken a parameter-free modelling approach that uses the methods of mathematical control theory to analyse, and ultimately accept or reject, whole classes of compartmental models. Any compartmental model can be thought of as one instance of a larger class or family of models. The class is determined by the model structure: that is, the number of compartments and the relationships between them, such as positive or negative feedback and feed-forward mechanisms, for example. The particular instance of the model is given by the set of values assigned to the parameters (rate constants and initial conditions) arising from the structure [70]. In the Cedersund method, models are systematically assessed against specific criteria based on structural details rather than features arising from the particular set of parameter values used to instantiate the models. The results of this analysis hold true irrespective of the feasibility of optimising the candidate model or models to experimental data. In [71] or [72], for example, this approach was applied to the early phase of insulin signalling to establish that insulin receptor internalisation is necessary for feedback mechanisms involving mass and information transfer.

### **3.4 Models of Akt Activation**

Numerous mathematical models of Akt activation have appeared in the literature. As Akt is an important crosstalk node in the cell, these modelling efforts have detailed its role in both insulin signalling [10, 45, 52, 73–77] and

other signalling pathways [78–82]. The models are based on a variety of cell types, such as Chinese-hamster ovary (CHO) cells [78], glial progenitor cells [81], HeLa cells [83], human adipocytes [73], human embryonic stem cells [74,75], mouse embryonic fibroblasts [84], NIH 3T3 fibroblasts [80], and rat hepatoma FAO cells [10]. Furthermore, although many of these studies model Akt activation in response to insulin, other growth factors have also been used, including fetal bovine serum [84], heregulin [78,85], insulin-like growth factor 1 (IGF-1) [81], platelet derived growth factor (PDGF) [80], and vascular endothelial growth factor (VEGF) [82]. Given the use of diverse cell types and stimuli, caution must be exercised when interpreting or comparing results from these disparate models.

### 3.4.1 Single Input Models

A number of studies based on the Sedaghat model have appeared in the literature. Giri and co-workers adapted the model to study the phenomenon of bistability caused by positive and negative feedback in the network [86]; Liu, *et al.*, employed the model in a study of glucose metabolism in hepatocytes [50]; Luni and Doyle simplified the model to study multi-drug therapy [47]; Huang and collaborators adapted the model to study the role of IRS1 and IRS2 in hepatic insulin signalling [54]; and Mathews and collaborators used the model in a systems analysis of self-renewal in human embryonic stem cells [74,75]. Being derived from the Sedaghat model, all these studies featured the same simple two-compartment treatment of Akt activation.

Park and co-workers studied the activation of Akt in NIH 3T3 fibroblasts in response to PDGF stimulation [80]. A mechanistic ODE model was used to describe this signalling pathway, however, the reduced version of this model used for the experimental data fitting featured only a single compartment of activated Akt.

Similarly, Romanelli and colleagues combined empirical studies and mathematical modeling to study the response of the PI3K-Akt signalling pathway

to IGF-1 stimulation in glial progenitor cells [81]. Their modelling predominantly focused on IGF-1 receptor dynamics, with the phosphorylated fraction of Akt as the primary model output. The treatment of Akt activation in this model was rudimentary, and the spatial distribution of Akt in the cell was not addressed.

Kubota, *et al.*, developed a computational model of the insulin signalling pathway from the insulin receptor to the downstream substrates of Akt: ribosomal protein S6 kinase (S6K); glucose-6-phosphatase (G6Pase); and glycogen synthase kinase-3 $\beta$  (GSK3 $\beta$ ) [10]. Although insulin receptor dynamics was treated with some detail, Akt activation was represented by a two-compartment system consisting of pools of unactivated and activated Akt.

Smith and colleagues developed a computational model of the regulation of insulin signalling by reactive oxide species in order to study the phenomenon of aging at the cellular level [53]. Their work focussed on the long-term regulation of downstream substrates of Akt, such as FOXO, rather than the short-term behaviour of the insulin signalling pathway. The Smith model featured a detailed treatment of the insulin receptor subsystem, with the inclusion of multiple insulin binding and receptor internalisation dynamics. Akt activation, however, was represented by a simple two-compartment model with pools of activated and un-activated Akt.

In contrast, Wang modelled the phosphorylation/dephosphorylation cycle of Akt in response to insulin with a four-compartment system that uses the full Michaelis-Menten kinetics [87]. That is to say, Akt in the Wang model existed in either the activated or unactivated state, and the intermediate states—where Akt is complexed with either its phosphorylating kinase or dephosphorylating phosphatase—were also explicitly modelled. The Wang paper consisted of singularity and bifurcation analyses of this system, and made no attempt to fit the model parameters to experimental data. Were this to be attempted, it is probable that this level of model complexity could

not be supported by the existing data, leading to some of the parameter values being unidentifiable.

The activation of Akt in response to vascular endothelial growth factor (VEGF) has also been modelled [82]. The authors' intent with this model was to study the highly transient behaviour of Gab2 (an upstream effector of Akt) in the VEGF signalling pathway. The model was based on mass-action kinetics and features a highly detailed treatment of Akt phosphorylation. As with the Wang model, the enzyme-substrate binding step for each biochemical reaction was explicitly modelled, with the added complexity of double phosphorylation. In common with the previously mentioned model, the experimental support for the estimation of all the parameters was possibly incomplete.

Goltsov, *et al.*, developed a computational model of the PTEN-PI3K-Akt signalling pathway to study the development of resistance to anti-cancer drugs in breast and ovarian cancer [88–90]. In their model, the double phosphorylation of Akt is explicitly modelled, with pools of unphosphorylated, singly-phosphorylated and doubly-phosphorylated Akt. Dalle Pezze and collaborators [83] also employed a three-pool model of Akt phosphorylation in their study of mTOR regulation by insulin. However, neither of these models depict the translocation of Akt directly.

Brännmark and colleagues from the Cedersund group developed an extensive mathematical model of insulin signalling to study the mechanisms of insulin resistance arising in type 2 diabetes [72]. Their model features a four-compartment subsystem of Akt activation (referred to as PKB) that tracks the phosphorylation and dephosphorylation of Akt in detail, and includes pools of unphosphorylated Akt; Akt singly-phosphorylated on Serine-473 (Ser473); Akt singly-phosphorylated on Threonine-308 (Thr308); and doubly-phosphorylated Akt.

As a generalisation, the models of Akt activation discussed thus far tend to be either rudimentary two-compartment models or, given the existing

experimental data, overly detailed in their treatment of Akt phosphorylation. One could say that the depiction of Akt phosphorylation seems to be either too simple, or too elaborate! Furthermore, in these studies Akt translocation has often been “lumped” into the activation step, rather than being explicitly modelled in its own right.

### 3.4.2 Crosstalk Models of Akt Signalling

An important sub-class of mathematical models of Akt activation are what may be termed “crosstalk” or systems biology models. One of the advantages that mathematical modelling has over other investigative techniques is the ability to study emergent properties that arise from complex interactions between multiple signalling pathways with comparative ease. Numerous examples of such systems biology models can be found in the Akt modelling literature. These studies investigate the interaction between the PI3K-Akt network and other signalling pathways such as mitogen activated protein kinase (MAPK) [78, 91, 92]; epidermal growth factor (EGF) [93, 94]; and mammalian target of Rapamycin (mTOR) [95, 96]. Crosstalk between three signal transduction pathways has also been studied: the PI3K-Akt, mTOR and MAPK pathways in [97]; and the PIP<sub>3</sub>-Akt, IGF-1, and EGF pathways in [94].

Hatakeyama [78] and colleagues studied the interaction between the MAPK pathway and PI3K-Akt signalling in CHO cells. This model treated Akt phosphorylation in detail, with three Akt pools representing singly-, doubly- and un-phosphorylated Akt. Similarly, Suresh Babu, *et al.*, employed a computational modelling approach to investigate the response of the MAPK and PI3K-Akt signalling pathways to stimulation with epidermal growth factor (EGF) and nerve growth factor (NGF) [92]. This model also tracked the phosphorylation and dephosphorylation of Akt in detail. In addition, Arkun investigated the key feedback loops involved in crosstalk between the MAPK and Akt signalling pathways, this time in response to insulin stimulation [91].

In this study, Akt signalling was represented by a reduced version of the Wang model, and thus featured only two Akt pools (activated and unactivated). None of these three models of combined Akt and MAPK signalling explicitly tracked the location Akt within the cell.

Nijhout and co-workers also studied the insulin-mTOR-MAPK network response to a variety of stimuli, such as insulin, amino acids and other growth factors [76]. Interestingly, the activation equation for each node in this network is a sigmoid (logistic) function of the input, defined as a weighted sum of upstream activators and inhibitors. Akt is represented as a single node in this network with the immediate upstream activator  $\text{PIP}_3$  and inhibitor PKC (protein kinase C). For all activation equations in the model, multiple phosphorylation steps, equilibrium reactions between kinases and phosphatases, and translocation dynamics were ignored.

The interaction between the mTOR and insulin signalling pathways was studied by Vinod and Venkatesh [95] and Bertuzzi, *et al.* [96]. Vinod and Venkatesh modelled the effect of amino acids on an integrated model of the insulin signalling pathway and mTOR. Akt activation in this study consisted of a two-compartment model with phosphorylated and unphosphorylated Akt pools linked to upstream and downstream components via ODEs that have the functional form of a Hill equation. In contrast, Bertuzzi, *et al.*, employed Michaelis-Menten kinetics to develop their rather detailed four-compartment submodel of Akt phosphorylation, which distinguishes between unphosphorylated Akt, Akt singly-phosphorylated on Ser473 or Thr308, and doubly-phosphorylated Akt.

Crosstalk between the EGF and insulin signalling pathways was investigated by Borisov, *et al.*, [93] and Zielinski, *et al.* [94]. In the Borisov paper, the double-phosphorylation and dephosphorylation of Akt was modelled with Michaelis-Menten reaction kinetics. In contrast to the previously outlined, purely deterministic models, Zielinski and co-workers developed a Boolean network model of crosstalk between the EGF, IGF-1, and insulin signalling

pathways. This model relied on stochastic signal propagation and was used to study the combinatorial stimulation of the EGF, IGF-1, and insulin receptors.

Crosstalk between three signal transduction pathways, namely PI3K-Akt, mTOR and MAPK, was studied in [97]. The PI3K-Akt subsystem in this model was largely drawn from Sedaghat, but employed a more elaborated description of Akt phosphorylation, resulting in a four-pool model which distinguished between unphosphorylated Akt, Akt singly-phosphorylated on Ser473 or Thr308, and doubly-phosphorylated Akt.

### 3.4.3 Translocation Models

In the mathematical modelling literature, comparatively detailed descriptions of Akt phosphorylation are commonplace. Numerous models discussed in Sections 3.4.1 and 3.4.2 featured a detailed treatment of the double-phosphorylation of Akt [72, 78, 82, 83, 88–90, 92, 96, 97]. However, models that address the spatial dependency of Akt activation or explicitly describe the Akt translocation process are rare. Two exceptions are the models of Bates, *et al.* [52], and Nim, *et al.* [84].

Bates and colleagues developed a mathematical model of growth regulation via Akt and the forkhead transcription factor, FOXO. In the downstream subsystems of this model, partial differential equations were used to describe the transport (advection and diffusion) of mobile proteins, such as Akt. However, all mobile components of this model shared common diffusivity and advection coefficients, presumably due to a dearth of experimental data suitable for estimating these constants.

In contrast, Nim and co-workers presented an ODE model of Akt activation in mouse embryonic fibroblasts. This compartmental model tracks the effect of a peak in PIP<sub>3</sub> activation on subsequent Akt activation and includes two Akt pools distinguished by location (plasma membrane and cytosol). This model

was used to investigate the implications of an unknown effect on each of the main steps of the canonical Akt activation pathway. This was done in order to either support or exclude certain hypotheses concerning the phenomenon of “overshoot” in the levels of Akt phosphorylated on Thr308.

### **3.5 Summary**

In this chapter, numerous models of the insulin signalling network have been discussed. The most comprehensive model of the insulin signalling pathway to date—the Sedaghat model—has been reviewed, along with some of the studies derived from it. An overview of modelling of two components of insulin signalling pathway—the insulin receptor subsystem and the Akt cycle—has also been given. In general, it can be seen that while the insulin receptor subsystem has been modelled in detail, models that directly depict the translocation of Akt in response to insulin are few.



# Chapter 4

## Mathematical Modelling Philosophy and Techniques

An overview of the mathematical modelling philosophy behind the thesis is presented in this chapter. This overarching philosophy naturally gives rise to a set of techniques for model development, model analysis, and parameter optimisation. For specific details concerning the implementation of these techniques, the reader is referred to the relevant chapter(s) in Part II of the thesis.

### 4.1 Modelling Approach

The three mathematical models that form the backbone of this thesis—the Receptor State Space model, the Akt Switch model, and the Akt Translocation model—are deterministic, ordinary differential equation (ODE) models of components of the insulin signalling pathway. The insulin receptor subsystem is the focus of the Receptor State Space model (Chapter 5); and the Akt activation cycle is modelled in the Akt Switch model (Chapter 6) and the

Akt Translocation model (Chapters 7 and 8). All three models are intended to be explanatory rather than predictive in a heuristic sense: they were developed to identify dominant processes and suggest possible mechanisms of regulation of the underlying biological system.

The approach taken in this work is that, in general, it is best to use the simplest model that can reproduce the salient features of the underlying biology: model complexity should only be increased when justified by the data available. This *principle of parsimony* (also known as “Ockham’s razor”) is particularly important when multiple submodels are to be linked together into a network, as it leads to more highly constrained data fitting and more straightforward model analysis. All three models presented in this thesis can be viewed as small components in a much larger network, either the insulin signalling pathway or in other signalling cascades, such as those of mTOR or MAPK. Consequently, two noteworthy simplifications have been made in the development of these models.

Firstly, the models are deterministic, even though the biochemical reactions being modelled are inherently stochastic. In this case, the deterministic model is a mean-field approximation representing the average behaviour of the underlying stochastic system. Provided that the population of chemical species is sufficiently large, this approximation will be a good one. In the absence of data indicating contrariwise, the greater computational tractability of a deterministic model makes it the preferred choice compared to its stochastic counterpart. Indeed, were one aiming to develop a stochastic model of a biochemical system, the development of a deterministic representation would still be a wise initial step.

Secondly, all three models are compartmental ODE models. In the case of Akt translocation, which involves changes in the intracellular distribution of Akt, it could be argued that a partial differential equation (PDE) model would be more appropriate. However, experimental data with sufficient spatial and temporal resolution to support the development of such a model does not currently exist. As noted in Section 3.4.3, there has been a previous

attempt to replace parts of the Sedaghat model, including the Akt activation cycle, with a PDE formulation (the Bates model [52]). This, however, required substantial simplifications—it could be argued over-simplifications—in which all mobile components of the model were assumed to share common diffusivity and advection coefficients. Instead, in the current work, compartmental ODE models have been employed. It should be borne in mind, however, that compartmental homogeneity is an inherent assumption of such modelling approaches.

## 4.2 Model Development

*This section is based on work presented in: CW Gray and ACF Coster. Models of Membrane-Mediated Processes: Cascades and Cycles in Insulin Action. In Wolkenhauer & Voit (Eds.), Systems Medicine: Integrative, Qualitative and Computational Approaches, Academic Press. To appear September 2020.*

Figure 4.1 shows a selection of simple two- and three-compartment models in which a reactant,  $R$ , is converted into a product,  $P$ . For each model, a schematic diagram is shown on the left and a typical time course on the right; the initial concentration of the product is  $P_0$ , and the steady state value is  $P^*$ . In each case, first order reaction kinetics have been assumed. This means that the rate of each reaction (depicted with an arrow in the diagram) depends linearly on the concentration of the reactant at the start of the arrow. Thus the time derivative of any component concentration is the sum of the incoming reactions minus the sum of the outgoing reactions. For example, in the three pool cycle shown in Figure 4.1 (d),

$$\frac{dP}{dt} = k_2I - k_3P,$$

where  $t$  is time.

The simplest possible scheme is shown in Figure 4.1 (a). In this case,  $R$  is converted to  $P$  via a single forward reaction with constant rate  $k$ . The

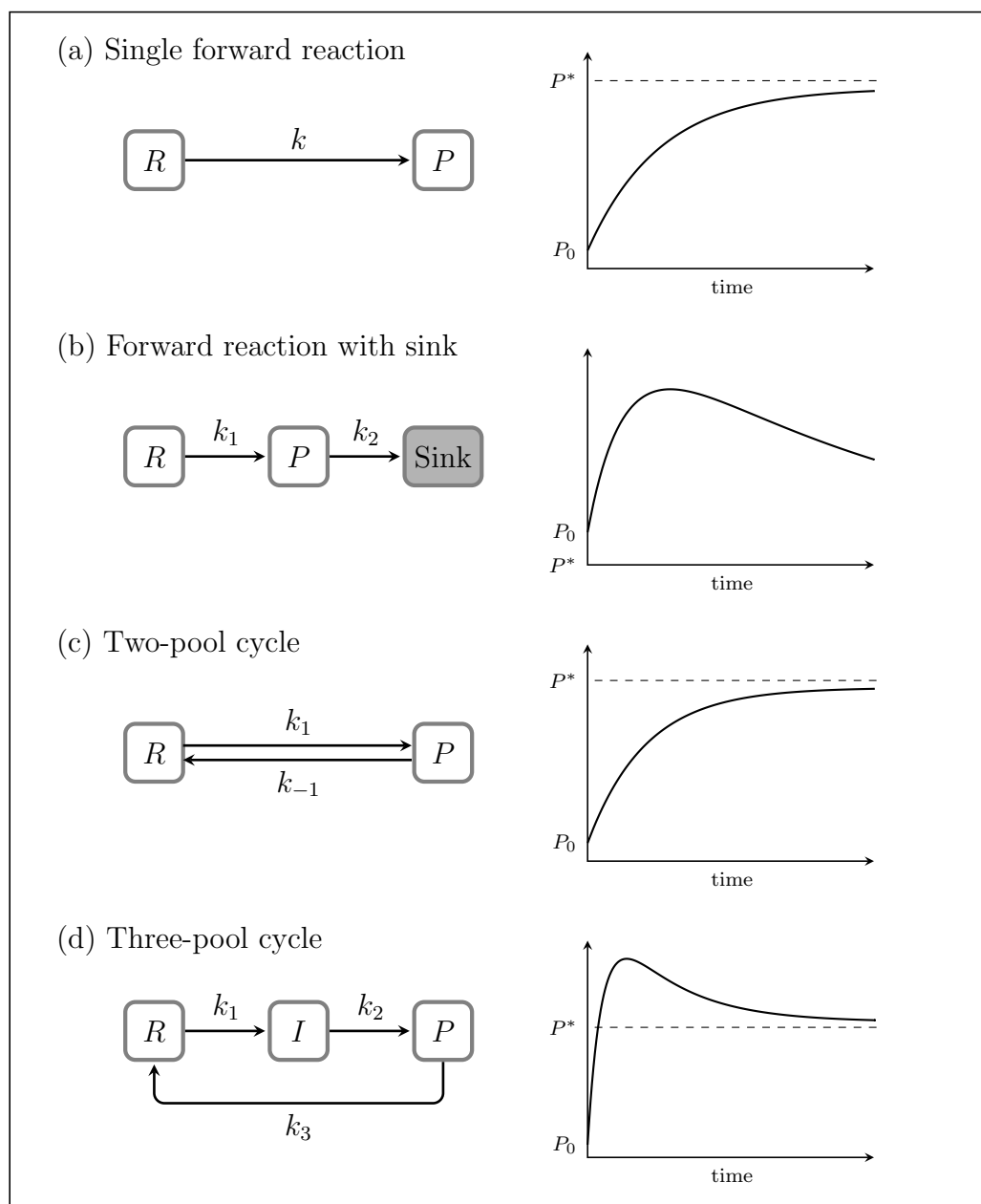


Figure 4.1: A schematic diagram of simple two- and three-compartment models is shown on the left; a typical time course from each model on the right. All rate constants ( $k$ ,  $k_1$ ,  $k_{-1}$ ,  $k_2$ ,  $k_3$ ) are positive. In each graph,  $R_0$  is the initial concentration of  $R$ ,  $P_0$  the initial concentration of  $P$ ,  $P_0 < R_0$ , and  $P^*$  is the steady state level of  $P$ . First order reaction kinetics have been assumed in each case. In (b),  $k_2 < k_1$ ; in (c),  $k_1 > k_{-1}$ ; and in (d),  $k_3 > k_1 > k_2$ .

solution for  $P$  is

$$P(t) = P_0 + R_0(1 - e^{-kt}),$$

where  $R_0$  is the initial concentration of  $R$ . The resulting time course is an exponential rise to the steady state value,  $P^* = P_0 + R_0$ , with a single time constant,  $\frac{1}{k}$ .

In contrast, Figure 4.1 (b) shows a forward reaction with a sink (shaded in grey). In other words, following conversion from  $R$  at the constant rate  $k_1$ ,  $P$  is consumed or otherwise leaves the system at the constant rate  $k_2$ . Consequently, the concentration of  $P$  typically increases at first, peaks, and then ultimately decreases to zero. In this case, the solution for  $P$  is a double exponential,

$$P(t) = \alpha e^{-k_1 t} + (P_0 - \alpha) e^{-k_2 t},$$

where  $\alpha = \frac{R_0 k_1}{k_2 - k_1}$  and  $k_1 \neq k_2$ . Note that the interplay of two rate constants of differing magnitude ( $k_1$  and  $k_2$ ) is necessary to produce a peak.

A two-compartment model with both forward and backward reactions is shown in Fig. 4.1 (c). The solution is a single exponential,

$$P(t) = P^* - (P^* - P_0) e^{-(k_1 + k_{-1})t},$$

where  $P^* = \frac{k_1}{k_1 + k_{-1}}(P_0 + R_0)$ , the steady state value. This results in a time course which is an exponential rise to the steady state value with a single time constant,  $\frac{1}{k_1 + k_{-1}}$ .

A three-pool cycle is shown in Figure 4.1 (d). In this model,  $R$  is converted to  $P$  via an intermediary,  $I$ . It is then converted back into  $R$  again. This has the solution

$$P(t) = \alpha e^{\lambda_1 t} + \beta e^{\lambda_2 t},$$

where

$$\lambda_1 = \frac{-(k_1 + k_2 + k_3) + \sqrt{\Delta}}{2},$$

$$\lambda_2 = \frac{-(k_1 + k_2 + k_3) - \sqrt{\Delta}}{2},$$

and

$$\Delta = (k_1 + k_2 + k_3)^2 - 4(k_1k_2 + k_2k_3 + k_1k_3).$$

Here the constants  $\alpha$  and  $\beta$  are determined by the initial conditions. This system, which is equivalent to a heavily damped harmonic oscillator [98], will exhibit overshoot under some conditions and is discussed more extensively in Chapter 7. Overshoot is an initial, rapid rise followed by a decrease or “roll-off” to a lower steady state value, and is an important aspect of some signalling pathways, such as Akt. Note that, as in Fig. 4.1 (b), at least two time constants, representing two processes that occur on sufficiently different time scales, are required to produce the overshoot behaviour.

Determining the relevant time scale is an important consideration in the construction of a mathematical model. Naturally, the choice of time scale will depend on the intended application of the model. Three significant time scales involved in signal transduction pathways are the time scales of biochemical activation (milliseconds to seconds); physical translocation (seconds to minutes); and protein synthesis (hours to days). In three out of the four models discussed in this section (the single forward reaction, the two pool cycle, and the three pool cycle), conservation has been assumed. That is to say,  $R + P$  (or in the case of the three-compartment model,  $R + P + I$ ) is constant at all times. This is called the quasi-steady state hypothesis, as it is often only approximately true over the time scale of interest. However, when invoked, the quasi-steady state hypothesis can lead to substantial simplifications.

As an example, compare the single forward reaction and the two-pool cycle, shown in Fig. 4.1 (a) and Fig. 4.1 (c), respectively. It is apparent that the

time courses and the forms of the solutions are substantially the same. Two differences are: the steady state levels, which differ by a factor of  $\frac{k_1}{k_1+k_{-1}}$ ; and the time constants,  $\frac{1}{k}$  compared to  $\frac{1}{k_1+k_{-1}}$ . That is, the two-pool model will reach a lower steady state value quicker than the single forward reaction. If  $k_1$  is much greater than  $k_{-1}$  (which is to say, if the forwards reaction occurs at a much faster rate than the back reaction) then  $\frac{k_1}{k_1+k_{-1}}$  is approximately one and  $\frac{1}{k_1+k_{-1}}$  is close to  $\frac{1}{k_1}$ . Thus the prudent mathematical modeller could invoke the quasi-steady state hypothesis and reduce the two constants to a single rate constant. In effect, this is the substitution of a single forward reaction for the two-pool cycle, and has the advantage of reducing the number of parameters in the model.

### 4.3 Model Analysis

Stability analysis is a standard method for analysing the long-term behaviour of a dynamical system (a system of ODEs). This involves finding and determining the stability of the *fixed points* of the system. If the time derivative of an  $n$ -dimensional dynamical system is given by

$$\frac{d\mathbf{x}}{dt} = \mathbf{F}(\mathbf{x}), \quad \text{where } \mathbf{F} : \mathbb{R}^n \rightarrow \mathbb{R}^n, \quad (4.1)$$

then a fixed point of the system is a point  $\hat{\mathbf{x}} \in \mathbb{R}^n$  where  $\mathbf{F}(\hat{\mathbf{x}}) = \mathbf{0}$ . Thus a dynamical system initially located at a fixed point will stay there indefinitely. The *stability* of a fixed point is determined by the behaviour of the system when slightly perturbed away from  $\hat{\mathbf{x}}$ .

Roughly speaking, fixed points can be categorised as either *stable* or *unstable*. If the system is perturbed away from a stable fixed point, the size of the perturbation decreases. In contrast, if the system is perturbed away from an unstable fixed point, the perturbation grows. Consequently, over time the system will return to a stable fixed point but move away from an unstable one.

For this reason, stable fixed points are sometimes referred to as attractors and unstable fixed points as repellers.

The stability of a non-linear dynamical system at a fixed point is typically determined by linearisation about the fixed point,  $\hat{\mathbf{x}}$ . A Taylor series approximation is used to re-write Equation 4.1 as

$$\frac{d\mathbf{x}}{dt} = \mathbf{F}(\hat{\mathbf{x}}) + \mathbf{J}(\hat{\mathbf{x}}) \cdot (\mathbf{x} - \hat{\mathbf{x}}) + \text{higher order terms},$$

where  $\mathbf{J}(\hat{\mathbf{x}})$ , the Jacobian, is the matrix of partial derivatives of  $\mathbf{F}$  evaluated at  $\hat{\mathbf{x}}$ . That is,

$$\mathbf{J} = \begin{bmatrix} \frac{\partial \mathbf{F}_1}{\partial x_1} & \dots & \frac{\partial \mathbf{F}_1}{\partial x_n} \\ \vdots & \ddots & \vdots \\ \frac{\partial \mathbf{F}_n}{\partial x_1} & \dots & \frac{\partial \mathbf{F}_n}{\partial x_n} \end{bmatrix}.$$

The stability of the system is determined, at least locally, by finding the eigenvalues of  $\mathbf{J}(\hat{\mathbf{x}})$ , provided that the eigenvalues have non-zero real part [99]. (If some of the eigenvalues have zero real part, then the higher order terms neglected in the linearisation need to be considered.) If all eigenvalues have negative real part, the fixed point is stable.

## 4.4 Parameter Optimisation

Once an initial model structure has been decided and preliminary stability analysis carried out, parameter optimisation is a natural next step. This means selecting a parameter set—rate constants and in some cases initial conditions for the model—to minimize the difference between the model output and the available experimental data. Although the emphasis here is on explanatory rather than predictive models, a model that cannot reproduce the significant features of the underlying biological system for any choice of parameter set clearly lacks explanatory power.

In this thesis, the focus is on identifying dominant processes operating in the system. Thus the primary motivation behind parameter optimisation is system identification rather than parameter estimation, per se. In general, the relative magnitudes of rate constants obtained from the parameter optimisation are of greater interest than the actual values obtained. It is hoped that from these results possible mechanisms of regulation can be inferred, and in some cases, more plausible model structures identified.

Non-linear least squares optimisation and simulated annealing were used for the parameter fitting. Other methodologies could have been employed: for instance, Bayesian methods could be used to determine the distribution of parameter values. Irrespective of parameter fitting method, a goodness-of-fit statistic that takes into account differing numbers of parameters must be used to compare rival model structures. For the non-linear least squares fitting in this study, the adjusted R-squared statistic was used.

Another important statistic related to the individual parameter values is the 95% confidence interval. In general, smaller confidence intervals are better. A large confidence interval indicates that a parameter has not been well identified. In particular, if the confidence interval includes zero, this means that the uncertainty is larger than the parameter value itself. Some authorities consider this evidence that the parameter has not been successfully identified [70]. Large confidence intervals could be due to the sparsity of the data used for fitting (a perennial problem with biological systems) or inherent problems with the proposed model structure. They also arise from the nature of the underlying system itself. Many biological processes exhibit multiple layers of regulation and considerable redundancy. Given the limitations of current experimental techniques, this may render some aspects of system behaviour *a priori* unidentifiable. Alternately, it may simply be that the model output is largely insensitive to changes to that particular parameter.

## 4.5 Parametric Sensitivity Analysis

Parametric sensitivity analysis (PSA) is a term describing a number of techniques used to understand the effect of parameter uncertainty on a mathematical or statistical model. Typically, the rate constants of a biological model are not known with any degree of certainty, if at all. Parameter values quoted in the literature are derived from measurements taken under diverse experimental conditions and may not reflect the behaviour of signalling molecules *in vivo* [100–102]. Many parameters must be inferred from data that is noisy or lacking in temporal and/or spatial resolution; often only relative, not absolute, measurements are available. Thus some form of PSA is an important step in the analysis and refinement of a mathematical model.

PSA methods can be categorized as either local or global. In local PSA, parameter values are varied about a reference point one at a time and the impact on some aspect of model output is assessed. The results of a local PSA may hold true only for a limited area of parameter space about the reference point of the analysis, particularly in the case of a non-linear dynamical system.

In contrast, global PSA is an attempt to assess the combinatorial effect of changes in multiple parameter values. There are a variety of global PSA techniques in the literature (see [100,103–106]), however, these methods typically have a computational burden that increases exponentially with the number of parameters under investigation. Furthermore, several studies have demonstrated that parameter rankings obtained from local and global PSA of the same system do not necessarily agree [102,107]. Thus local and global PSA are not interchangeable. However, given the relative computational tractability of a local PSA, it can be used as an initial investigation of the parameter space of the model.

PSA—either local or global—is performed with respect to some criterion that reflects an important aspect of model behaviour. In this thesis, the term *metric* is used to refer to some quantifiable aspect of model behaviour, and should not be confused with the mathematical use of the same term. Examples of metrics include: the area under the curve; the maximum value; the peak timing (that is, the time taken to reach the maximum value); and the initial gradient. Which metrics should be used and the priority given them in the PSA depends on the purpose of the mathematical model and should be informed by what is already known about downstream signalling.

A successful local PSA can lead to greater insight into the underlying biology, and even improved experimental design [103, 108]. The identification of sensitive and insensitive parameters can suggest potential mechanisms of regulation for the behaviour of interest, even if only in a negative way, as a behaviour cannot be controlled by a process to which it is insensitive. In addition, this knowledge can be used to design experiments that more accurately measure the sensitive parameters or identify possible therapeutic targets.

Furthermore, PSA can lead to improved parameter optimisation and model development. Parameters identified as insensitive can be set to their nominal values, and the remaining sensitive parameters fitted to experimental data in a more highly constrained fashion. Alternately, the model could be simplified by a process of model reduction informed by the results of the PSA. An example of the simplification of the insulin receptor subsystem of the Sedaghat model based on a local PSA is given in Chapter 5.

## 4.6 Summary

In this thesis, gaining insight into the underlying biology is a key motivation behind the choice of models and techniques. From the development of the initial model structure, to its analysis and optimisation, the emphasis is on

determining the dominant processes and modes of regulation in operation. The next part of the thesis presents the original work undertaken using this approach to explore the translocation and activation of Akt in response to insulin.

## Part II

# Mathematical Models of Akt Translocation and Phosphorylation



# Chapter 5

## Preliminary Study on the Insulin Signalling Network

### 5.1 Introduction

*This chapter is based on work presented in: CW Gray and ACF Coster. A receptor state space model of the insulin signalling system in glucose transport. Mathematical Medicine and Biology: A Journal of the IMA, 32(4):457–473, 2015.*

In this chapter, the Receptor State Space model is proposed as a simpler, more streamlined alternative to the insulin receptor subsystem of the Sedaghat model. This is done for two purposes: to demonstrate some of the mathematical techniques described in Chapter 4 that can be used to study signal transduction pathways; and to provide further context for the models of Akt activation which are discussed in Chapters 6–8. The Receptor State Space model, while preserving the same input-output relation of the original Sedaghat subsystem, was analytically tractable and computationally efficient. Furthermore, it overcame some of the limitations of the Sedaghat model, such as the non-conservation of insulin receptor numbers and stiffness of the differential equations.

## 5.2 Methods

### 5.2.1 Analysis of the Sedaghat Model

A local parametric sensitivity analysis (PSA) of the full Sedaghat model was the major theme of my masters thesis [69]. As the results of the PSA strongly informed the development of the Receptor State Space model, the important points of the analysis are summarized here.

The simpler feed-forward version of the Sedaghat model was used for the PSA. A diagram of the full Sedaghat model is given in Chapter 3 (see Figure 3.1). The output metric for the PSA was the time integral of GLUT4 at the plasma membrane ( $x_{21}$ ) over a 60 minute interval. The state variable  $x_{21}$  is located at the end point of the cascade in the downstream subsystem, however, the model reduction detailed subsequently was limited to the insulin receptor subsystem. The differential equations, initial conditions, and parameter values of the Sedaghat insulin receptor subsystem are listed in Table 5.1; and an enlarged diagram of the system is given in Figure 5.1.

#### Stability Analysis

A linear stability analysis of the Sedaghat model was performed by a conventional procedure as described in Section 4.3. It confirmed that the model has no true fixed points, however, a quasi-steady state in the basal condition (that is, at the vector of initial conditions but with zero insulin input) was found.

The absence of fixed points is caused by the non-conservation of insulin receptors (in the insulin receptor subsystem) and GLUT4 (in the downstream subsystem). The differential equation given for  $x_6$  (intracellular insulin receptors) in the Sedaghat model is

$$\frac{dx_6}{dt} = k_5 - k_{-5}x_6 + k_6(\text{PTP})(x_7 + x_8) + k_4x_2 - k_{-4}x_6,$$

Table 5.1: Differential equations, initial conditions and parameter values of the insulin receptor subsystem from the Sedaghat model.

<b>Differential Equations</b>
$\frac{dx_2}{dt} = k_{-1}x_3 + k_{-3}(\text{PTP})x_5 - k_1x_1x_2 + k_{-4}x_6 - k_4x_2$
$\frac{dx_3}{dt} = k_1x_1x_2 - k_{-1}x_3 - k_3x_3$
$\frac{dx_4}{dt} = k_2x_1x_5 - k_{-2}x_4 + k_{-4'}x_7 - k_{4'}x_4$
$\frac{dx_5}{dt} = k_3x_3 + k_{-2}x_4 - k_2x_1x_4 - k_{-3}(\text{PTP})x_4$ $+ k_{-4'}x_8 - k_{4'}x_4$
$\frac{dx_6}{dt} = k_5 - k_{-5}x_6 + k_6(\text{PTP})(x_7 + x_8) + k_4x_2 - k_{-4}x_6$
$\frac{dx_7}{dt} = k_{4'}x_4 - k_{-4'}x_7 - k_6(\text{PTP})x_7$
$\frac{dx_8}{dt} = k_{4'}x_4 - k_{-4'}x_8 - k_6(\text{PTP})x_8$
<b>Initial Conditions</b>
$x_2(0) = 9 \times 10^{-12} \text{M}$
$x_3(0) = 0$
$x_4(0) = 0$
$x_5(0) = 0$
$x_6(0) = 1 \times 10^{-13} \text{ M}$
$x_7(0) = 0$
$x_8(0) = 0$
<b>Parameter Values</b>
$k_1 = 6 \times 10^7 \text{ M}^{-1} \text{ min}^{-1}$
$k_{-1} = 0.20 \text{ min}^{-1}$
$k_2 = k_1$
$k_{-2} = 100 k_{-1}$
$k_3 = 2500.00 \text{ min}^{-1}$
$k_{-3} = k_{-1}$
$k_4 = \frac{k_{-4}}{9}$
$k_{-4} = 0.003 \text{ min}^{-1}$
$k_{4'} = 2.1 \times 10^{-3} \text{ min}^{-1}$
$k_{-4'} = 2.1 \times 10^{-4} \text{ min}^{-1}$
$k_5 = \begin{cases} 10 k_{-5} \text{ M min}^{-1} & \text{if } x_6 + x_7 + x_8 > 1 \times 10^{-13}, \\ 60 k_{-5} \text{ M min}^{-1} & \text{otherwise} \end{cases}$
$k_{-5} = 1.67 \times 10^{-18} \text{ min}^{-1}$
$k_6 = 0.461 \text{ min}^{-1}$
$\text{PTP} = 1.0$
$\text{IR}_p = 8.97 \times 10^{-13} \text{ M}$

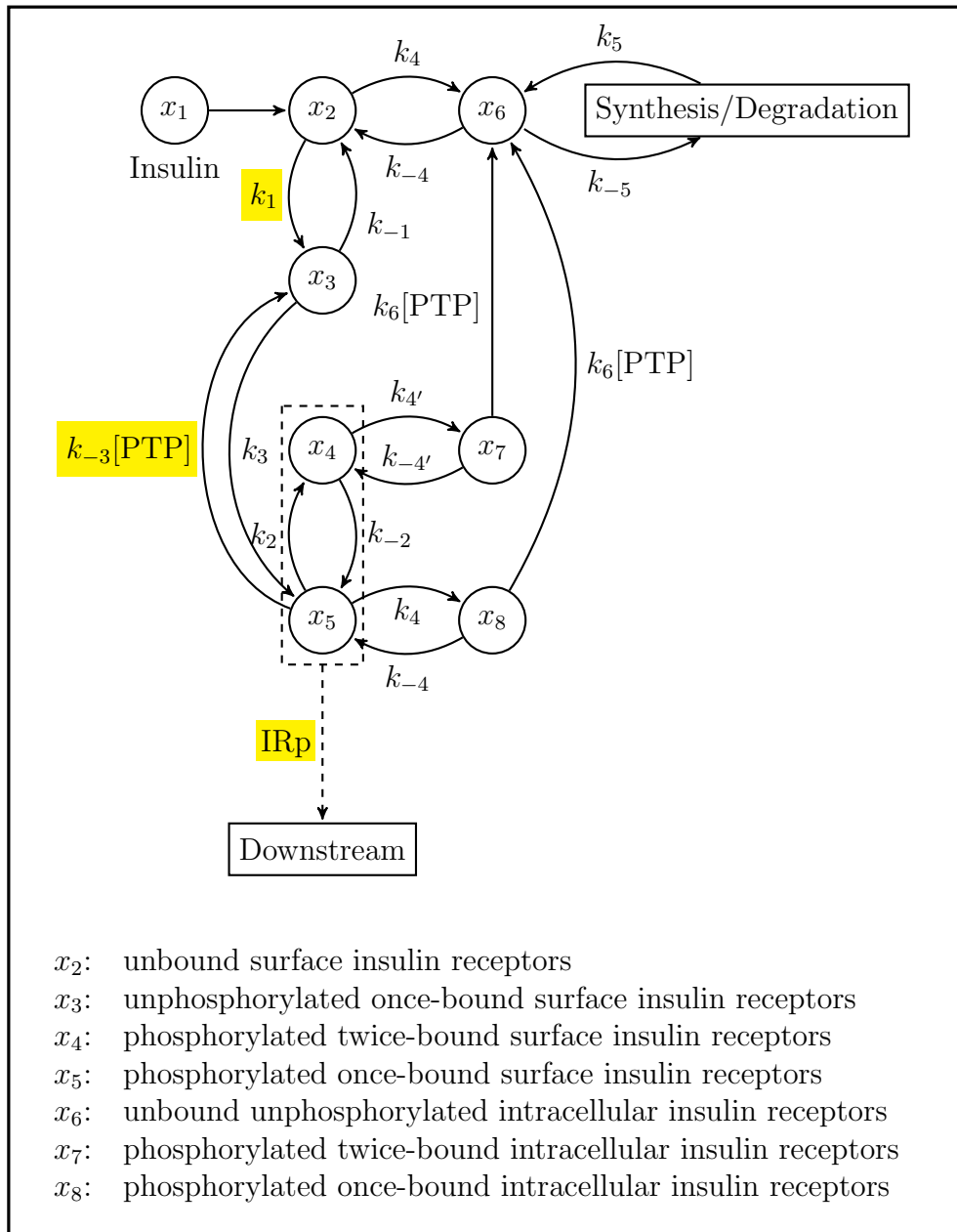


Figure 5.1: A schematic diagram of the insulin receptor subsystem from the Sedaghat model. Nodes in the diagram represent state variables; edges represent chemical reactions. Parameters sensitive for glucose transport have been highlighted in yellow.

where  $k_5$  is the rate of synthesis and  $k_{-5}$  the rate of degradation of intracellular insulin receptors. These parameters are defined as

$$k_{-5} = 1.67 \times 10^{-18} \text{ min}^{-1},$$

and

$$k_5 = \begin{cases} 10k_{-5} & \text{if } x_6 + x_7 + x_8 > 1 \times 10^{-13}, \\ 60k_{-5} & \text{otherwise.} \end{cases}$$

It can be seen that the rate of synthesis generally substantially exceeds the rate of degradation, although both rates are small, being of the order of MATLAB's machine precision [109]. The small magnitude of these rates makes their numerical analysis somewhat difficult. However, when the model was simulated with a constant insulin input of 100 nM for 240 minutes an increase of approximately 4.4% in total receptor numbers, mainly in the variables  $x_2$  and  $x_6$ , was observed. Indeed, an increase of 0.4% was found even when the model was simulated for 240 minutes with zero insulin input.

The Jacobian of the system in the basal condition was also found, and numerical calculation of the eigenvalues confirmed that the differential equations of the insulin receptor subsystem are stiff [50, 55].

### Parametric Sensitivity Analysis

A local PSA of the Sedaghat model was carried out by simulating the model over a 60 minute interval in MATLAB (R2014a Mathworks 2014). When GLUT4 is at the plasma membrane, glucose can flow down its concentration gradient into the cell. Thus the time integral of GLUT4 expressed at the plasma membrane (the glucose transport) was chosen as the metric for the PSA. The percentage change in the glucose transport ( $\Delta GT$ ) was calculated as model parameters were individually perturbed by  $\pm 5\%$  and  $\pm 10\%$ .

Of a wide variety of possible insulin input profiles, an initial fifteen minute insulin pulse over a total 60 minute simulation was chosen. This pulsatile delivery profile facilitated the study of both the transition from basal to maximal GLUT4 expression and also the relaxation back to the basal state. A logarithmic scale of insulin concentrations (0.1 nM, 1 nM, 10 nM and 100 nM) was used. This scale spanned both the physiological and experimental range of insulin levels [110, 111].

For each parameter in the model, a four-tuple representing  $\Delta GT$  at the various insulin concentrations was calculated. These four-tuples were then clustered in MATLAB using the Euclidean metric and classified as either sensitive (causing a substantial change in the glucose transport) or insensitive (causing little or no change in the glucose transport). The majority of parameters from the insulin receptor subsystem were insensitive across all four insulin levels; the parameters PTP and IRp were sensitive at all insulin levels; and the rate constants  $k_1$  and  $k_{-3}$  were sensitive at low insulin levels only. These sensitive parameters have been highlighted in yellow in Figure 5.1. For all sensitive parameters, a decline in sensitivity at higher concentrations of insulin was evident. For further details of the parametric sensitivity analysis, and for a full ranking of parameters by sensitivity, please consult [69] or [112].

### 5.2.2 Model Reduction

Following the local PSA of the Sedaghat model, a model reduction of the insulin receptor subsystem was carried out. The goals of the model reduction were threefold:

- to preserve the input-output relation of the insulin receptor subsystem from the original Sedaghat model;
- to conserve insulin receptor numbers; and

- to reduce the stiffness of the differential equations in the Sedaghat insulin receptor subsystem.

Model reduction necessarily entails the sacrifice of some degree of biological complexity, however, it is hoped that this loss of realism is compensated for by gains in computational and analytic tractability.

### 5.2.3 The Receptor State Space Model

Model reduction was carried out by the removal of insensitive states and parameters. Only two processes in the Sedaghat insulin receptor subsystem were sensitive for glucose transport: the forward reaction pathway from  $x_2$  through to  $x_4$  and  $x_5$  via  $x_3$ , which featured the sensitive rate constant  $k_1$ ; and the backward pathway from  $x_4$  and  $x_5$  to  $x_2$ , containing the multiplicative combination  $(\text{PTP})k_{-3}$ . Thus a simplified Receptor State Space model was proposed. The equations for this model are as follows:

$$\frac{dy_2}{dt} = r_{-1}y_3 - r_1y_1y_2, \quad (5.1)$$

$$\frac{dy_3}{dt} = r_1y_1y_2 - r_{-1}y_3, \quad (5.2)$$

where  $t$  is time;  $y_1$  is the extracellular insulin input;  $y_2$  is the concentration of unbound insulin receptors; and  $y_3$  is the concentration of both singly- and doubly-bound receptors. In other words,  $y_2$  corresponds to  $x_2$  and  $y_3$  corresponds to the sum of the variables  $x_4$  and  $x_5$  from the Sedaghat model. Thus  $y_3$ , modulated by the factor IRp, takes on the role of propagating the insulin signal to the downstream subsystem. The rate constant of the forward pathway is  $r_1$ , which most closely corresponds to  $k_1$  in the original model; and  $r_{-1}$  is the backward rate constant, broadly corresponding to  $(\text{PTP})k_{-3}$ . A schematic diagram of the model is shown in Figure 5.2.

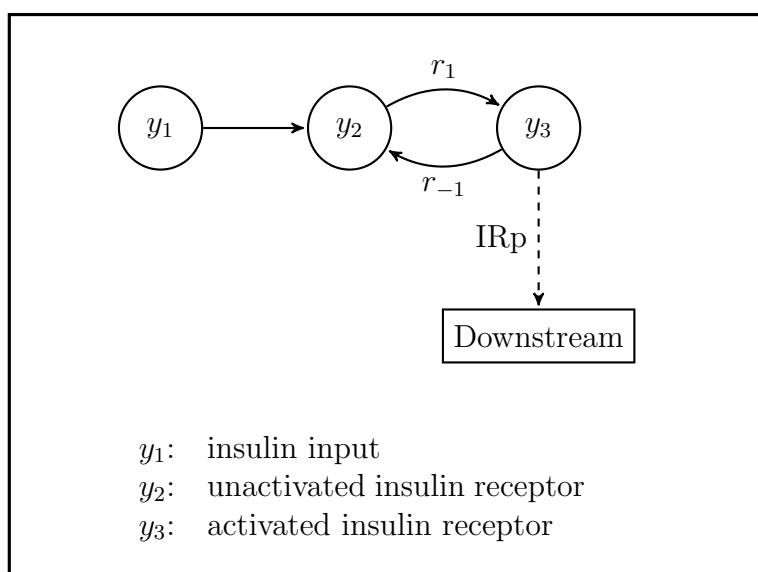


Figure 5.2: A schematic diagram of the Receptor State Space model. Nodes in the diagram represent state variables; edges represent chemical reactions.

## 5.3 Results

### 5.3.1 Rate Constants

Rate constants for the new model were determined by simulated annealing in MATLAB (R2014a Mathworks 2014), using the output ( $x_{21}$ ) of the Sedaghat model as a benchmark. The corresponding initial conditions and rate constants from the Sedaghat model ( $k_1$  and  $k_{-3}$ ) were used as a seed for the simulated annealing algorithm. The values obtained are given in Table 5.2, and were similar to those of the corresponding rate constants in the original Sedaghat model. Differential equations and initial conditions for the model are listed in Table 5.2, and the MATLAB code is given in Appendix A.1.

### 5.3.2 Fixed Points

The fixed points of the system were found analytically. As it was assumed that insulin receptor numbers are conserved,  $y_2 + y_3 = R$ , where the constant  $R$  represents the total number of receptors. Substituting this into Equation (5.2), and assuming a fixed value of  $y_1$ , the equation

$$\frac{dy_3}{dt} = r_1 y_1 R - (r_1 y_1 + r_{-1}) y_3 = f(y_3), \quad (5.3)$$

is obtained. From this equation it can be seen that there is a fixed point of the system at  $y_1 = 0$ ,  $y_3 = 0$ , representing the basal (unstimulated) state. Furthermore,  $y_3^*$ , the insulin stimulated steady state value of  $y_3$ , is given by

$$y_3^* = \frac{r_1 y_1 R}{r_1 y_1 + r_{-1}} = R - \frac{R r_{-1}}{r_1 y_1 + r_{-1}}.$$

The stability of this fixed point can be determined by linearising about  $y_3^*$ . Since  $y_1$ ,  $r_1$ , and  $r_{-1}$  are all positive,  $f'(y_3^*) = -(r_1 y_1 + r_{-1})$ , which is clearly

Table 5.2: State variables, differential equations, initial conditions and parameter values of the Receptor State Space model.

Variable	Chemical Species
$y_1$	Insulin input
$y_2$	Unbound surface insulin receptor
$y_3$	Bound surface insulin receptor
Differential Equation	Initial Condition
$\frac{dy_2}{dt} = r_{-1}y_3 - r_1y_1y_2$	$y_2(0) = 9 \times 10^{-13}$ M
$\frac{dy_3}{dt} = r_1y_1y_2 - r_{-1}y_3$	$y_3(0) = 0$ M
Parameter	Value
$y_1$	$1 \times 10^{-7}$ M if $t < 15$ , 0 otherwise
$r_1$	$6 \times 10^7$ M <sup>-1</sup> min <sup>-1</sup>
$r_{-1}$	0.202 min <sup>-1</sup>

negative. This implies that  $y_3^*$  is a stable fixed point, with characteristic time scale,  $\tau$ , given by

$$\tau = \frac{1}{|f'(y_3^*)|} = \frac{1}{r_1 y_1 + r_{-1}}.$$

Figure 5.3(a) shows time courses of insulin receptor activation for the Receptor State Space model. In all cases, a constant insulin input of  $y_1 = 10$  nM but with varying initial conditions was used. The existence of a single, stable fixed point is evident. In contrast, Figure 5.3(b) shows time courses of insulin receptor activation for varying insulin concentrations but with a constant zero initial condition for  $y_3$ , demonstrating that both  $y_3^*$  and  $\tau$  are functions of the insulin concentration.

### 5.3.3 The Analytic Solution

The simplified equations of the Receptor State Space model are amenable to analytic solution. Given a fixed value of  $y_1$ , if the derivative of  $y_3$  is non-zero, reciprocals of both sides of Equation 5.3 can be taken to obtain

$$\begin{aligned} \frac{dt}{dy_3} &= \frac{1}{r_1 y_1 R - (r_1 y_1 + r_{-1}) y_3} \\ &= \left( \frac{1}{r_1 y_1 + r_{-1}} \right) \left( \frac{1}{y_3^* - y_3} \right). \end{aligned}$$

Thus

$$y_3(t) = y_3^* - \alpha e^{-(r_1 y_1 + r_{-1})t},$$

where  $\alpha = y_3^* - y_3(0)$ .

Time courses of insulin receptor activation in response to a fifteen-minute insulin pulse for the Sedaghat and Receptor State Space models are shown in Figure 5.4(a). Insulin receptor activation ( $x_4 + x_5$  in Sedaghat;  $y_3$  in the Receptor State Space model) represents the output of the insulin receptor subsystem that is propagated downstream. As can be seen in the figure, there is a slight divergence between the two models during the ‘plateau’ phase

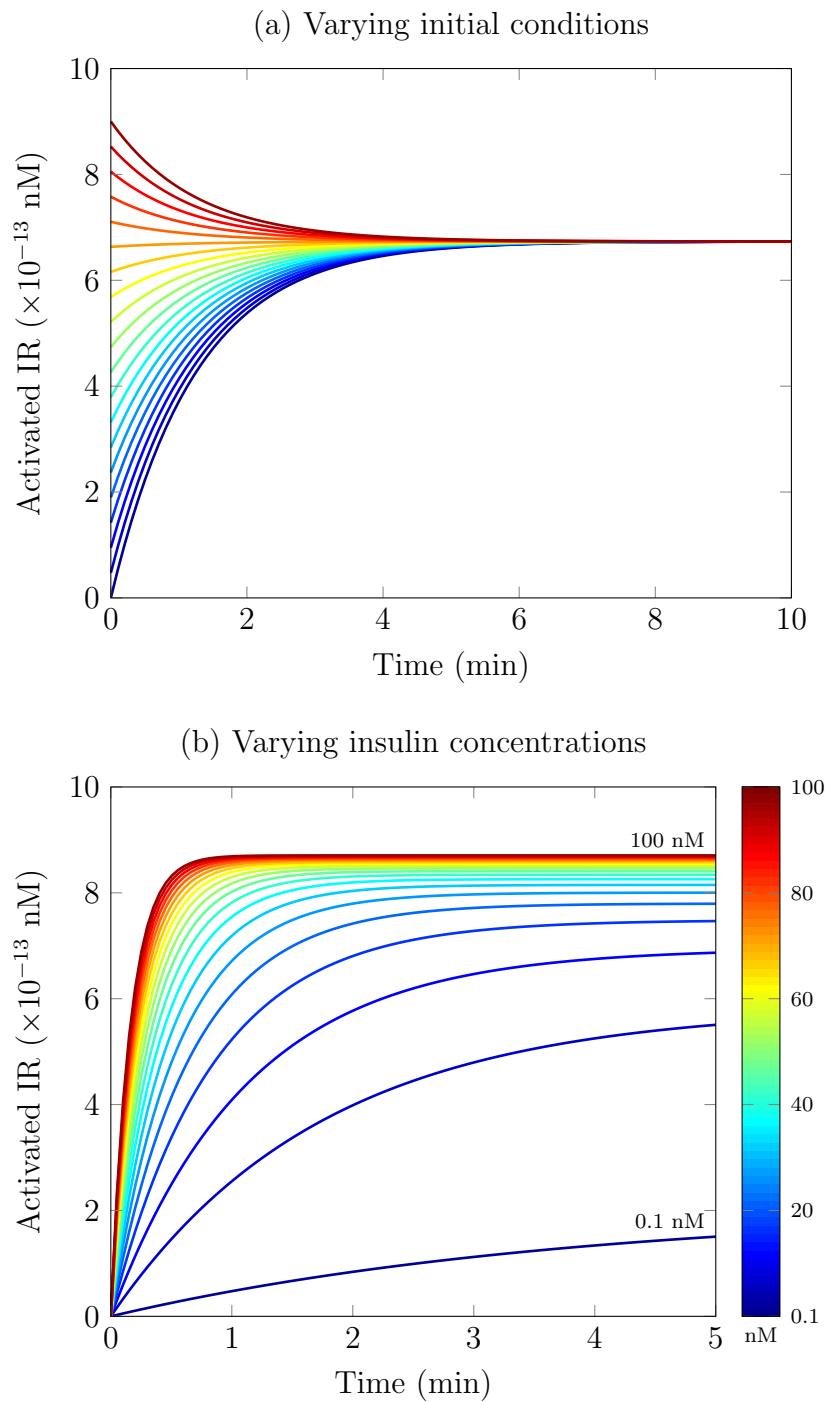


Figure 5.3: Time course of insulin receptor (IR) activation for the Receptor State Space model for (a) constant insulin (10 nM) and varying initial conditions; and (b) varying insulin concentrations. Parameter values used are listed in Table 5.2.

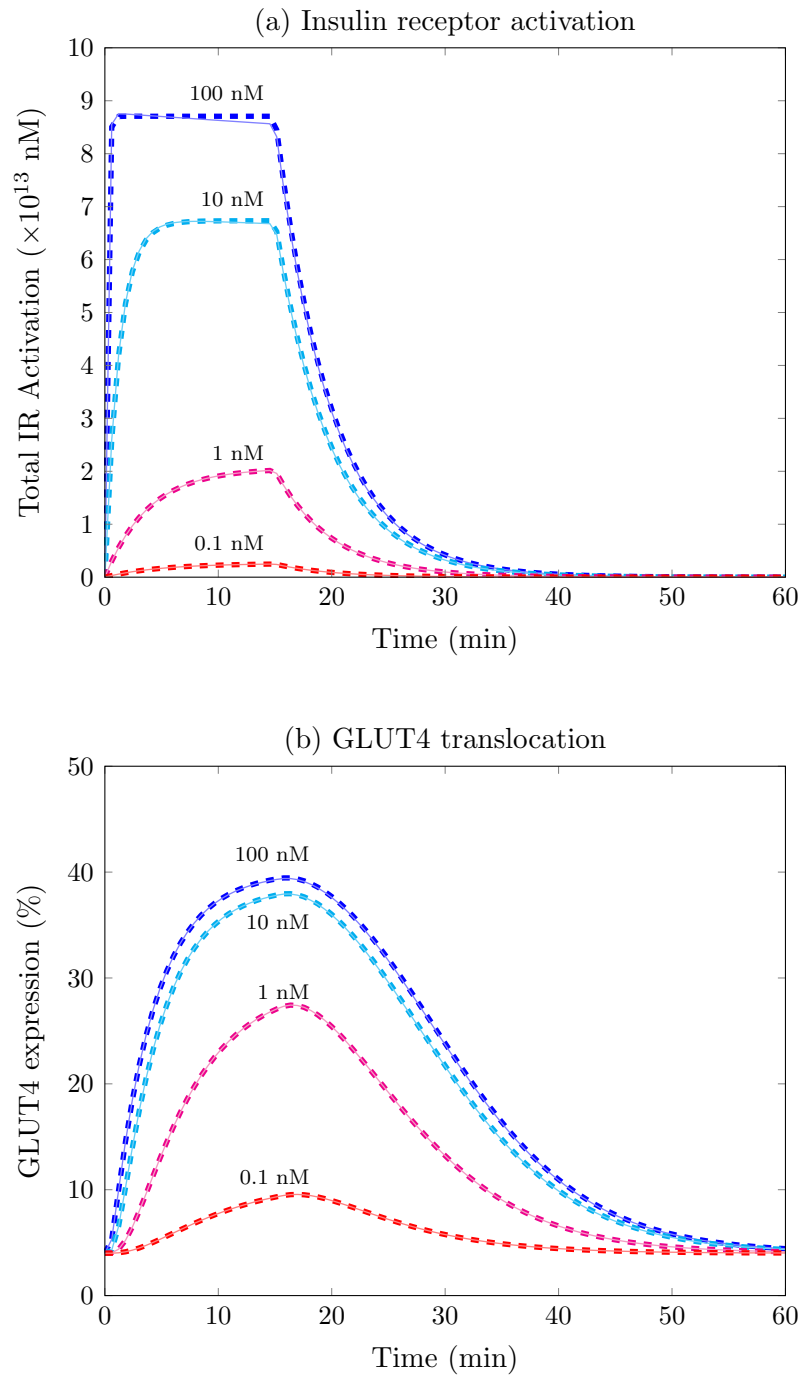


Figure 5.4: A comparison of (a) insulin receptor (IR) activation; and (b) GLUT4 translocation for the two models for varying insulin concentrations. Receptor State Space model outputs are indicated by dashed lines; Sedaghat model outputs by unbroken lines. The input was a fifteen-minute insulin pulse of 0.1 nM (red), 1 nM (magenta), 10 nM (cyan) or 100 nM (blue).

of activation at high insulin concentrations. At low insulin concentrations, neither of the models reaches the plateau and so the two outputs match closely. In contrast, Figure 5.4(b) shows a comparison of the final output—the GLUT4 expression at the plasma membrane—of the two models. In both cases, the downstream subsystem of the Sedaghat model has been coupled to the output of the respective insulin receptor subsystems. As can be seen in this figure, the output of the system utilising the Receptor State Space model is practically identical to that of the Sedaghat model at all insulin levels tested.

## 5.4 Discussion

Mathematical analysis of the Sedaghat model revealed a lack of conservation of insulin receptors and stiffness in the equations of the insulin receptor subsystem. In at least two subsequent papers that use the Sedaghat model [47, 51], the insulin receptor subsystem was modified by removing the insulin receptor degradation/synthesis terms to make a closed system. Thus, it is desirable to reduce the model in such a fashion that insulin receptor numbers are conserved and, if possible, improve the computational tractability of the model by developing a non-stiff system of equations.

The Receptor State Space model results from eliminating all but the two sensitive pathways of the Sedaghat insulin receptor subsystem. That is, in the Receptor State Space model, only the forward reaction pathway from  $x_2$  to  $x_5$  and the backward pathway from  $x_5$  to  $x_2$  are retained. Hence the Receptor State Space model features only three state variables, namely:  $y_1$ , the extracellular insulin input;  $y_2$ , the un-activated surface insulin receptors; and  $y_3$ , the activated surface insulin receptors. Thus, the processes of receptor internalisation, recycling, synthesis and degradation were omitted; and the secondary binding of insulin to the surface receptor has been lumped into the receptor activation step. Consequently, only the state variable  $y_3$ , modulated by the factor IRp, propagates the signal downstream.

In the Receptor State Space model the conservation of insulin receptor numbers is made explicit. As a result, for this subsystem at least, a fixed point at high insulin exists and an analytic solution can be found. (However, as the system reduction is limited to the top of the signalling cascade, this does not resolve the issue of non-conservation of GLUT4 in the downstream subsystem.)

It should also be noted that the total number of receptors differs by 10% between the two models, at least initially. In the Sedaghat model it is assumed that only 90% of the total receptor concentration is expressed at the plasma membrane, with the remainder present in the internalisation/recycling pathway. In contrast, the Receptor State Space model only includes surface receptors, hence the lower number of receptors. Furthermore, since the number of insulin receptors is not conserved in the Sedaghat model, the disparity between the two models increases the longer the simulation is run.

Parameter values for the Receptor State Space model were determined by simulated annealing, using the output of the Sedaghat model as a benchmark. The time constants of the dominant processes in the Sedaghat insulin receptor subsystem were preserved. The output of the two models—Sedaghat and the system utilising the Receptor State Space model—are closely matched over the entire range of insulin concentrations tested, as seen in Figure 5.4.

## 5.5 Summary

In this chapter, an alternative to the insulin receptor subsystem of the Sedaghat model has been described. This model retains the input-output relation of the original model, but is non-stiff. This reduces computational time and results in a system that is analytically tractable. Furthermore, the non-conservation of insulin receptors in the Sedaghat model has been eliminated. Consequently, the Receptor State Space model is a viable alternative to the insulin receptor subsystem of the Sedaghat model for situations where: the

internal dynamics of the insulin receptor subsystem can be safely ignored; the model is to be embedded as a component of a larger multi-scale system; simulations over long time periods are necessary; or many simulations are required.

However, the Receptor State Space model only addresses issues in the Sedaghat model arising from the upper portion of the signalling cascade. The limitations discussed in Section 3.2.2 that arise from the downstream subsystem remain. In particular, the process of Akt translocation and activation was only given a cursory treatment in the Sedaghat model. This lacuna will be addressed in the following chapters.

# Chapter 6

## The Akt Switch Model

### 6.1 Introduction

*This chapter is based on work presented in: CW Gray and ACF Coster. The Akt switch model: Is location sufficient? Journal of Theoretical Biology, 98:103–111, 2016.*

Akt functions as a pivotal nutrient sensor in the mammalian cell, coordinating proliferation and growth with metabolism. In insulin-sensitive cells, the primary metabolic role of Akt is the regulation of glucose uptake, which is achieved by the redistribution of GLUT4 from the cell interior to the plasma membrane [25, 28, 113]. Under basal conditions, the vast majority of GLUT4 is sequestered within the cell. However, in response to the insulin signal, GLUT4-laden vesicles travel to and fuse with the plasma membrane, providing a channel for glucose to selectively diffuse down its concentration gradient into the cell. In this signal transduction pathway, Akt acts as a vital, intermediate amplifier of the insulin signal [15, 28, 29].

However, insulin signalling as mediated by Akt poses somewhat of an enigma, as the time and dose-response characteristics of Akt and its substrates are not always well correlated [17, 29, 114]. Recent evidence suggests that Akt derives

signalling specificity from its cellular location—either at the plasma membrane or within the cytosol—and not merely its phosphorylation state. Gonzalez and McGraw have shown that the greater efficacy of Akt2 for GLUT4 translocation *vis-à-vis* Akt1 is largely due to the propensity of the former to accumulate at the plasma membrane [16]. Ng and colleagues have demonstrated that the time and dose characteristics of several metabolic effectors of Akt, such as AS160 and GLUT4, cluster more closely with those of the pAkt fraction at the plasma membrane, rather than total pAkt [17]. Furthermore, there is evidence suggesting that the initial rate of Akt phosphorylation (that is, immediately following insulin application), and not just the absolute level reached, is an important determinant of downstream signalling [10, 29].

As discussed in Chapter 3, numerous mathematical models of Akt activation can be found in the literature [10, 45, 52, 73–82, 84, 85, 115, 116]. With a few exceptions, none of these models address the spatial dependency of Akt activation or describe the Akt translocation process in any detail. In this chapter, a four-compartment ODE model that tracks both the location and biochemical state of Akt in 3T3-L1 adipocytes is presented. This simple, linear model is composed of four state variables and six rate constants. It has a readily derived analytic solution and is computationally tractable. Analysis of the behaviour of this dynamical system demonstrates that some of the apparent anomalies of Akt signalling can be explained by distinguishing between the two activation subprocesses—translocation and phosphorylation—particularly if these two processes occur on time scales that differ by several orders of magnitude.

## 6.2 Method

### 6.2.1 Experimental Data

Dose response and time course data were obtained from the raw data of Ng, *et al.* [17]. In these experiments, 3T3-L1 adipocytes were stimulated with a constant dose of insulin (1 or 100 nM) for a specified time (0 s, 15 s, 30 s, 60 s, 5 min, 30 min). Levels of Ser-473 phosphorylation were assessed by Western blot and normalized to the steady state (30 min) value obtained with 100 nM insulin. Three experimental replicates were carried out at an insulin concentration of 1 nM and four at a concentration of 100 nM.

The data is shown in Figure 6.1. As can be seen in this figure, there is an initial rapid rise in pAkt, followed by a distinct overshoot. After approximately one minute, levels of pAkt decrease more slowly to a steady state. This rapid rise and overshoot is a robust feature of Akt activation that is evident in numerous experiments [10, 17, 29, 78, 80, 83, 117]. A single exponential curve cannot capture this feature of the data: at least two processes, with time constants that differ by at least three orders of magnitude, are in operation. A double exponential, in contrast, describes the data well. The relative phosphorylated fraction of pAkt ( $y$ ) as a function of time ( $t$  min) was fitted to a double exponential of the form  $y = ae^{-bt} - ce^{-dt}$ . Table 6.1 shows the parameter values, 95% confidence intervals, and adjusted R-squared obtained for both the 100 nM insulin and 1 nM insulin data. Note that in both cases, the time constants obtained ( $b$  and  $d$ ) differ by several orders of magnitude. This demonstrates that at least two subprocesses operating on widely different timescales are required to explain the data.

The overshoot behaviour of Akt is thought to be intimately connected to its role as a crosstalk node between metabolic and mitogenic signalling pathways within the cell [17,29,84]. How a diverse range of signals is encoded by a comparatively small number of signalling pathways is an intriguing conundrum in

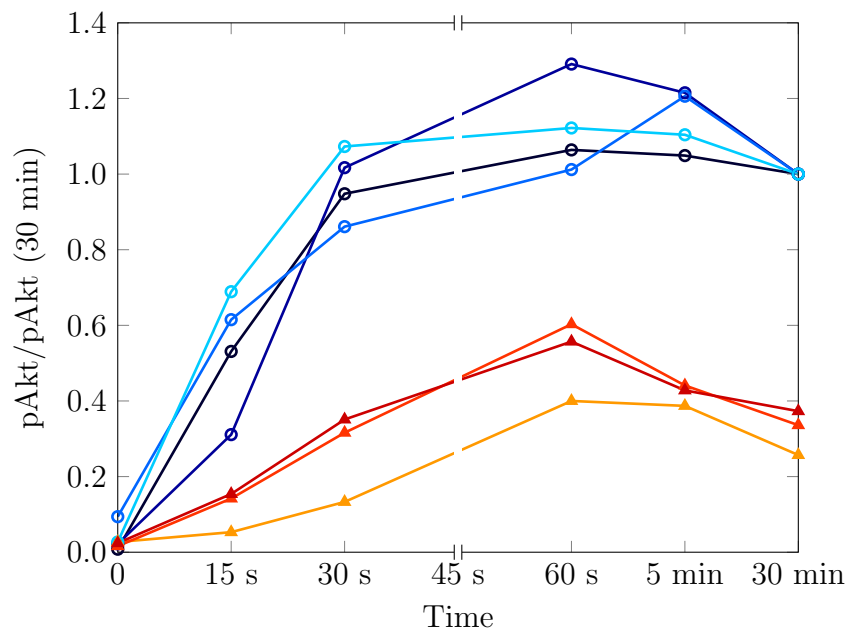


Figure 6.1: Relative phosphorylated Akt as function of time from Ng, *et al.* [17]. Blue-toned hues and open circles represent the four experimental runs conducted at an insulin concentration of 100 nM. Red-toned hues and filled triangles represent the three experimental runs conducted with a 1 nM insulin concentration. In all cases, the insulin concentration was held constant throughout the experimental run. Total pAkt has been normalized to the steady state (30 min) value of the 100 nM data.

Table 6.1: Parameter values obtained from fitting the relative phosphorylated fraction of pAkt ( $y$ ) as a function of time in minutes ( $t$ ) for the 100 nM insulin and 1 nM insulin data to a double exponential of the form  $y = ae^{-bt} - ce^{-dt}$ .

Insulin (nM)	Parameter	Value	Confidence Interval
100	$a$	1.203	(0.1091, 1.314)
	$b$	0.006276 min <sup>-1</sup>	(0.001116, 0.01144)
	$c$	1.183	(1.33, 1.036)
	$d$	2.77 min <sup>-1</sup>	(1.97, 3.57)
Adjusted R-squared:		0.9363	
1	$a$	0.511	(0.3673, 0.6547)
	$b$	0.01637 min <sup>-1</sup>	(-0.0007458, 0.03349)
	$c$	0.5239	(0.3528, 0.6949)
	$d$	1.837 min <sup>-1</sup>	(0.5466, 3.127)
Adjusted R-squared:		0.7455	

cell biology: one possibility is that different information is encoded by different temporal aspects of the signal. For instance, in the case of Akt, the downstream metabolic effectors must respond rapidly to the insulin signal to ensure the prompt clearance of glucose from the blood. In contrast, the mitogenic effects of Akt take place on a much slower time scale, and thus could be encoded by steady state values or even tied to the attainment of a threshold value of pAkt. The initial rapid phosphorylation could be a key signalling motif for some downstream components, whereas the steady state phosphorylation level could control the behaviour of other, slower acting components. Hence, it is essential that the model both replicate the overshoot observed in the experimental data and produce appropriate steady state values.

## 6.2.2 Model Development

The Akt Switch model is a deterministic compartmental model that tracks both the translocation and phosphorylation of Akt. A major aim of the modelling was to develop the simplest model that reproduces the important features of the experimental data. Although investigation of the metabolic function of Akt in insulin signalling was the primary motivation for developing the model, the resulting model can be readily extended to encompass the mitogenic effects as well.

Figure 6.2 is a diagram of the Akt Switch model. As there are at least two subprocesses involved in Akt activation (translocation and phosphorylation), all Akt in the cell is assumed to be present in one of two locations, in either the phosphorylated or the unphosphorylated state. Thus there are four compartments in the model: unphosphorylated Akt in the cytosol ( $A_c$ ); phosphorylated Akt in the cytosol ( $P_c$ ); unphosphorylated Akt at the plasma membrane ( $A_p$ ); and phosphorylated Akt at the plasma membrane ( $P_p$ ). These variables are normalized to the total Akt pool, which is assumed to be constant over the duration of the simulations in this study. Thus at all times,  $A_c + P_c + A_p + P_p = 1$ .

In the basal state, approximately 5% of Akt is located at the plasma membrane, with the remaining 95% in the cytosol; negligible amounts are phosphorylated in either location [17]. Thus the initial conditions of the model are  $A_c(0) = 0.95$ ,  $A_p(0) = 0.05$ , and  $P_c(0) = P_p(0) = 0$ . The effect of the initial condition as a parameter was also explored.

The four rate constants in the model represent the rate of translocation of Akt from cytosol to plasma membrane ( $k_{out}$ ); the rate of translocation of Akt from plasma membrane to cytosol ( $k_{in}$ ); the rate of phosphorylation of Akt at the plasma membrane ( $k_{on}$ ), and the rate of dephosphorylation of Akt ( $k_{off}$ ). Furthermore, it is assumed that the rate of translocation of Akt (both to and from the plasma membrane) is independent of its phosphorylation state, and that the dephosphorylation rate is independent of location.

It is thought that insulin up-regulates both the translocation of Akt from cytosol to plasma membrane and the phosphorylation of Akt at the plasma membrane. In the model, the parameter  $\psi$  represents the insulin-dependent spatial distribution of Akt between the cytosol and the plasma membrane. Thus  $\psi = \frac{k_{out}}{k_{in}}$  (or alternately,  $k_{out} = \psi k_{in}$ ). Similarly,  $\phi$  represents the equilibrium between Akt and pAkt in the cell, and so  $\phi = \frac{k_{on}}{k_{off}}$ . It is assumed that both  $\psi$  and  $\phi$  are functions of the insulin concentration. The differential equations of the model expressed in terms of  $\psi$ ,  $\phi$ ,  $k_{in}$  and  $k_{off}$  are presented in Table 6.2, along with the initial conditions. MATLAB code for simulating the model is given in Appendix A.2.

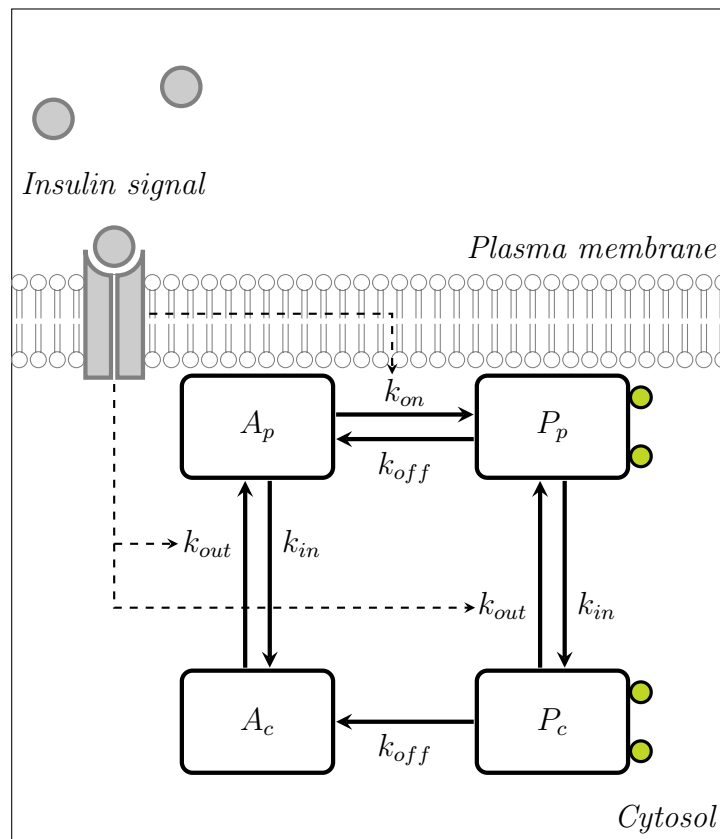


Figure 6.2: Diagram of the Akt Switch model. This four-compartment model tracks both the location—cytosol and plasma membrane—and biochemical state of cellular Akt. The effect of insulin on the system is shown by the dashed line.

Table 6.2: Variables, differential equations and initial conditions of the Akt Switch model.

<b>Variables</b>	
$A_c$	Unphosphorylated Akt in the cytosol
$P_c$	Phosphorylated Akt in the cytosol
$A_p$	Unphosphorylated Akt at the plasma membrane
$P_p$	Phosphorylated Akt in the cytosol
<b>Equations</b>	
$\frac{dA_c}{dt}$	$= k_{off}P_c - \psi k_{in}A_c + k_{in}A_p$
$\frac{dP_c}{dt}$	$= k_{in}P_p - (k_{off} + \psi k_{in})P_c$
$\frac{dA_p}{dt}$	$= k_{off}P_p + \psi k_{in}A_c - (\phi k_{off} + k_{in})A_p$
$\frac{dP_p}{dt}$	$= \phi k_{off}A_p + \psi k_{in}P_c - (k_{in} + k_{off})P_p$
$A_c + P_c + A_p + P_p = 1, P = P_c + P_p$	
<b>Initial Conditions</b>	
$A_c(0)$	$= 0.95$
$P_c(0)$	$= 0.00$
$A_p(0)$	$= 0.05$
$P_p(0)$	$= 0.00$

### 6.2.3 Parameter Optimisation

Parameters from the Akt Switch model were fitted to the experimental data using non-linear regression via the Levenberg-Marquardt method (fit algorithm) in MATLAB (R2015b Mathworks 2015). The tolerance for the minimum change in the finite difference gradient was  $1 \times 10^{-8}$  and the maximum was 0.1. The maximum number of iterations allowed for the fit was 400 and the maximum number of function evaluations was 600. The termination tolerance on the model value was  $1 \times 10^{-6}$ , as was the termination tolerance on the coefficient values. The confidence intervals for the parameters were calculated from the Jacobian. The confidence bounds for fitted coefficients were given by  $C = b \pm t\sqrt{S}$ , where  $b$  is the vector of coefficients produced by the fit;  $t$  depends on the confidence level, and is computed using the inverse of Student's  $t$  cumulative distribution function; and  $S$  is the covariance matrix of the coefficient estimates,  $(X^T X)^{-1}s^2$ , where  $X$  is the Jacobian of the fitted values with respect to the coefficients,  $X^T$  is the transpose of  $X$ , and  $s^2$  is the mean squared error. The parameters were constrained to be non-negative.

The fit was weighted to correct for the discrepancy in the number of experimental replicates between the two insulin concentrations (3 for 1 nM versus 4 for 100 nM) and additionally the non-uniform spread of time-points. Half the measurements were taken during the first minute of the experimental run, that is, during the 'up-stroke' of the overshoot. However, the model must replicate not only the overshoot, but also the relaxation back to steady state. Obtaining correct steady state values is particularly important as the experimental data is normalized to the steady state levels of the 100 nM insulin data. Consequently, time-points after 1 min were more heavily weighted than earlier times. Choice of seed-values for the parameter fitting was informed by the double exponential fit shown in Table 6.1.

## 6.3 Results

### 6.3.1 Analytic Solution

The system of differential equations in Table 6.2 can be written in matrix form for the vector of states  $\mathbf{x} = (A_c, P_c, A_p, P_p)^T$ . Then  $\mathbf{x}' = \mathbf{M}\mathbf{x}$  where

$$\mathbf{M} = \begin{pmatrix} -\psi k_{in} & k_{off} & k_{in} & 0 \\ 0 & k_{in} & 0 & -(k_{off} + \psi k_{in}) \\ \psi k_{in} & 0 & -(\phi k_{off} + k_{in}) & k_{off} \\ 0 & \psi k_{in} & \phi k_{off} & -(k_{in} + k_{off}) \end{pmatrix}.$$

The matrix  $\mathbf{M}$  has eigenvalues

$$\lambda_1 = 0, \quad \lambda_2 = -(1 + \psi)k_{in}, \quad \lambda_3 = -\frac{\gamma + \sqrt{\Delta}}{2}, \quad \lambda_4 = -\frac{\gamma - \sqrt{\Delta}}{2},$$

where

$$\gamma = (\psi + 1)k_{in} + (\phi + 2)k_{off},$$

and

$$\Delta = [(\psi + 1)k_{in} - \phi k_{off}]^2 + 4\phi k_{in}k_{off}.$$

The zero eigenvalue,  $\lambda_1$ , is due to the conserved quantity  $A_c + P_c + A_p + P_p = 1$ . This means that the system could be rewritten as a three-by-three dynamical system, and the corresponding zero eigenvalue eliminated. Clearly  $\lambda_2$  is real and negative, as all parameters in the model are non-negative. Similarly,  $\Delta$  is positive, and consequently  $\lambda_3$  and  $\lambda_4$  are real. Furthermore,

$$\begin{aligned} \gamma^2 - \Delta &= [(\psi + 1)k_{in} + (\phi + 2)k_{off}]^2 - [(\psi + 1)k_{in}\phi k_{off}]^2 - 4\phi k_{in}k_{off} \\ &= [2(\psi + 1)k_{in} + 2k_{off}][2(\phi + 1)k_{off}] - 4\phi k_{in}k_{off} \\ &= 4(\psi\phi + \psi + 1)k_{in}k_{off} + 4(\phi + 1)k_{off}^2 > 0, \end{aligned}$$

so  $\gamma$  has greater magnitude than  $\sqrt{\Delta}$ , and hence  $\lambda_3$  and  $\lambda_4$  are negative. Thus all non-zero eigenvalues are real and negative, which implies that the steady state of the system is asymptotically stable.

The steady state values of the system ( $A_c^*$ ,  $P_c^*$ ,  $A_p^*$ ,  $P_p^*$ ) are given by

$$\begin{aligned} A_c^* &= \frac{(\psi + 1)k_{in} + (\phi + 1)k_{off}}{(\psi + 1)[k_{in} + (\phi + 1)(k_{off} + \psi k_{in})]}, \\ P_c^* &= \frac{\psi\phi k_{in}}{(\psi + 1)[k_{in} + (\phi + 1)(k_{off} + \psi k_{in})]}, \\ A_p^* &= \frac{\psi[k_{off} + (\psi + 1)k_{in}]}{(\psi + 1)[k_{in} + (\phi + 1)(k_{off} + \psi k_{in})]}, \\ P_p^* &= \frac{\psi\phi(k_{off} + \psi k_{in})}{(\psi + 1)[k_{in} + (\phi + 1)(k_{off} + \psi k_{in})]}. \end{aligned}$$

Much of the experimental work in the literature reports the total phosphorylated fraction of Akt, irrespective of location. In the current model, this quantity corresponds to the sum of  $P_p$  and  $P_c$ , and has a steady state value,  $P^*$ , given by

$$P^* = \frac{\psi\phi[k_{off} + (\psi + 1)k_{in}]}{(\psi + 1)[k_{in} + (\phi + 1)(k_{off} + \psi k_{in})]}.$$

### 6.3.2 The Parameter Space

Figure 6.3 shows a series of time courses of total Akt activation (pAkt) for various values of  $\psi$ , with all other parameters fixed. It is apparent from this figure that the model exhibits two distinct types of behaviour. For low values of  $\psi$  there is a rapid rise in output during the first few minutes of simulation. This is followed by a slower decline to a steady state value which is reached within 15 minutes of simulation time. In contrast, at higher  $\psi$  values pAkt increases monotonically to the steady state value. These two modes of behaviour will subsequently be referred to as *overshoot* and *monotonic increase*, respectively.

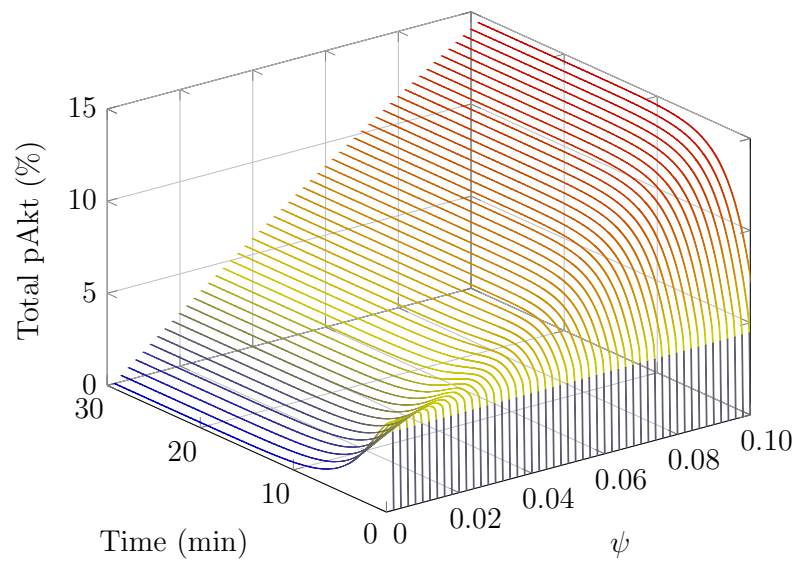


Figure 6.3: Time course of the Akt Switch model showing pAkt as a percentage of total Akt for various values of  $\psi$ . Other model parameters were held constant at typical values of  $A_p(0) = 0.05$ ,  $\phi = 32$ ,  $k_{in} = 0.43$ , and  $k_{off} = 0.62$ . Note the presence of the two behaviour regimes: overshoot at lower values of  $\psi$ ; monotonic increase at higher values.

Figure 6.4 shows a series of time courses of total Akt activation for varying values of  $\phi$ . In this figure,  $\phi$  was varied from one order of magnitude less to one order of magnitude more than  $\psi$ . In contrast to Figure 6.3, the overshoot behaviour is less pronounced, but still evident, particularly at higher  $\phi$  values. However, it should be noted that even when  $\phi$  is an order of magnitude greater than  $\psi$ , the amount of total pAkt in the steady state is still very low, at less than 1% of the total Akt pool. This indicates that  $\phi$  needs to be several orders of magnitude larger than  $\psi$  for the model to exhibit biologically realistic behaviour.

The influence of initial conditions on the transient behaviour of the model is demonstrated in Figure 6.5. In this figure, the initial fraction of Akt in the unphosphorylated state at the plasma membrane (that is,  $A_p(0)$ ) was varied from zero to ten percent. It can be seen that some Akt must initially be present at the plasma membrane for the model to exhibit overshoot behaviour.

The influence of  $A_p(0)$  on the behaviour of the model is further illustrated by Figure 6.6. The model was simulated for values of  $\psi$  and  $\phi$  over a logarithmic range. The behaviour of the model was classified as overshoot if the difference between final and maximal values of pAkt was greater than  $10^{-5}$  and as monotonic increase otherwise. The contour lines on this plot show the demarcation line between the overshoot and monotonic increase regimes as a function of  $A_p(0)$ .

### 6.3.3 Optimised Parameter Values

The model parameters were fitted to the time course data via non-linear least squares optimisation. A steady state (30 min) phosphorylation of 5% of the total Akt pool was set as the end-point for the 100 nM insulin data [29], and all data sets were re-normalized to this level. In the model, the translocation rate is  $k_{out} = \psi k_{in}$ . Similarly, the phosphorylation rate is  $k_{off} = \phi k_{on}$ . That

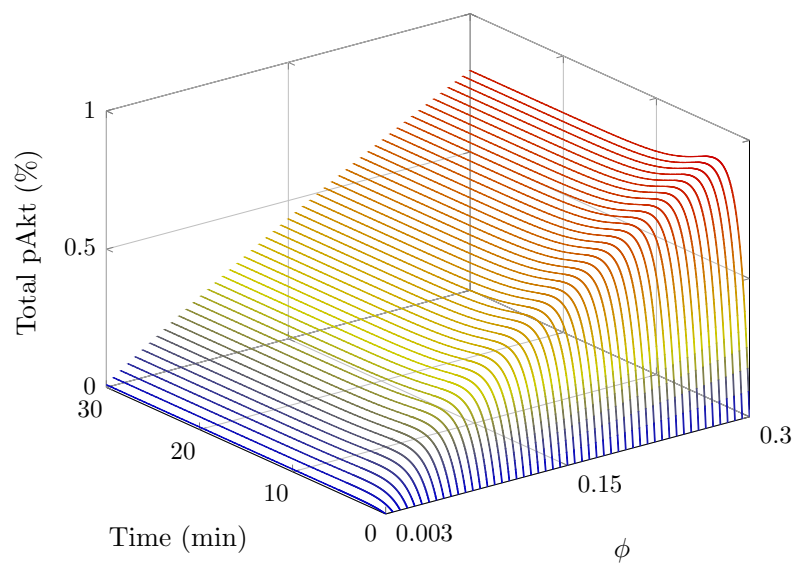


Figure 6.4: Time course of the Akt Switch model showing the pAkt as a percentage of total Akt for various values of  $\phi$ . Other model parameters were held constant at typical values of  $A_p(0) = 0.05$ ,  $\psi = 0.032$ ,  $k_{in} = 0.43$ ,  $k_{off} = 0.62$ .

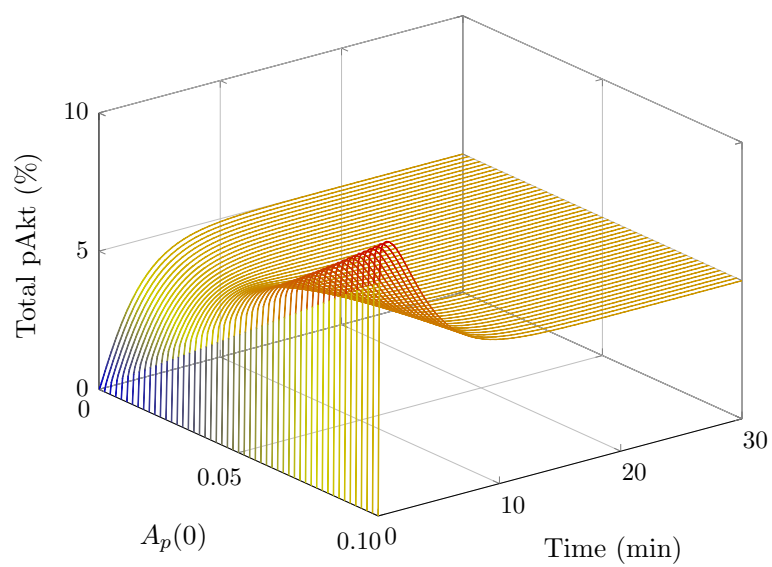


Figure 6.5: Time course of the Akt Switch model showing the pAkt as a percentage of total Akt for various values of  $A_p(0)$ . Other model parameters were held constant at typical values of  $\psi = 0.032$ ,  $\phi = 32$ ,  $k_{in} = 0.43$ ,  $k_{off} = 0.62$ .

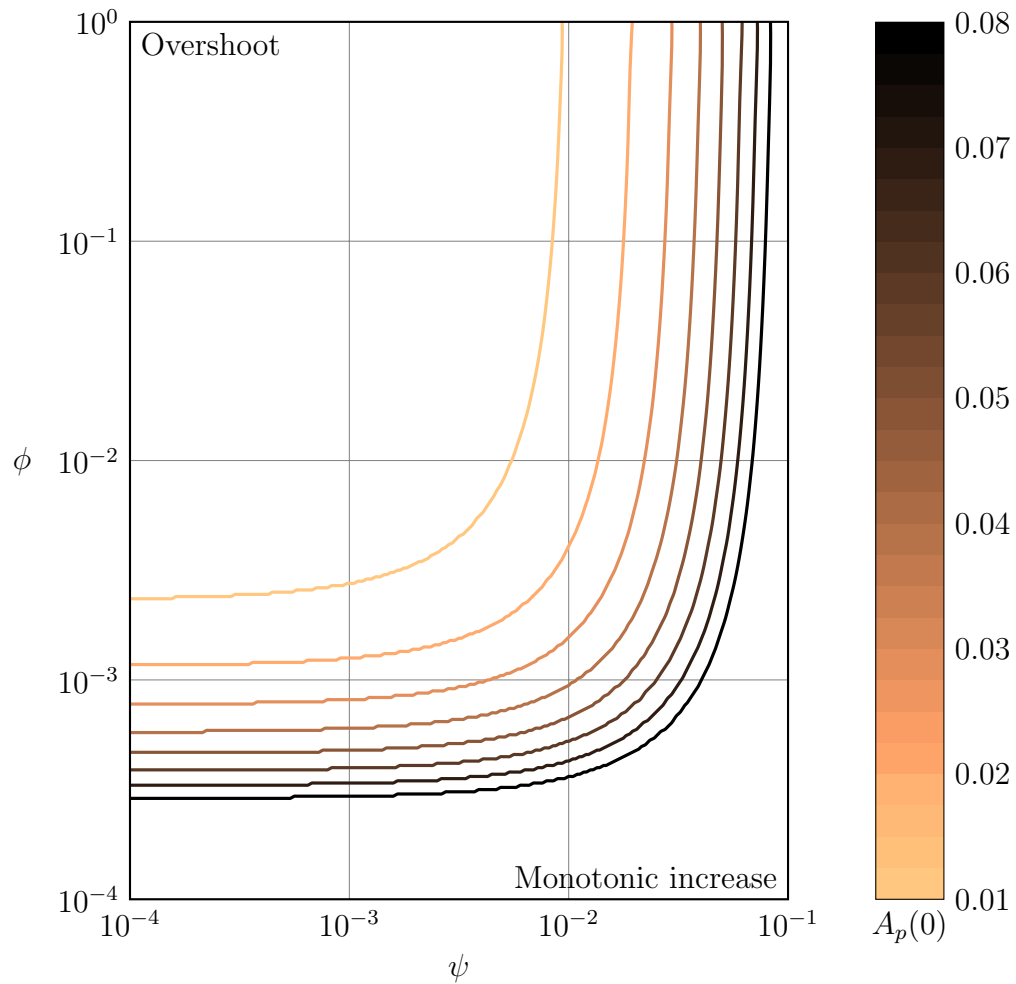


Figure 6.6: Phase transition diagram of the Akt Switch model for various values of  $\psi$  and  $\phi$ . The parameters  $k_{in}$  and  $k_{off}$  were held constant at typical values of 0.43 and 0.62, respectively. The thick lines show the change of regime (from monotonic increase to overshoot) for a given initial condition.

is, it is assumed that  $k_{in}$  and  $k_{off}$  are insulin independent but that  $\psi$  and  $\phi$  are insulin dependent. Thus, when simultaneously optimising the data from both the 1 nM and 100 nM experiments,  $k_{in}$  and  $k_{off}$  are common, but two values for each of  $\psi$  and  $\phi$  ( $\psi_1$  and  $\psi_{100}$ ;  $\phi_1$  and  $\phi_{100}$ ) were employed.

Given the amount of data, unconstrained fits of  $\phi_{100}$  and  $\phi_1$  unsurprisingly produced ill-conditioned Jacobians that resulted in very large confidence intervals. As a double exponential fitted directly to the raw data rather than the model output (see Section 6.2.1) had showed that the two major time constants in the system differ by at least three orders of magnitude,  $\phi_{100}$  was constrained to be one thousand times  $\psi_{100}$  and the fit was repeated. This allowed much narrower 95% confidence intervals to be obtained for the other parameters, which were allowed to vary freely. Values obtained for  $k_{in}$ ,  $k_{off}$ ,  $\psi_{100}$ ,  $\psi_1$  and  $\phi_1$  are shown in Table 6.3.

The output of the model for a 100 nM insulin input (Fig 6.7(a)); and a 1 nM insulin input (Fig 6.7(b)) is shown in comparison with the experimental data in Figure 6.7. The insets in these two plots show the first two minutes of simulation in greater detail.

### 6.3.4 Analysis of Model Behaviour

An analysis of the model optimised to the experimental data (the optimised model) was carried out by simulating the model with the parameter values listed in Table 6.3. Maximum values of  $P_p$  and  $P_c$  and the time taken to reach the maximum ( $t_{max}$ ) at both insulin concentrations were found. The overshoot, defined as the difference between the maximum value and the final value at 30 minutes as a percentage of the final value, was also calculated. In addition, initial activation rates of  $P_p$  and  $P_c$  were found by fitting the model output from  $t = 0$  to  $t = t_{max}$  to a single exponential curve,  $y = 1 - e^{-kt}$ . The values of these metrics are shown in Figure 6.8.

Table 6.3: Optimised parameter values of the Akt Switch model with 95% confidence intervals. The adjusted R-squared for this fit was 0.9732.

<b>Parameter</b>	<b>Value</b>	<b>Confidence Interval</b>
$k_{in}$	0.55 min <sup>-1</sup>	(0.19, 0.91)
$k_{off}$	0.35 min <sup>-1</sup>	(0.010, 0.60)
$\psi_1$	0.014	(0.0041, 0.023)
$\psi_{100}$	0.023	(0.011, 0.034)
$\phi_1$	2.2	(0.46, 4.0)

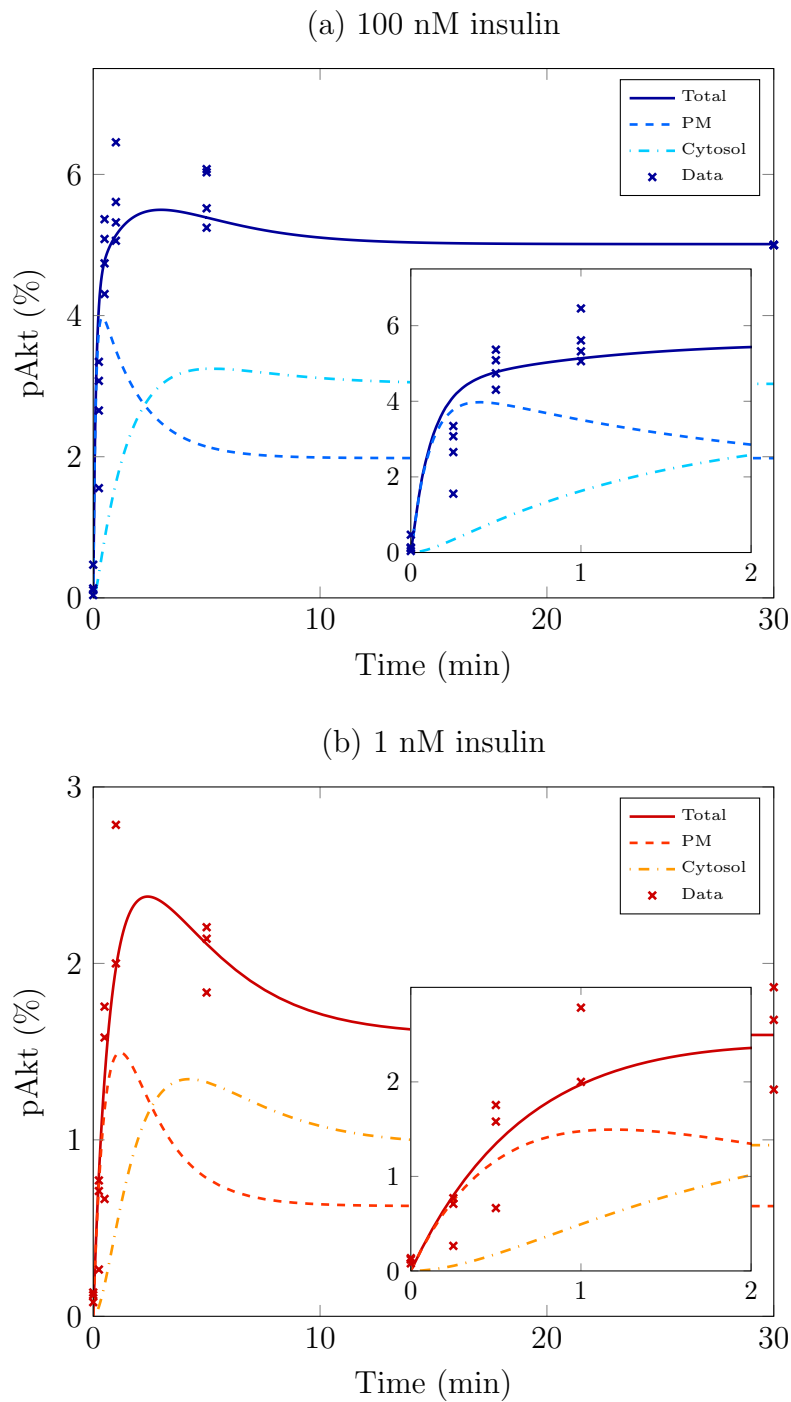


Figure 6.7: Output of the optimised Akt Switch model showing pAkt at the plasma membrane (PM), in the cytosol, and total pAkt as a percentage of total Akt in comparison with the experimental data for (a) 100 nM insulin and (b) 1 nM insulin. The insets show the first two minutes in detail.

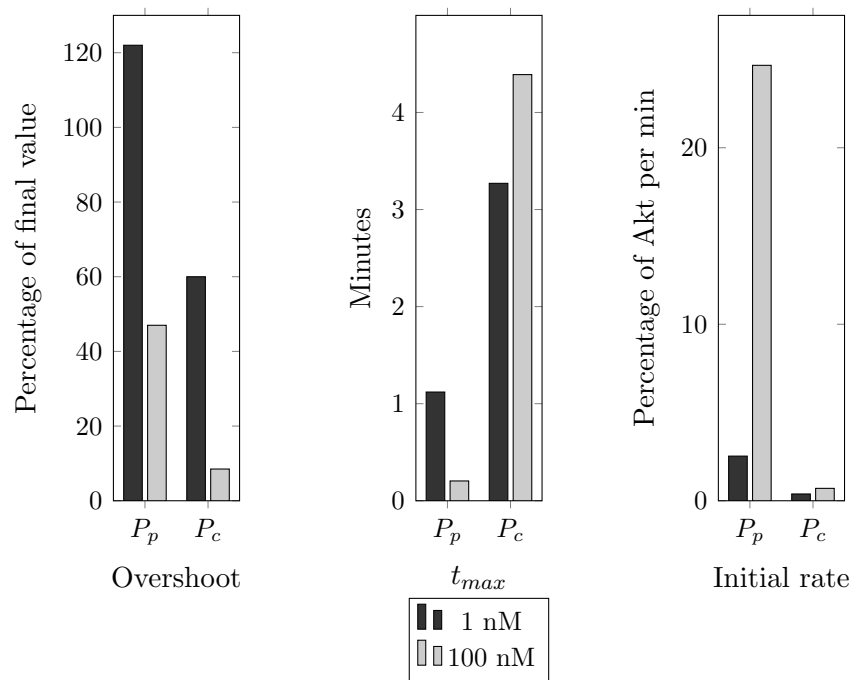


Figure 6.8: The behaviour of the optimised Akt Switch model, showing the overshoot as a percentage of the corresponding final value; the time taken to reach the maximum value ( $t_{max}$ ); and the initial rate of activation for both the plasma membrane ( $P_p$ ) and cytosolic fractions ( $P_c$ ) of Akt for insulin concentrations of 1 and 100 nM.

## 6.4 Discussion

The Akt switch model is able to reproduce the experimental data, both qualitatively and quantitatively. When simulated with the parameter set for 100 nM insulin given in Table 6.3, the Akt Switch model reaches a steady state within 15–20 minutes that has 5% of the total Akt pool phosphorylated (Figure 6.7(a)). This level of Akt phosphorylation is known to be sufficient for maximal GLUT4 translocation [17, 29, 114]. Furthermore, both the physiological (1 nM) and high (100 nM) insulin parameter sets found in the current work preserve the initial overshoot of Akt phosphorylation, as is seen in the literature [10, 17, 29, 80, 117]. Thus both the transient and the steady state behaviour of the model are consistent with the experimental evidence.

Parameter values obtained for the model are in broad agreement with those found in the literature. Park and colleagues give a deactivation rate of Akt (albeit in a different cell type) of  $0.56 \text{ min}^{-1}$  and Gao, *et al.*, found that Akt1 was dephosphorylated at Ser473 by PHLPP with a half time of  $0.53 \pm 0.08 \text{ min}$  [80, 118], corresponding to a deactivation rate of approximately  $1.9 \text{ min}^{-1}$ . The  $k_{off}$  value found in the current work ( $0.35 \text{ min}^{-1}$ ) is of the same order of magnitude at the value found by Gao.

In contrast, little is known about the insulin-stimulated translocation of Akt from the cytosol to the plasma membrane, and almost nothing of a quantitative nature [20, 21]. It is well known that PI3K inhibitors, such as Wortmannin, inhibit Akt activation by preventing the formation of  $\text{PIP}_3$  at the plasma membrane. It has also been shown that Akt translocation (and hence activation) can be inhibited in a PI3K-independent manner by ceramide [119, 120]. This indicates that the insulin signal diverges into two separate paths—one controlling translocation and the other phosphorylation—at some point above PI3K in the signalling network. In the Akt Switch model, these two points of regulation are embodied by the parameters  $\psi$  and  $\phi$ .

The parameter  $\psi$  represents the equilibrium distribution of Akt between the cytosolic and plasma membrane pools. Carvalho and colleagues have found

that the translocation of Akt to the plasma membrane approximately doubled when human fat cells taken from non-diabetic subjects were stimulated with insulin [121]. This is in agreement with values of 0.014 and 0.023 obtained for  $\psi_1$  and  $\psi_{100}$ , respectively, in the current work. It should be noted that the Carvalho study used a different cell type (primary human adipocytes) and measured the steady state difference between basal insulin and 6.9 nM insulin, rather than the 1 and 100 nM data used for data fitting in the current work. However, it has been found that the ED50 (the dose required to obtain 50% of the maximal effect) of insulin for GLUT4 translocation is approximately 1 nM [17], so 6.9 nM is likely near maximal stimulation.

Given that Akt translocation is insulin-regulated, one possible mechanism is that of active transport by molecular motors. In this scenario, the Akt is packed into transport vesicles, with the strength of the insulin signal determining either the number or the Akt-loading of the vesicles. Average velocities for vesicles transported by molecular motors range from 0.8 to 1  $\mu\text{ms}^{-1}$  in the literature [122, 123]. The cell radius of a typical mouse adipocyte is approximately 25  $\mu\text{m}$  (calculated from an average cross-sectional area of about 2150  $\mu\text{m}^2$  reported in [124]). Assuming that the Akt travels a distance equal to the radius, this results in a transit time of 25–33 s. Given the (implausible) assumption that all unphosphorylated Akt in the cytosol is available for transport, this yields an insulin-stimulated translocation rate constant of about two, which is two orders of magnitude greater than the  $\psi_{100}$  value found in the parameter fitting. This indicates that if an active transport process is involved, only a small percentage of the cytosolic Akt pool is available for transport.

An alternative transportation mechanism is a ‘retention-and-release’ model that relies on diffusion to move the Akt to the plasma membrane. In this model, the unactivated Akt is initially bound to structures on, or near, the endoplasmic reticulum. Some fraction of the bound Akt is released in an insulin-sensitive manner, and then diffuses to the plasma membrane. Bates reports a diffusivity for Akt of 25  $\mu\text{m}^2 \text{min}^{-1}$ , based on the assumption

that 5% of the Akt pool diffuses [52]. This yields an insulin-stimulated translocation rate of the same order of magnitude as those found in the current work. It is interesting to note that both these translocation models (active transport and retention and release) can only be reconciled with the rate constants found if a large portion of the cytosolic Akt pool is not available for transport at any given time. This is a reasonable assumption: unactivated cytosolic Akt ( $A_c$  in the model) is a diverse pool, including both freshly synthesized and recycled Akt. It would appear that even newly synthesized Akt must form a complex with PDK1 in the cytosol prior to translocation and phosphorylation [30]. Furthermore, once Akt is activated at the plasma membrane, it travels to a variety of cellular locations, including the plasma membrane, the cytosol, and the nucleus [19]. Once activated, the Akt must be recycled before it can participate afresh in the insulin signalling process. At a minimum, the recycling of Akt involves steps such as: dephosphorylation; return to the cytosol; some form of sorting or sub-localisation within the cytosol; and complexing with PDK1. Thus it is plausible that a large fraction of the  $A_c$  pool is present in the recycling pathway. This may also explain the extremely low threshold of Akt activation observed in GLUT4 translocation: at any given time, only a small fraction of the total Akt pool is available to respond to the insulin signal. Clearly, this is an area requiring further investigation.

Rather more is known about the process of phosphorylation at the plasma membrane [19, 35, 37]. Studies in the literature typically report pAkt levels, either in the whole cell or (rarely) at the plasma membrane. In either case, this measure is the culmination of both the translocation and the phosphorylation processes. Little could be found in the literature specifically concerning the rate of phosphorylation. However, overshoot in Akt levels is a commonly observed phenomenon at both high and physiological levels of insulin, and this type of behaviour cannot be produced by a single dominating time constant—it requires at least two time constants, differing by several orders of magnitude. Furthermore, since translocation is synonymous with the physical movement of signalling components, whereas phosphory-

lation involves a chemical change *in situ*, it is reasonable to assume that phosphorylation is the faster process.

A number of alternative parameter fitting scenarios were attempted to determine if the parameters given in Table 6.3 represent a truly minimal set. As can be seen in this table, the 95% confidence interval of  $\psi_1$  and  $\psi_{100}$  overlap to a large extent, which could suggest that the same  $\psi$  value can be used for both the 100 nM and 1 nM insulin simulations. However, when the data was fitted with a single  $\psi$  value, overshoot behaviour at the physiological insulin level disappeared and a biologically unrealistic value for  $\phi_{100}$  ( $10^8$ ) was obtained. Similarly, forcing the same  $\phi$  value for both insulin treatments resulted in the loss of overshoot behaviour at 100 nM insulin. A third scenario, where the ratios of  $\psi_{100} : \phi_{100}$  and  $\psi_1 : \phi_1$  were constant was also attempted, but this too resulted in the loss of overshoot behaviour at the higher insulin level. The failure of these alternative parameter fitting scenarios indicates that insulin control of both  $\psi$  and  $\phi$  is necessary to obtain a good fit to the experimental data. Although there were slight discrepancies at very early times (see inset, Figure 6.7), this was due to delays between the application of insulin and the response in Akt phosphorylation, delays which are not explicitly embodied in the model. (The role of time delays in Akt translocation is a topic that will be explored in greater depth in Chapter 8.) This also accords with what has been reported in the literature concerning Akt activation: namely, that translocation and phosphorylation are controlled by distinct mechanisms that diverge considerably upstream from Akt.

As can be seen in Figures 6.5 and 6.6, the initial amount of unphosphorylated Akt at the plasma membrane,  $A_p(0)$ , is also an important determinant of model behaviour. In the absence of Akt at the plasma membrane, Akt translocation becomes rate-limiting for phosphorylation and consequently the model exhibits monotonic increase, even when the rate of phosphorylation is high. As explained previously, the parameter  $\psi$  represents the equilibrium distribution of Akt between the cytosol and plasma membrane for a given level of insulin stimulation. In the basal state, the rate of phosphorylation is

negligible, which gives a steady state value for unphosphorylated Akt at the plasma membrane ( $A_p^*$ ) of  $\frac{\psi_0}{1 + \psi_0}$ . The parameter fitting yielded a  $\psi_1$  value of 0.014;  $\psi_0$  will be lower still, resulting in a low value of  $A_p^*$ . It can be seen from the phase transition diagram in Figure 6.6 that this value is too low to produce an overshoot in pAkt upon stimulation.

*In vivo*, insulin is secreted in a pulsatile fashion, which is thought to be necessary for normal glucose homeostasis [125]. It has been shown that glucose clearance from the blood is enhanced by pulsatile insulin delivery [126], and dysregulation of pulsatile secretion, particularly of the high frequency modes, is known to be an early symptom of pre-diabetes [127]. It is possible that the regular secretion of small pulses of insulin serves to ‘prime’ the insulin signalling pathway so that it can respond rapidly and effectively. One way that this might happen is by maintaining a larger pool of Akt at the plasma membrane than would otherwise occur in the basal state. Clearly the interplay between steady state values, initial conditions, and periodic inputs in the model is an area requiring further investigation.

The Akt Switch model also shows that it is possible to control downstream signalling with different temporal profiles. There are differences in the initial rate, overshoot and maximal time profiles of Akt activation under various levels of insulin stimulation. These differences are further amplified by location. This is because the two pools of activated Akt ( $P_c$  and  $P_p$ ) display distinct responses to the same insulin input. When simulated with the parameter values listed in Table 6.3, the plasma membrane fraction had a much larger overshoot than the cytosolic fraction, and reached a maximum much quicker (see Figures 6.7 and 6.8). In addition, observed initial activation rates of the plasma membrane fraction are much more sensitive to the insulin concentration than those of the cytosolic fraction: whereas the initial activation rate of  $P_c$  increased two-fold between 1 and 100 nM insulin, the initial activation rate of  $P_p$  increased by one order of magnitude. This is of particular interest, as there is evidence to suggest that activation of Akt substrates is more closely correlated with the initial rate of Akt phosphorylation

than the maximum level reached [29]. The existence of two pAkt pools in the model provides a mechanism for the differential regulation of downstream substrates, and suggests ways in which the model can be fruitfully extended in the future.

The model is capable of further refinement should appropriate experimental data become available. For instance, more data from time points after the overshoot in Akt activation is observed—say between 5 and 15 minutes—would further elucidate the relaxation of the system back to steady state. In addition, it has been posited that the translocation and phosphorylation of Akt are insulin regulated, and the parameter values obtained in the current work provide point estimates of this relationship. Data from a greater number of insulin concentrations would permit the interpolation of the behaviour of the system under a wider range of stimuli: the physiological range (0.1–1.5 nM insulin) is of particular interest. Such data would also allow the relaxation of some of the parameter constraints in the model. The ultimate (if improbable) data would be time series that track all four Akt pools. Nonetheless, the proposed model is able to replicate all the major features of the data that is currently available.

## 6.5 Summary

The Akt Switch model is a simple, linear, four-compartment ODE model of Akt activation. It embodies the main features of this important cross-talk node and is consistent with the existing experimental data. The model provides a means for the differential regulation of downstream components without requiring complex feedback mechanisms. Experimental data sufficient to support a more complicated model of Akt activation does not exist at the current time. However, should such data come to light, the model presented here is amenable to extension and adaptation.

The Akt Switch model elucidates how differential downstream regulation can be effected via a node that appears to act as a low-threshold switch. The key is location: simply allowing for two cellular locations opens up the possibility of dissimilar temporal activation profiles in initial rate, time to maximum activation, and steady state values.

# Chapter 7

## The Akt Translocation Model

### 7.1 Introduction

*This chapter is based on work that has been presented in: CW Gray and ACF Coster. Crosstalk in transition: The translocation of Akt. Journal of Mathematical Biology, 78(4):919–942, 2019*

In this chapter, a three-compartment model of Akt translocation is presented. The four-compartment Akt Switch model presented in Chapter 6 employed two spatial Akt pools: one in the cytosol and one at the plasma membrane. It was able to reproduce important features of the experimental data, including a substantial initial overshoot in pAkt. In the Akt Switch model, overshoot arose from the interaction between phosphorylation, which is fast, and translocation, which is slow. These two processes were assigned single, dominant time constants that differed by three orders of magnitude. However, subsequent experimental work has shown that overshoot is evident within the translocation process itself, independent of phosphorylation state [128]. Consequently, the Akt Translocation model was developed to investigate the translocation of Akt in greater detail. In this chapter, the model is defined and some preliminary mathematical analysis is carried out. In Chapter 8, the model is optimised to experimental data, yielding further insights into the underlying biology.

## 7.2 Method

### 7.2.1 Model Development

A good mathematical model of Akt translocation should reproduce salient features of both the transient and steady state behaviour seen in the experimental data. More specifically, the transient behaviour should manifest an overshoot in Akt localised to the plasma membrane (Akt-PM); and realistic steady state values should be produced in both the basal and insulin stimulated states. It is known that Akt functions as an ultra-sensitive switch in the insulin signalling cascade [15, 28], operating within only 5–22% of its dynamic range [29]. Overshoot—an initial rapid rise in Akt-PM upon stimulation followed by a slower decrease to a steady state value—is also a robust and widely observed feature of Akt activation. In the literature, overshoot in Akt activation is reported in response to many types of stimulation, including insulin [10, 17, 29, 78, 80, 83, 117]. Moreover, overshoot, or at least a high initial rate of Akt activation, is thought to be a crucial trigger of downstream processes in the insulin signalling pathway [29].

Mathematically, a minimum of three compartments is required to produce overshoot behaviour: a two-compartment model can only exhibit an exponential rise or decay determined by the balance of on- and off-rates. Clearly, the Akt translocation process involves at least one ‘internal’ or cytosolic pool and one ‘external’ or plasma membrane-docked pool where activation takes place. The Akt Translocation model has a third, intermediate or ‘primed’ pool, containing Akt which is primed for docking, but has not yet received the signal to do so. This compartment could represent Akt that is physically located in close proximity to the plasma membrane, or alternately, in an intermediate, but necessary, biochemical state prior to translocation to the inner leaflet of the plasma membrane. The addition of a third pool can also be justified based on the current understanding of the biology, as it is thought that Akt forms a complex with PDK1 in the cytosol prior to recruitment to the plasma membrane [15, 30].

Figure 7.1 shows a diagram of the Akt Translocation model. The three compartments consist of a cytosolic pool of Akt ( $x_1$ ); a primed pool representing Akt primed for docking at the plasma membrane ( $x_2$ ); and a membrane-bound pool located on the inner leaflet of the plasma membrane ( $x_3$ ). As this model focuses on the translocation process only, the Akt is not distinguished by phosphorylation state in any of the compartments. Thus each compartment could contain Akt in either the activated or the unactivated state. Furthermore, it has been assumed that the total amount of Akt is constant (at least on the time-scale of translocation events) and has been normalized to one.

The transition between any two compartments is approximated by a single reaction that represents the combined effect of the forward and back reactions, as explained in Section 4.2. This results in three major rate constants:  $k_1$ , the rate of transition into the primed pool (the priming rate);  $k_2$ , the rate of docking at the plasma membrane (the docking rate); and  $k_3$ , the rate of recycling from plasma membrane to cytosol (the recycling rate). Since each compartment potentially contains both phosphorylated and unphosphorylated Akt, these rate constants represent a weighted average rate of both subtypes of Akt. Whilst other effects are possible, in this chapter it is assumed that the insulin signal changes the docking rate only. This transition is represented by changes to the parameter  $\alpha$ . Initially, the system is assumed to be a steady state corresponding to  $\alpha = \alpha_1$ . At time  $t = 0$ , the value of  $\alpha$  undergoes a step change to  $\alpha_2$ . The equations, variables and parameters for the model are presented in Table 7.1.

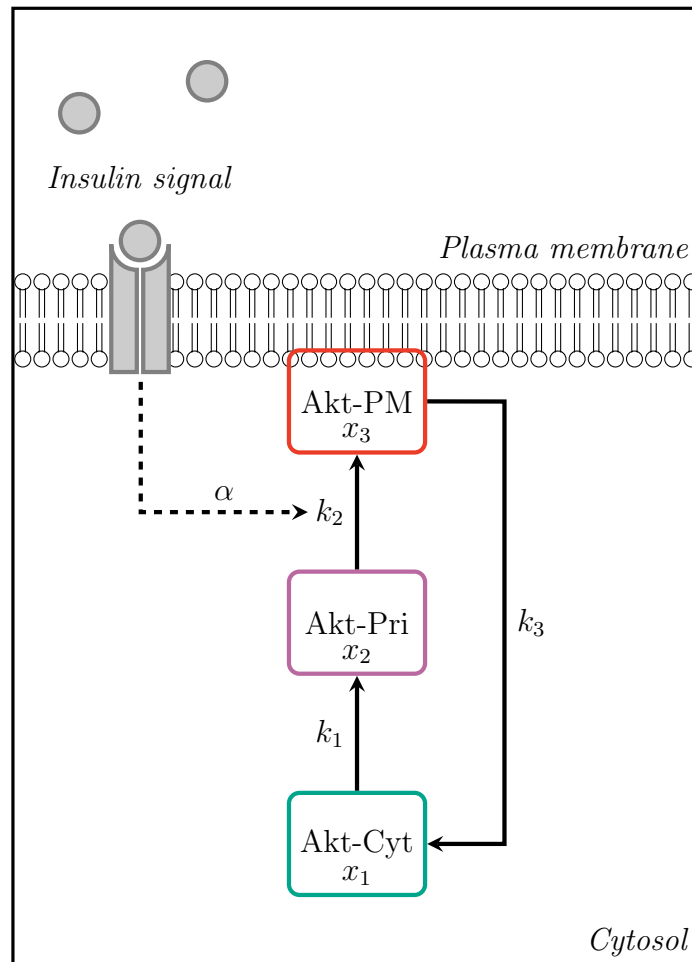


Figure 7.1: Diagram of the Akt Translocation model. All Akt in the cell is in one of three pools: the cytosolic pool (Akt-Cyt,  $x_1$ ); the primed pool (Akt-Pri,  $x_2$ ); or the plasma membrane-bound pool (Akt-PM,  $x_3$ ). The effect of the insulin signal on the system is represented by the multiplicative factor  $\alpha$ .

Table 7.1: Variables, parameters, and differential equations of the Akt Translocation model.

<b>Variables</b>	
$x_1$ :	Akt in the cytosol (Akt-Cyt)
$x_2$ :	Akt in the primed pool (Akt-Pri)
$x_3$ :	Akt docked at the plasma membrane (Akt-PM)
<b>Parameters</b>	
$k_1$ :	Rate of transition into the primed state
$k_2$ :	Rate of Akt docking at the plasma membrane
$k_3$ :	Rate of Akt recycling from plasma membrane to cytosol
$\alpha$ :	The effect of the insulin signal on the system.
<b>Equations</b>	
$\frac{dx_1}{dt}$	$= -k_1x_1 + k_3x_3$
$\frac{dx_2}{dt}$	$= k_1x_1 - \alpha k_2x_2$
$\frac{dx_3}{dt}$	$= \alpha k_2x_2 - k_3x_3$
$x_1 + x_2 + x_3 = 1, \forall t.$	

## 7.3 Results

### 7.3.1 Mathematical Analysis

#### Non-Dimensionalisation

Insight into the behaviour of a dynamical system can be gleaned from non-dimensionalisation. The actual values of the parameters in a dynamical system are an artefact of the units of measurement used. When a system is non-dimensionalised, the variables are re-scaled to be dimensionless. This can highlight relationships between variables and parameters that are intrinsic to the system. At the very least, it will yield a system with fewer parameters (see [129] or [130]).

The system of equations in Table 7.1 can be written in matrix form for the vector of states  $\mathbf{x} = (x_1, x_2, x_3)^T$ . Then  $\mathbf{x}' = \mathbf{M}\mathbf{x}$ , where

$$\mathbf{M} = \begin{pmatrix} -k_1 & 0 & k_3 \\ k_1 & -\alpha k_2 & 0 \\ 0 & \alpha k_2 & -k_3 \end{pmatrix}. \quad (7.1)$$

Let  $\hat{x}_1 = \frac{x_1}{z_1}$ ,  $\hat{x}_2 = \frac{x_2}{z_2}$ ,  $\hat{x}_3 = \frac{x_3}{z_3}$  and  $\tau = \frac{t}{t_0}$ , where  $z_1$ ,  $z_2$ ,  $z_3$  and  $t_0$  are constants yet to be determined. By the chain rule,

$$\frac{dx_1}{dt} = \frac{dx_1}{d\hat{x}_1} \cdot \frac{d\hat{x}_1}{d\tau} \cdot \frac{d\tau}{dt} = \left(\frac{z_1}{t_0}\right) \frac{d\hat{x}_1}{d\tau}.$$

Similarly,  $\frac{dx_2}{dt} = \left(\frac{z_2}{t_0}\right) \frac{d\hat{x}_2}{d\tau}$ , and  $\frac{dx_3}{dt} = \left(\frac{z_3}{t_0}\right) \frac{d\hat{x}_3}{d\tau}$ .

In terms of the new variables, Equation 7.1 can be written as  $\frac{d\hat{\mathbf{x}}}{d\tau} = \mathbf{N}\hat{\mathbf{x}}$ , where

$$\mathbf{N} = t_0 k_2 \begin{pmatrix} -\frac{k_1}{k_2} & 0 & \frac{k_3}{k_2} \begin{pmatrix} z_3 \\ z_1 \end{pmatrix} \\ \frac{k_1}{k_2} \begin{pmatrix} z_1 \\ z_2 \end{pmatrix} & -\alpha & 0 \\ 0 & \alpha \begin{pmatrix} z_2 \\ z_3 \end{pmatrix} & -\frac{k_3}{k_2} \end{pmatrix}.$$

Set  $t_0 = \frac{1}{k_2}$ , let  $z_1 = z_2 = z_3$ , and define the relative rates  $r_1 = \frac{k_1}{k_2}$  and  $r_3 = \frac{k_3}{k_2}$ . Then  $\frac{d\hat{\mathbf{x}}}{d\tau} = \mathbf{R}\hat{\mathbf{x}}$ , where the matrix  $\mathbf{R}$  is given by

$$\mathbf{R} = \begin{pmatrix} -r_1 & 0 & r_3 \\ r_1 & -\alpha & 0 \\ 0 & \alpha & -r_3 \end{pmatrix}.$$

In effect, for this particular non-dimensionalisation, only the time variable has been re-scaled in terms of the docking rate of Akt. Consequently, in the following discussion the re-scaled time variable,  $\tau$ , will be used; but for the sake of convenience,  $\hat{x}_1$ ,  $\hat{x}_2$ , and  $\hat{x}_3$  will be referred to by their original variable names,  $x_1$ ,  $x_2$ , and  $x_3$ .

### Steady States and Stability

The elementary symmetric polynomials in the relative rates  $\alpha$ ,  $r_1$ , and  $r_3$  occur repeatedly in the ensuing discussion. The elementary symmetric polynomials are

$$s_1(\alpha) = \alpha + r_1 + r_3$$

and

$$s_2(\alpha) = \alpha r_1 + \alpha r_3 + r_1 r_3.$$

These polynomials have been defined as functions of  $\alpha$  since the parameter  $\alpha$  takes on different values to represent the level of insulin stimulation.

As a three-by-three matrix,  $\mathbf{R}$  has three eigenvalues,

$$\lambda_0 = 0, \quad \lambda_1(\alpha) = \frac{-s_1(\alpha) + \sqrt{\Delta(\alpha)}}{2}, \quad \lambda_2(\alpha) = \frac{-s_1(\alpha) - \sqrt{\Delta(\alpha)}}{2},$$

where  $\Delta(\alpha) = [s_1(\alpha)]^2 - 4s_2(\alpha)$ . The zero eigenvalue,  $\lambda_0$ , arises from the assumption of Akt conservation: namely, that  $x_1 + x_2 + x_3 = 1$  at all times. In effect, this assumption reduces the dimension of the system by one.

The stability of the system can be determined by considering the two non-zero eigenvalues,  $\lambda_1$  and  $\lambda_2$ . The sign of  $\Delta$  depends on the values of  $r_1$ ,  $r_3$  and  $\alpha$ : if they are of similar magnitude, then  $\Delta$  is negative; if one is much larger than the others, or only one parameter is smaller, then  $\Delta$  is positive. When  $\Delta$  is positive,  $s_1(\alpha)$  has a greater magnitude than  $\sqrt{\Delta}$ , and so both eigenvalues are negative. If  $\Delta$  is negative, the eigenvalues are complex. However, even in this case, the real parts of  $\lambda_1$  and  $\lambda_2$  are negative. Thus in all cases, over time the system will converge from any initial condition to a stable steady state or fixed point,  $\mathbf{x}^*(\alpha)$ , given by

$$\mathbf{x}^*(\alpha) = \frac{1}{s_2(\alpha)}(\alpha r_3, r_1 r_3, \alpha r_1)^T, \quad (7.2)$$

which is the eigenvector corresponding to the zero eigenvalue.

## Derivation of the Harmonic Oscillator Equation

A major focus of the current work is the study of the transient behaviour of the system as it moves between one steady state and another. These changes in steady state correspond to changes in the value of  $\alpha$ . Initially, it is assumed that the system is in a steady state with an  $\alpha$  value of  $\alpha_1$ . Thus  $\mathbf{x}(0) = \mathbf{x}^*(\alpha_1)$ . However, at  $\tau = 0$ ,  $\alpha$  is switched to a second value,  $\alpha_2$ . Thus the system potentially undergoes two types of transition: a low-high transition, where  $\alpha_1 < \alpha_2$ ; and a high-low transition, where  $\alpha_1 > \alpha_2$ . *In vitro* experiments often measure the transition from basal (zero) to extremely high

insulin, that is  $\alpha_1 \ll \alpha_2$ . *In vivo*, this is more likely a low-high transition where  $\alpha_1$  and  $\alpha_2$  are more similar in value. High-low transitions are problematic in experimental work, as rapid removal of the insulin signal is difficult to achieve.

The system represented by the equations in Table 7.1 can be re-written as an instance of the damped harmonic oscillator equation. The ordinary differential equations (ODEs) of the Akt Translocation model expressed in terms of the relative rates  $r_1$ ,  $r_3$ , and  $r_2 = \alpha$  are

$$x_1' = r_3x_3 - r_1x_1, \quad (7.3)$$

$$x_2' = r_1x_1 - \alpha x_2, \quad (7.4)$$

$$x_3' = \alpha x_2 - r_3x_3, \quad (7.5)$$

where the prime denotes differentiation with respect to  $\tau$ . The conservation relation  $x_1 + x_2 + x_3 = 1$  can be substituted into Equation (7.4) to eliminate the variable  $x_1$ . Then

$$x_2' = r_1 - (r_1 + \alpha)x_2 - r_1x_3. \quad (7.6)$$

Moreover, as  $\alpha \neq 0$ , Equation (7.5) can be rearranged as

$$x_2 = \frac{1}{\alpha}(x_3' + r_3x_3).$$

This can be differentiated once more to obtain

$$x_2' = \frac{1}{\alpha}(x_3'' + r_3x_3').$$

Substituting these last two equations into Equation (7.6) and simplifying gives the second order ODE

$$x_3'' + s_1(\alpha)x_3' + s_2(\alpha)(x_3 - x_3^*) = 0. \quad (7.7)$$

If we make the change of variable  $X_3(\tau) = x_3(\tau) - x_3^*(\alpha)$ , then

$$X_3'' + s_1(\alpha)X_3' + s_2(\alpha)X_3 = 0. \quad (7.8)$$

Since all the rate constants in the model are positive, so are  $s_1(\alpha)$  and  $s_2(\alpha)$ . Thus Equation (7.8) is an instance of the damped harmonic oscillator equation.

### The Analytic Solution

Since  $\alpha = \alpha_2$  for  $\tau \geq 0$ , the general solution to Equation (7.7) is

$$x_3(\tau) = x_3^*(\alpha_2) + Ae^{\lambda_1\tau} + Be^{\lambda_2\tau}, \quad (7.9)$$

where  $A$  and  $B$  are constants determined by the initial conditions of the system, and  $\lambda_1$ ,  $\lambda_2$ , and  $\Delta$  denote the values of these quantities when  $\alpha = \alpha_2$ . That is,

$$\lambda_1 = \frac{-s_1(\alpha_2) + \sqrt{\Delta}}{2},$$

$$\lambda_2 = \frac{-s_1(\alpha_2) - \sqrt{\Delta}}{2},$$

and

$$\Delta = [s_1(\alpha_2)]^2 - 4s_2(\alpha_2).$$

To determine the values of  $A$  and  $B$ , recall that initially the system is in a steady state with  $\alpha = \alpha_1$ . Thus it can be seen from Equation (7.2) that  $x_3(0) = \frac{\alpha_1 r_1}{s_2(\alpha_1)}$ . Substituting  $\tau = 0$  into Equation (7.9) and re-arranging,

$$A + B = \frac{\alpha_1 r_1}{s_2(\alpha_1)} - \frac{\alpha_2 r_1}{s_2(\alpha_2)} = -\frac{r_1^2 r_3 (\alpha_2 - \alpha_1)}{s_2(\alpha_1) s_2(\alpha_2)}.$$

Moreover, differentiating Equation (7.9),

$$x'_3(\tau) = \lambda_1 A e^{\lambda_1 \tau} + \lambda_2 B e^{\lambda_2 \tau}, \quad (7.10)$$

which implies that  $x'_3(0) = \lambda_1 A + \lambda_2 B$ . However, from Equation (7.5),

$$\begin{aligned} x'_3(0) &= \alpha_2 x_2(0) - r_3 x_3(0) \\ &= \alpha_2 \frac{r_1 r_3}{s_2(\alpha_1)} - r_3 \frac{r_1 \alpha_1}{s_2(\alpha_1)} \\ &= \frac{(\alpha_2 - \alpha_1) r_1 r_3}{s_2(\alpha_1)}. \end{aligned}$$

Thus

$$\lambda_1 A + \lambda_2 B = \frac{(\alpha_2 - \alpha_1) r_1 r_3}{s_2(\alpha_1)}.$$

Putting these results together in matrix form,

$$\begin{pmatrix} 1 & 1 \\ \lambda_1 & \lambda_2 \end{pmatrix} \begin{pmatrix} A \\ B \end{pmatrix} = \frac{(\alpha_2 - \alpha_1) r_1 r_3}{s_2(\alpha_1)} \begin{pmatrix} -\frac{r_1}{s_2(\alpha_2)} \\ 1 \end{pmatrix}.$$

Now

$$\begin{pmatrix} 1 & 1 \\ \lambda_1 & \lambda_2 \end{pmatrix}^{-1} = \frac{1}{\sqrt{\Delta}} \begin{pmatrix} -\lambda_2 & 1 \\ \lambda_1 & -1 \end{pmatrix},$$

and so

$$\begin{aligned} \begin{pmatrix} A \\ B \end{pmatrix} &= \frac{(\alpha_2 - \alpha_1) r_1 r_3}{s_2(\alpha_1) \sqrt{\Delta}} \begin{pmatrix} \frac{r_1 \lambda_2}{s_2(\alpha_2)} + 1 \\ -\frac{r_1 \lambda_1}{s_2(\alpha_2)} - 1 \end{pmatrix} \\ &= C \begin{pmatrix} r_1 \lambda_2 + s_2(\alpha_2) \\ -r_1 \lambda_1 - s_2(\alpha_2) \end{pmatrix}, \end{aligned}$$

where  $C = \frac{(\alpha_2 - \alpha_1) r_1 r_3}{s_2(\alpha_1) s_2(\alpha_2) \sqrt{\Delta}}$ .

### 7.3.2 The Parameter Space

The harmonic oscillator equation is a canonical second order ODE discussed extensively in many introductory texts on the theory of differential equations, such as [131–133], for instance. The standard treatment in most texts is to write the equation in the form

$$X_3'' + 2\zeta\omega_0 X_3' + \omega_0^2 X_3 = 0, \quad (7.11)$$

where  $\omega_0$  is the natural frequency (that is, the notional frequency of the undamped system) and  $\zeta$  is the damping coefficient, a dimensionless ratio that crucially determines the behaviour of the system. In terms of parameters from the current model,  $\omega_0 = \sqrt{s_2(\alpha_2)}$  and  $\zeta = \frac{s_1(\alpha_2)}{2\sqrt{s_2(\alpha_2)}}$ .

Four solution types can be distinguished based on the value of  $\zeta$ . When  $\zeta = 0$ , the system is undamped and the solutions are purely sinusoidal. That is, the system oscillates indefinitely about the equilibrium position with a constant amplitude at a frequency of  $\omega_0$ . In the current model, all rate constants are strictly positive, so  $\zeta > 0$ . Hence this situation does not apply directly; nonetheless, the natural frequency,  $\omega_0$ , remains an important concept in the analysis of the three damped solution types.

The three damped solution types are termed under-damped, over-damped, and critically-damped. If  $0 < \zeta < 1$ , then the system is under-damped. The solutions display damped oscillations with quasi-frequency  $\omega_1 = \omega_0\sqrt{1-\zeta^2}$  inside an exponential decay envelope given by  $e^{-\lambda t}$ , where  $\lambda = \omega_0\zeta$ . In contrast, the system is over-damped if  $\zeta > 1$ , with the borderline case of critical damping when  $\zeta = 1$ . In both these cases, there are no oscillations, but the system could overshoot: this is when the solution passes through the equilibrium position once in the transient phase before asymptotically approaching the equilibrium. It also entails the existence of an extremum that is distinct from the steady state value (either higher or lower).

### Conditions for Overshoot

In the Akt Translocation model, overshoot will occur if  $r_1 < \alpha_2 + r_3$ , in which case the system reaches an extremum of

$$x_3^*(\alpha_2) + m \exp\left(-\frac{s_1(\alpha_2)}{2\sqrt{\Delta}} \ln \gamma\right),$$

where  $\gamma = \frac{r_1 + \lambda_2}{r_1 + \lambda_1}$  and  $m = \left(\frac{(\alpha_2 - \alpha_1)r_1r_3}{s_2(\alpha_1)s_2(\alpha_2)}\right) \sqrt{(r_1 + \lambda_1)(r_1 + \lambda_2)}$ .

In order to prove this, consider the over-damped case, where  $\Delta > 0$  and hence  $\lambda_1$  and  $\lambda_2$  are both real and negative. If there is an overshoot in  $x_3$ , then  $x_3$  reaches an extremum (a peak or a trough) for some  $\hat{\tau} > 0$ . At this time  $x_3'(\hat{\tau}) = 0$ . This means that, from Equation (7.10),

$$\begin{aligned}\lambda_1 A e^{\lambda_1 \hat{\tau}} &= -\lambda_2 B e^{\lambda_2 \hat{\tau}} \\ e^{(\lambda_1 - \lambda_2) \hat{\tau}} &= -\frac{\lambda_2 B}{\lambda_1 A} \\ \hat{\tau} &= \frac{1}{\sqrt{\Delta}} \ln \gamma,\end{aligned}$$

where  $\gamma = -\frac{\lambda_2 B}{\lambda_1 A}$ . If  $\hat{\tau}$  is real valued and positive, then  $\gamma > 1$ . Now

$$\gamma = -\frac{\lambda_2 B}{\lambda_1 A} = \frac{\lambda_2 [r_1 \lambda_1 + s_2(\alpha_2)]}{\lambda_1 [r_1 \lambda_2 + s_2(\alpha_2)]}.$$

Since  $\lambda_1$  and  $\lambda_2$  are the roots of the characteristic polynomial of Equation (7.7),  $\lambda_1 \lambda_2 = s_2(\alpha_2)$ . Thus

$$\gamma = \frac{r_1 + \lambda_2}{r_1 + \lambda_1}.$$

Consequently, if  $\hat{\tau}$  is real-valued, then  $(r_1 + \lambda_1)$  and  $(r_1 + \lambda_2)$  have the same sign (both are negative in the over-damped case). Furthermore, if  $\hat{\tau} > 0$  then  $|r_1 + \lambda_2| > |r_1 + \lambda_1|$ . It is this last condition that limits the size of  $r_1$  in the

case of an overshoot, since if  $|r_1 + \lambda_2| > |r_1 + \lambda_1|$ , then

$$\begin{aligned} \left| r_1 + \frac{-s_1(\alpha_2) - \sqrt{\Delta}}{2} \right| &> \left| r_1 + \frac{-s_1(\alpha_2) + \sqrt{\Delta}}{2} \right| \\ \left| r_1 - \alpha_2 - r_3 - \sqrt{\Delta} \right| &> \left| r_1 - \alpha_2 - r_3 + \sqrt{\Delta} \right| \\ \left| \sqrt{\Delta} - (r_1 - \alpha_2 - r_3) \right| &> \left| \sqrt{\Delta} + (r_1 - \alpha_2 - r_3) \right|. \end{aligned}$$

Given that  $\sqrt{\Delta} > 0$ , this inequality holds only if  $r_1 - \alpha_2 - r_3 < 0$ . That is, if  $r_1 < \alpha_2 + r_3$ .

### Large Damping

As will be demonstrated shortly, damping in the model is always ‘large’. This means that, even in the under-damped case, any oscillations rapidly die out after the switch from  $\alpha_1$  to  $\alpha_2$ . In the context of an experiment, once the amplitude of the oscillations is smaller than the experimental error, they are no longer detectable.

Under-damping in a harmonic oscillator occurs when  $0 < \zeta < 1$ . The exponential decay envelope for the oscillations is given by the decreasing exponential  $e^{-\lambda t}$ , where  $\lambda = \omega_0 \zeta$ . As a result, when  $\zeta$  is large (close to one), the exponential decay envelope rapidly narrows, and the solution curves manifest as simple overshoots that rapidly approach equilibrium.

In terms of parameters from the Akt Translocation model,

$$\zeta = \frac{s_1(\alpha_2)}{2\sqrt{s_2(\alpha_2)}}.$$

Thus

$$\zeta^2 - \frac{3}{4} = \frac{[s_1(\alpha_2)]^2}{4s_2(\alpha_2)} - \frac{3}{4}.$$

Recall that  $s_1(\alpha_2) = r_1 + \alpha_2 + r_3$  and  $s_2(\alpha_2) = r_1\alpha_2 + \alpha_2r_3 + r_1r_3$ . This implies that

$$\begin{aligned}\zeta^2 - \frac{3}{4} &= \frac{r_1^2 + \alpha_2^2 + r_3^2 + 2s_2(\alpha_2)}{4s_2(\alpha_2)} - \frac{3}{4} \\ &= \frac{r_1^2 + \alpha_2^2 + r_3^2 - s_2(\alpha_2)}{4s_2(\alpha_2)} \\ &= \frac{r_1^2 + \alpha_2^2 + r_3^2 - (r_1\alpha_2 + \alpha_2r_3 + r_1r_3)}{4s_2(\alpha_2)}.\end{aligned}$$

A simple application of the inequality of arithmetic and geometric means shows that, for all positive numbers,  $r_1$ ,  $r_3$ , and  $\alpha_2$ ,

$$r_1^2 + \alpha_2^2 + r_3^2 \geq r_1\alpha_2 + \alpha_2r_3 + r_1r_3.$$

Thus  $\zeta^2 - \frac{3}{4} \geq 0$  and hence  $\zeta \geq \frac{\sqrt{3}}{2} \approx 0.866$ . This means that  $\zeta$  is always close to the critically damped value, even in the under-damped case. Consequently the model can produce only two broad modes of behaviour, namely *overshoot* and *monotonic increase*.

### The Delta Surface

As the model contains only three relative rates— $r_1$ ,  $r_3$  and  $\alpha$ —it is easy to visualise the parameter space in three dimensions. The system is under-damped if  $0 < \zeta < 1$  and over-damped if  $\zeta > 1$ , or, equivalently, if  $\Delta < 0$  or  $\Delta > 0$ . The surface in Figure 7.2 shows  $\Delta$  on the vertical axis as a function of  $r_1$  and  $r_3$  when  $\alpha = 1$ . A horizontal slice corresponding to  $\Delta = 0$  can be taken through this surface to create a two dimensional plot, as illustrated in the plot in Figure 7.3. (Due to the inherent symmetry in the roles of the parameter values in the model, similar plots can be produced when either  $r_1$  and  $r_3$  is held constant.) The curve thus created is a parabola that touches the coordinate axes at  $(\alpha, 0)$  and  $(0, \alpha)$ , dividing the plane into four distinct regions. The single under-damped region (B), where  $\Delta < 0$ , lies inside

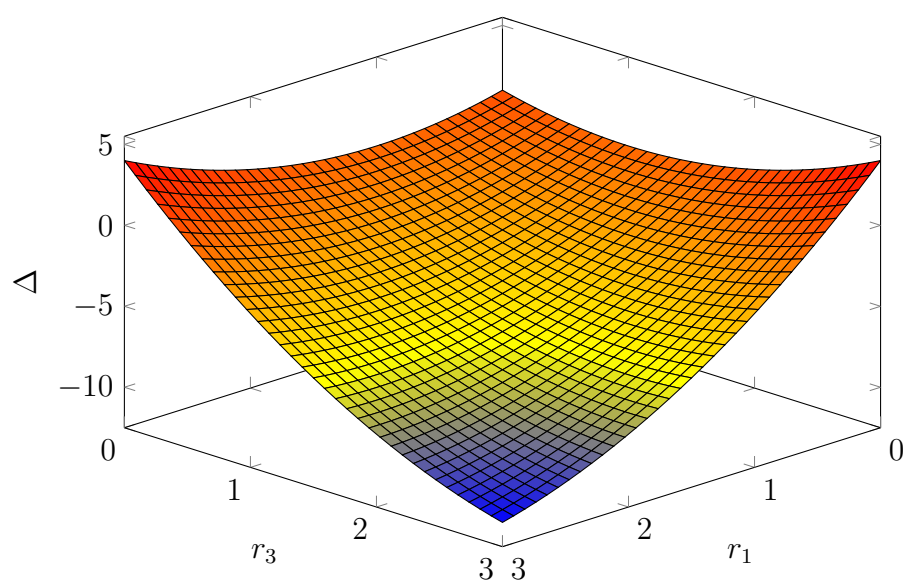


Figure 7.2: The  $\Delta$ -surface as a function of  $r_1$  and  $r_3$  for a constant value of  $\alpha = 1$ . A horizontal slice corresponding to  $\Delta = 0$  can be taken through this surface to create a parabola (see Figure 7.3).

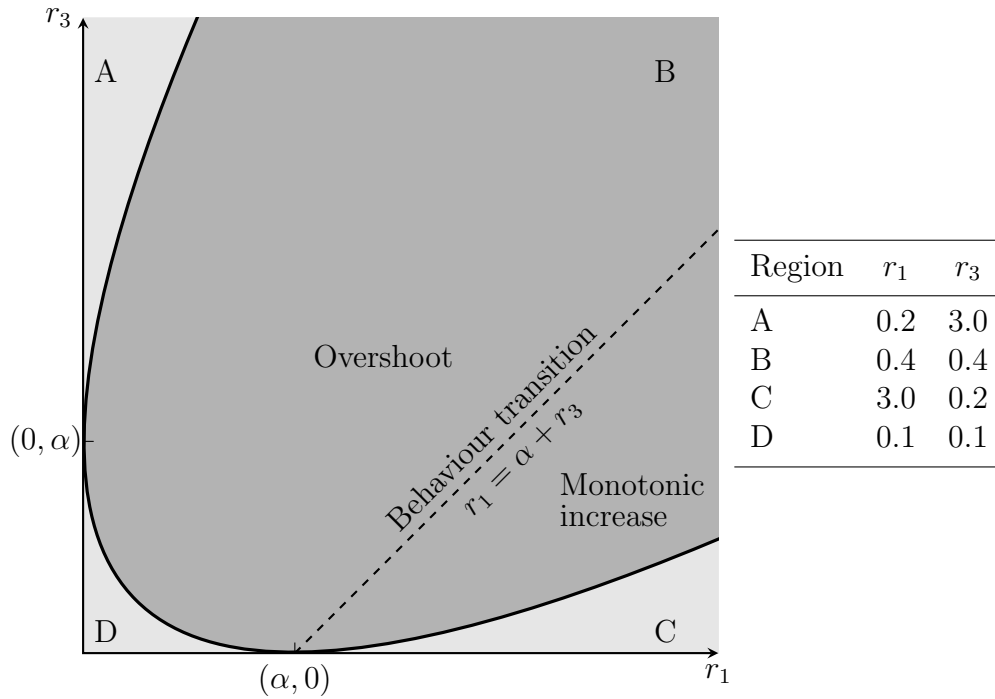


Figure 7.3: Regions of parameter space. The curve shown in the plot is a parabola that demarcates the under-damped and over-damped regions of parameter space ( $\Delta = 0$ ). The darkly shaded area (B) inside the curve is the under-damped region ( $\Delta < 0$ ). The over-damped region ( $\Delta > 0$ ) is divided into three non-contiguous areas: A (small  $r_1$ , large  $r_3$ ); C (large  $r_1$ , small  $r_3$ ); and D (small  $r_1$  and  $r_3$ ).

the parabola. In contrast, the over-damped region outside the parabola is divided into three non-contiguous areas: A, with small  $r_1$  and large  $r_3$ ; C, with large  $r_1$  and small  $r_3$ ; and D with small  $r_1$  and  $r_3$ . The dashed line,  $r_1 = \alpha + r_3$ , represents the behaviour transition of the system, from overshoot in the upper left of the plot to monotonic increase in the lower right. Thus overshoot in  $x_3$  occurs in regions A, D, and part of B, but not in C.

### 7.3.3 Crosstalk in Transition

Figure 7.4 shows the output of simulations with parameter sets representative of the four regions of parameter space. In each plot, the system is initially in a steady state with  $\alpha = \alpha_1$  for  $-5 < \tau < 0$ . The value of  $\alpha$  changes to  $\alpha_2$  at time  $\tau = 0$ . Solid curves shows the low-high transition, where  $\alpha_1 = 0.5$  and  $\alpha_2 = 1$ ; dashed curves shows the high-low transition with the values of  $\alpha_1$  and  $\alpha_2$  reversed. The dotted black lines represent the steady state values. Within any given plot, the other rates ( $r_1$  and  $r_3$ ) were held constant across both conditions.

Interestingly, the high-low transition in  $\alpha$  values is not a simple vertical reflection of the low-high transition in any of the four regions but rather exhibits some degree of hysteresis. This can be seen most clearly in the simulation with the Region B parameter set, where the Akt-PM values for the low-high transition reaches a peak that is both greater in magnitude and earlier than the corresponding trough for the high-low transition. Similar phenomena can be seen in the simulations from the other three regions of parameter space.

This asymmetry in the roles of  $\alpha_1$  and  $\alpha_2$  is further illustrated in three important downstream signalling metrics: the (scaled) time to the extremum (Figure 7.5); the size of the extremum as a fraction of total Akt (Figure 7.6); and the initial gradient of the Akt-PM pool,  $x'_3(0)$  (Figure 7.7). For all these metrics, the Region A parameter set with  $r_1 = 0.2$  and  $r_3 = 3$  has been used, but values of  $\alpha_1$  and  $\alpha_2$  have been varied as indicated.

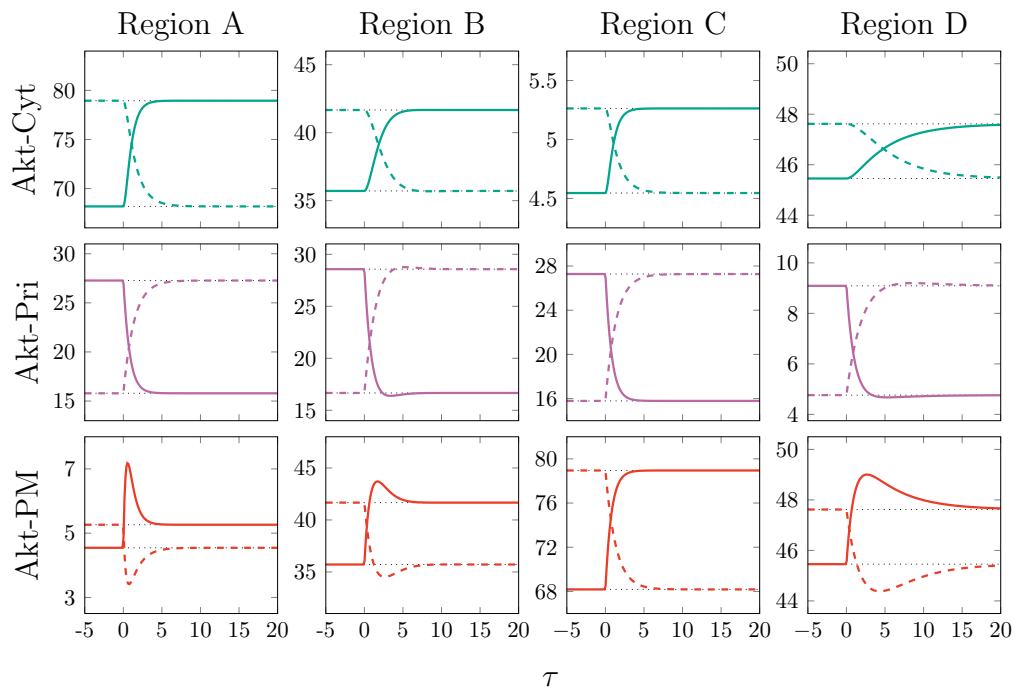


Figure 7.4: The output of the Akt Translocation model. Time courses of cytosolic Akt (Akt-Cyt,  $x_1$ ), primed Akt (Akt-Pri,  $x_2$ ), and Akt at the plasma membrane (Akt-PM,  $x_3$ ) for the four regions of parameter space are shown in blue, purple, and red, respectively. Step increases in insulin are shown with solid lines; step decreases with dashed lines. Steady state levels are shown as black dotted lines.

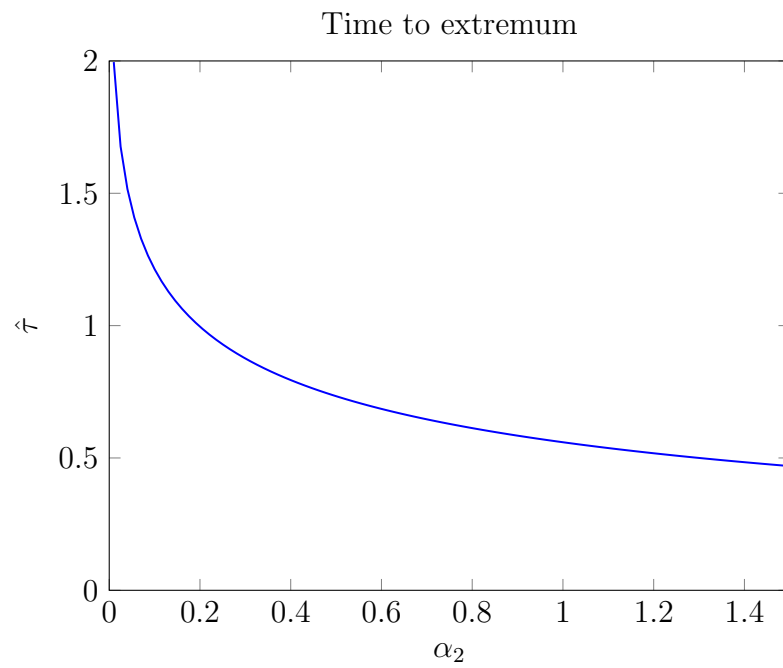


Figure 7.5: The time to the extremum,  $\hat{\tau}$ , as a function of  $\alpha_2$  with  $r_1 = 0.2$  and  $r_3 = 3$ .

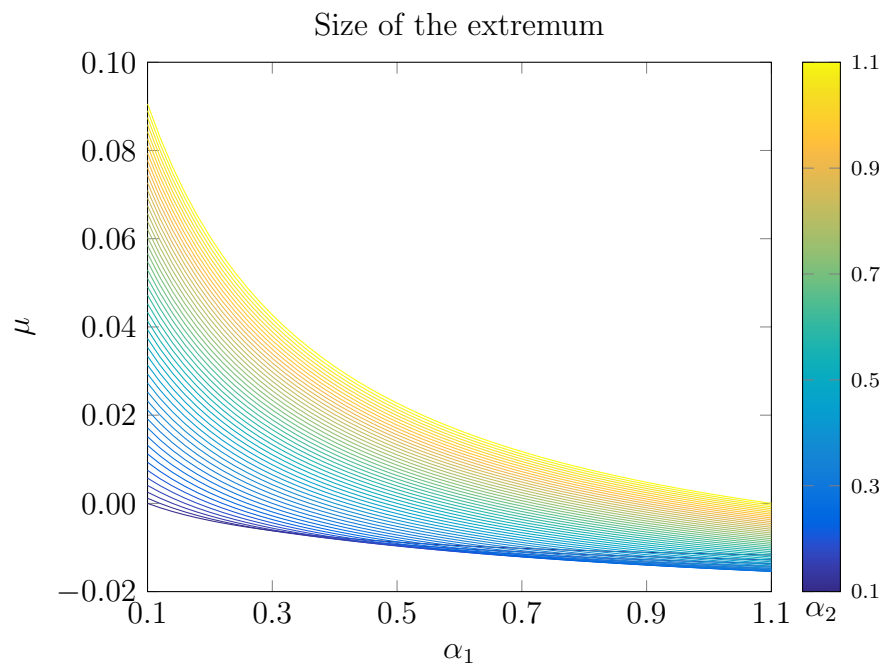


Figure 7.6: The size of the extremum,  $\mu$ , as a fraction of total Akt shown as a function of  $\alpha_1$  and  $\alpha_2$  with  $r_1 = 0.2$  and  $r_3 = 3$ . (Negative values indicate a trough.) The value of  $\alpha_2$  is shown in the colour bar on the right.

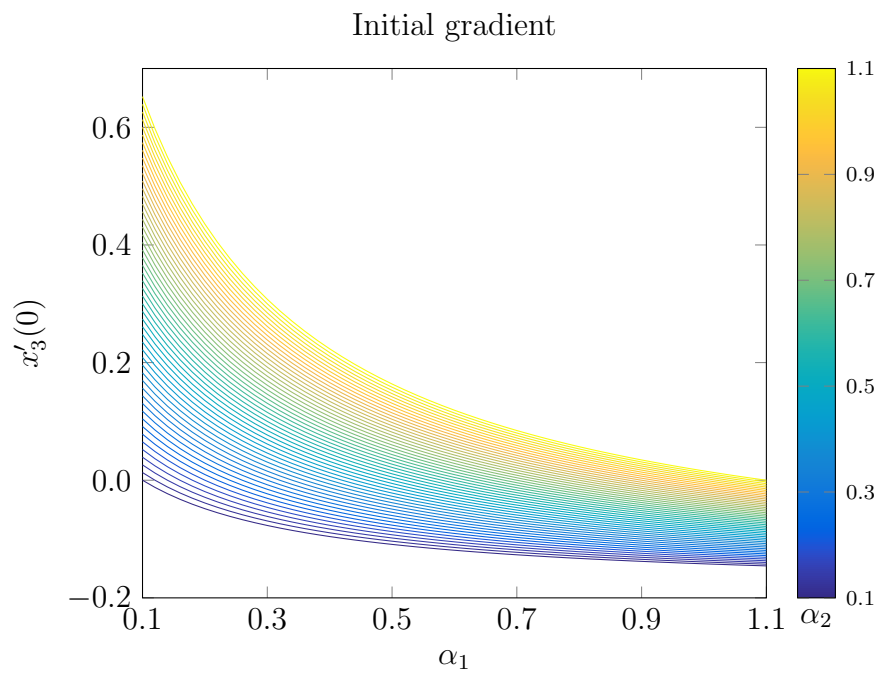


Figure 7.7: The initial gradient as a function of  $\alpha_1$  and  $\alpha_2$  with  $r_1 = 0.2$  and  $r_3 = 3$ . The value of  $\alpha_2$  is shown in the colour bar on the right.

The time to the extremum (when it exists) is independent of  $\alpha_1$ . Recall that the time to extremum,  $\hat{\tau}$ , is given by

$$\hat{\tau} = \frac{1}{\sqrt{\Delta}} \ln \left( \frac{r_1 + \lambda_2}{r_1 + \lambda_1} \right).$$

Now

$$\begin{aligned} \frac{r_1 + \lambda_2}{r_1 + \lambda_1} &= \frac{r_1 - \alpha_2 - r_3 - \sqrt{\Delta}}{r_1 - \alpha_2 - r_3 + \sqrt{\Delta}} \\ &= 1 - \frac{2\sqrt{\Delta}}{r_1 - \alpha_2 - r_3 + \sqrt{\Delta}} \\ &= 1 + \frac{2\sqrt{\Delta}}{\alpha_2 + (r_3 - r_1) - \sqrt{\Delta}}. \end{aligned}$$

Furthermore,

$$\begin{aligned} \lim_{\alpha_2 \rightarrow 0} \sqrt{\Delta} &= \lim_{\alpha_2 \rightarrow 0} \sqrt{[s_1(\alpha_2)]^2 - 4s_2(\alpha_2)} \\ &= \sqrt{(r_1 + r_3)^2 - 4r_1r_3} \\ &= |r_1 - r_3|. \end{aligned}$$

Note that in the overshoot case, if  $\alpha_2$  approaches zero, then  $r_1 < r_3$ , so  $|r_1 - r_3| = r_3 - r_1$ . Thus

$$\lim_{\alpha_2 \rightarrow 0} \hat{\tau} = \lim_{\alpha_2 \rightarrow 0} \frac{1}{r_3 - r_1} \ln \left( 1 + \frac{2(r_3 - r_1)}{\alpha_2} \right).$$

So as  $\alpha_2$  approaches zero,  $\hat{\tau}$  increases without bound as illustrated in Figure 7.5. Furthermore, as  $\alpha_2$  increases,  $\hat{\tau}$  decreases, irrespective of the value of  $\alpha_1$ .

In contrast, the size of the extremum—that is, the difference between the height of the extremum and the final steady state value—is a function of both  $\alpha_1$  and  $\alpha_2$ , but is not symmetric in these two variables. Let  $\mu$  be the

extreme value (maximum or minimum) of  $x_3$  in the overshoot case. Then

$$\begin{aligned}
\mu &= x_3^*(\alpha_2) + Ae^{\lambda_1 \hat{\tau}} + Be^{\lambda_2 \hat{\tau}} \\
&= x_3^*(\alpha_2) + Ae^{\lambda_1/\sqrt{\Delta} \ln \gamma} + Be^{\lambda_2/\sqrt{\Delta} \ln \gamma} \\
&= x_3^*(\alpha_2) + A \exp \left[ \left( \frac{1}{2} - \frac{s_1(\alpha_2)}{2\sqrt{\Delta}} \right) \ln \gamma \right] \\
&\quad + B \exp \left[ \left( -\frac{1}{2} - \frac{s_1(\alpha_2)}{2\sqrt{\Delta}} \right) \ln \gamma \right] \\
&= x_3^*(\alpha_2) + m \exp \left( -\frac{s_1(\alpha_2)}{2\sqrt{\Delta}} \ln \gamma \right),
\end{aligned}$$

where  $m = A\sqrt{\gamma} + B/\sqrt{\gamma}$ . Now

$$\begin{aligned}
m &= A\sqrt{\gamma} + \frac{B}{\sqrt{\gamma}} \\
&= C[r_1\lambda_2 + s_2(\alpha_2)] \sqrt{\frac{\lambda_2[r_1\lambda_1 + s_2(\alpha_2)]}{\lambda_1[r_1\lambda_2 + s_2(\alpha_2)]}} \\
&\quad - C[r_1\lambda_1 + s_2(\alpha_2)] \sqrt{\frac{\lambda_1[r_1\lambda_2 + s_2(\alpha_2)]}{\lambda_2[r_1\lambda_1 + s_2(\alpha_2)]}} \\
&= C \left( \sqrt{\frac{\lambda_2}{\lambda_1}} - \sqrt{\frac{\lambda_1}{\lambda_2}} \right) \sqrt{[r_1\lambda_1 + s_2(\alpha_2)][r_1\lambda_2 + s_2(\alpha_2)]}.
\end{aligned}$$

Recall that  $\lambda_1\lambda_2 = s_2(\alpha_2)$ . Thus the equation can be simplified as

$$\begin{aligned}
m &= C \left( \frac{|\lambda_2 - \lambda_1|}{\sqrt{\lambda_1\lambda_2}} \right) \sqrt{(r_1\lambda_1 + \lambda_1\lambda_2)(r_1\lambda_2 + \lambda_1\lambda_2)} \\
&= C|\lambda_2 - \lambda_1| \sqrt{(r_1 + \lambda_1)(r_1 + \lambda_2)}.
\end{aligned}$$

Since  $C = \frac{(\alpha_2 - \alpha_1)r_1r_3}{s_2(\alpha_1)s_2(\alpha_2)\sqrt{\Delta}}$ , and  $\lambda_2 - \lambda_1 = \sqrt{\Delta}$ ,

$$m = \left( \frac{(\alpha_2 - \alpha_1)r_1r_3}{s_2(\alpha_1)s_2(\alpha_2)} \right) \sqrt{(r_1 + \lambda_1)(r_1 + \lambda_2)}.$$

If  $\gamma$  is positive, then so is  $(r_1 + \lambda_1)(r_1 + \lambda_2)$ . Consequently, if  $\alpha_2 > \alpha_1$  then  $m > 0$ . In this case,  $\mu > x_3^*(\alpha_2)$  and represents a peak. Conversely, if  $\alpha_2 < \alpha_1$  then  $m < 0$  and  $\mu$  represents a trough.

As demonstrated in Figure 7.6, as  $\alpha_1$  increases or  $\alpha_2$  decreases, the size of the extremum decreases, with the positive peaks becoming less pronounced and the negative overshoot decreasing in magnitude (it should be noted that negative values on the vertical axis in this plot denote a trough rather than a peak).

The dependence of the initial gradient of Akt-PM,  $x_3'(0)$ , on the parameters  $\alpha_1$  and  $\alpha_2$  is illustrated in Figure 7.7. The initial gradient of the plasma membrane pool,  $x_3'(0)$ , is given by

$$\begin{aligned} x_3'(0) &= \alpha_2 x_2(0) - r_3 x_3(0) \\ &= \alpha_2 \left( \frac{r_1 r_3}{s_2(\alpha_1)} \right) - r_3 \left( \frac{r_1 \alpha_1}{s_2(\alpha_1)} \right) \\ &= (\alpha_2 - \alpha_1) \frac{r_1 r_3}{s_2(\alpha_1)} \\ &= (\alpha_2 - \alpha_1) x_2(0). \end{aligned}$$

Consequently, the initial gradient is directly proportional to both the difference in the final and initial  $\alpha$  values ( $\alpha_2 - \alpha_1$ ) and the initial size of the primed pool,  $x_2(0)$ . As it is assumed that the system starts in a steady state with  $\alpha = \alpha_1$ ,  $x_2(0)$  is also a function of  $\alpha_1$ .

## 7.4 Discussion

In the Akt Translocation model, the system transitions from one steady state, where initially  $\alpha = \alpha_1$ , to a second steady state with  $\alpha = \alpha_2$ . The large damping inherent in the model guarantees that the transition occurs in one of two ways: Akt-PM can overshoot, where the extreme value and steady state differ; or increase monotonically, with the extreme value and steady state coinciding. These two types of behaviour are typified by the simulations with the parameter set from Region A (overshoot) and Region C (monotonic increase), both shown in Figure 7.3.

The simulation plots in Figure 7.3 also illustrate that the steady state values of the system and the relative size of the overshoot peak or trough varies markedly between the different regions of parameter space. In Region A, Akt-PM has a low steady state value and a relatively large overshoot peak/trough. It is thus the region that produces the most biologically realistic simulations. In Region B (the ostensibly underdamped region), Akt-PM has a higher steady state value and a relatively modest overshoot peak, at least for parameter values to the upper right of the dashed line. Region C can only produce simulations that manifest monotonic increase. Region D, whilst producing overshoot, has a more delayed time to extreme value, and takes much longer to approach steady state. The plots in Figure 7.3 show the behaviour of the system for  $-5 \leq \tau \leq 10$ . By the end of this time, only the Region D plot has not yet reached steady state, although it does so within a scaled time of 30. These differences in simulations from the various regions of parameter space demonstrate the fact that different information, occurring on radically different time scales, can be encoded into the transitory and steady state behaviour of the model. As Akt is activated at the plasma membrane, the dynamics of translocation have a direct bearing on the subsequent activation and downstream signalling.

It is known that Akt has a wide variety of substrates [19, 31, 37], which can be broadly classified as metabolic and/or mitogenic effectors. The short half-

life of insulin in the blood (approximately 5 min [4]) necessitates a rapid response from the metabolic effectors of Akt. Rapidly responding substrates of Akt may be activated in an ultra-sensitive switch-like manner once a certain threshold of Akt phosphorylation is attained. Alternately, there is evidence to suggest that some Akt substrates are sensitive to the initial gradient of Akt phosphorylation, independent of ultimate phosphorylation levels [29]. Both these aspects of downstream signalling can be encoded into the transient behaviour of the model by a judicious choice of parameter values, which permits the fine-tuning of details such as the peak height (size of the extremum), peak timing (time to extremum), and the initial gradient of Akt-PM.

In contrast, growth, proliferation, and cell fate decisions—the purview of the mitogenic effectors of Akt—occur on much longer timescales as they involve changes to gene expression levels and protein synthesis. It is possible that activation of the slow-responding substrates of Akt is linked to long term changes in Akt activation levels, an aspect of the steady state behaviour of the model that can also be manipulated through parameter choice. As shown in Figure 7.3 (Region A–D), the model is capable of producing a wide range of values for both the basal and insulin-stimulated steady states.

Another illustration of how the transient and steady state attributes of the dynamics could differentially drive downstream signalling is given in Figure 7.5. Here, the time to the extremum is a non-linear function of  $\alpha_2$  only. The extremum time decreases as  $\alpha_2$  is increased (Figure 7.5(a)). In contrast, the size of the extremum and the initial gradient respond to changes in both  $\alpha_1$  and  $\alpha_2$ , as shown in Figure 7.5(b) and (c).

Thus far the discussion has focussed almost exclusively on the role of  $x_3$  (Akt-PM) in the model. This is because  $x_3$  represents a pool of Akt that is able to be phosphorylated and become biologically active. This pool can also be readily observed experimentally using, for instance, total internal reflection fluorescence (TIRF) microscopy [128]. However, the analysis carried out here (the transformation to a second order ODE) can be repeated for the other two variables. The inherent mathematical symmetry of the model ensures that

the resulting solutions are structurally identical, but with the rate constants permuted, reflecting the cyclic nature of the model. This permutation of rate constants guarantees that at most one pool in the model can manifest overshoot. For instance, when a parameter set from Region A is used to simulate all three pools in the model,  $x_3$  overshoots, but  $x_1$  and  $x_2$  show monotonic increases, similar to the  $x_3$  solution curves from Region C.

Although  $x_1$  and  $x_2$  have similar solution curves (albeit with different steady state values),  $x_2$  is of particular relevance to the initial gradient of  $x_3$ . In the model, it is assumed that the system starts in a steady state, and consequently, there is some Akt in the primed pool ( $x_2$ ) available for translocation to, and subsequent activation at, the plasma membrane. As shown in Equation 7.2, the steady state values are a function of the insulin-sensitive parameter,  $\alpha$ . Thus the initial condition is a function of the initial value of  $\alpha = \alpha_1$ . As  $x_2^*(\alpha)$  lacks an  $\alpha$  containing term in the numerator, it can be seen that the initial  $x_1$  and  $x_3$  pools are enriched at the expense of the  $x_2$  pool if the value of  $\alpha_1$  is increased. Since the initial gradient is a linear function of  $x_2(0)$ , this depletion of the  $x_2$  pool has ramifications for subsequent downstream signalling.

The hysteretic effect on the system caused by changes to the initial condition is further demonstrated by the low-high transitions (solid curves) and the high-low transitions (dashed curves) shown in Figure 7.3 (Region A–D). It is clear that for all four regions of parameter space, the steady state levels for the low-high and high-low transitions are the same, however, the transitions exhibit an obvious asymmetry. Low-high transitions are typical of much experimental work in this area. High-low transitions, in contrast, are much harder to conduct experimentally, as it is difficult to rapidly lower the concentration of insulin once it has been applied.

It is possible to block or attenuate the insulin signal upstream from Akt with a number of different inhibitors. For instance, the PIP<sub>3</sub> pool can be depleted by either the direct dephosphorylation of PIP<sub>3</sub> by PTEN [134] or the inhibition of PI3K by agents such as Wortmannin or LY294002 [35,37,135]. Alternately,

the recruitment of Akt to the plasma membrane can be prevented in a PI3K-independent manner by ceramide or NSC126188 [20, 119, 120, 136], however, as the Akt translocation process itself is currently not well understood, the precise mechanism involved is not known. Furthermore, these inhibitors can have other, off-target effects in cells. Wortmannin, for example, undergoes irreversible binding and is toxic to cells after prolonged use [37].

In contrast, the behaviour of the system during a high-low transition can be readily inferred from the mathematical model by simply exchanging the values of  $\alpha_1$  and  $\alpha_2$ . Moreover, this can be done repeatedly to simulate the pulsatile release of insulin that occurs *in vivo*. Thus the underlying dynamics of the system can be investigated without confounds caused by the timing or duration of external perturbations. In particular, pulsatile and/or periodic insulin stimulation is an obvious next step in the analysis of the current model, and will no doubt raise issues of both timing and depletion that require investigation.

The mathematical modelling of complex phenomena always entails simplifications of some kind, often significant ones. For example, in the analysis of the current model, it was assumed that insulin only affects the docking rate (that is,  $k_2$  or the relative rate  $\alpha$ ). It is possible that insulin also directly affects the rate of recycling from plasma membrane to cytosol ( $k_3$ ) or even the priming rate ( $k_1$ ). In addition, these translocation rates may vary depending on the phosphorylation state of Akt. For instance, a differential recycling rate for phosphorylated Akt in the  $x_3$  pool could lead to membrane retention of this fraction. Since  $k_3$  in the current model is a weighted average of recycling rates for both subtypes of Akt, this is equivalent to making  $k_3$  indirectly insulin dependent. Since the phosphorylation state of Akt is not explicitly tracked in the current model, it is not possible to distinguish between these two scenarios—a direct influence of insulin on  $k_3$ , or an indirect influence mediated by phosphorylation state. The investigation of such hypotheses is better suited to an expanded model of the dynamics that includes compartments for both phosphorylated and un-phosphorylated Akt. This refinement thus constitutes a natural next step in the development of the model.

The preliminary aim of this model was to recapitulate *in silico* the type of behaviour reported in the literature. This behaviour has been inferred from *in vitro* experiments, and will necessarily differ to some extent from that of the *in vivo* system. However, the techniques and insights obtained from modelling the *in vitro* observations will contribute to the development of a more realistic description of the *in vivo* behaviour. In order for this ultimate aim to be achieved, more experimental data from the *in vivo* context would be required. Prior to this, information from *in vitro* systems would be useful in determining future directions. For example, techniques such as reversible cryo-arrest [137] or plasma membrane lawns can help to determine both the spatial distribution and activation state of Akt. In addition, data taken using insulin concentrations in the physiological range will probably yield more accurate descriptions of the *in vivo* system. Investigations using primary adipocytes rather than cultured cells lines may also highlight differences between *in vitro* and *in vivo* systems. In particular, further measurements of the high to low transition would be useful to determine the parameter regimes observed under different conditions.

## 7.5 Summary

In this chapter, a simple, deterministic, three-compartment ordinary differential equation model of Akt translocation *in vitro* has been presented. The Akt Translocation model can reproduce the salient features of Akt translocation in a manner that is consistent with the existing experimental data. After recasting the model in terms of relative rates, and taking the conservation relation into account, it can be seen that the system is mathematically equivalent to a damped harmonic oscillator. This framework permits an analysis of both the steady state and transient behaviour of the model over the entire parameter space and the elucidation of conditions for the manifestation of overshoot, a biologically significant feature of Akt translocation.

Further investigation of the dynamics of the model has also revealed an inherent hysteresis brought about by changes to the initial conditions. This asymmetry in system behaviour will have ramifications in pulsatile and periodic forcing scenarios, which are ubiquitous in biological signalling networks. In the next chapter, this model is optimised to experimental data to provide further insight into the underlying biology of the system.



# Chapter 8

## Time Delays and Dominant Processes

### 8.1 Introduction

*This chapter is based on work presented in: CW Gray and ACF Coster. From Insulin to Akt: Time Delays and Dominant Processes. Journal of Theoretical Biology. Online 19 August 2020. <https://doi.org/10.1016/j.jtbi.2020.110454>*

In Chapter 7, the Akt Translocation model—a deterministic three compartment ODE model of Akt translocation in response to insulin—was presented and analysed. In this model, it was assumed that all Akt in the cell exists in one of three pools: a cytosolic pool (Akt-Cyt); a primed pool (Akt-Pri); and a plasma membrane-docked pool (Akt-PM); and that the predominant effect of insulin is an increase in the docking rate (that is, the rate at which Akt transitions between the primed pool and the plasma membrane docked pool). The model was able to reproduce the salient features of Akt translocation with a minimum of assumptions. In the current chapter, the parameters of this model are optimised to experimental data obtained from TIRF microscopy of 3T3-L1 adipocytes under insulin stimulation at both physiological (1 nM) and very high (100 nM) concentrations.

As an outcome of the parameter optimisation, the time delay between the application of insulin and the Akt translocation response has been quantified. For physiological insulin, a delay of approximately 0.4 min was found, indicating constraints on the timing of upstream signalling processes between the insulin receptor and Akt. Intriguingly, it was found that a further transition from physiological insulin to higher stimuli did not incur a delay.

In addition, the parameter optimisation to such widely divergent insulin levels suggested that the dominant processes regulating the appearance of Akt at the plasma membrane differ with the insulin concentration. For physiological insulin, the release of Akt to the plasma membrane in response to the insulin signal was rate limiting. This is consistent with the assumptions of the mathematical analysis in Chapter 7. In contrast, at high insulin levels, regulation of the recycling of Akt from the plasma membrane to the cytosol was also required.

## 8.2 Method

### 8.2.1 The Data

The time course data for the parameter optimisation of the model was from Norris, *et al.* [128] (Figure 8.1). In this study, the translocation dynamics of Akt2 in fully differentiated 3T3-L1 adipocytes was measured by total internal reflection fluorescence (TIRF) microscopy. TIRF microscopy is a live cell imaging technique in which molecules of interest (in this case, Akt2) are tagged with fluorophores. A beam of light of a given frequency incident on the sample excites fluorophores within a narrow region near the plasma membrane only. This narrow region (on the order of 100-200 nm) is termed the TIRF zone. Patches of cell are repeatedly imaged as insulin is applied, and the movement of fluorescently tagged Akt into and out of the TIRF zone can be measured.

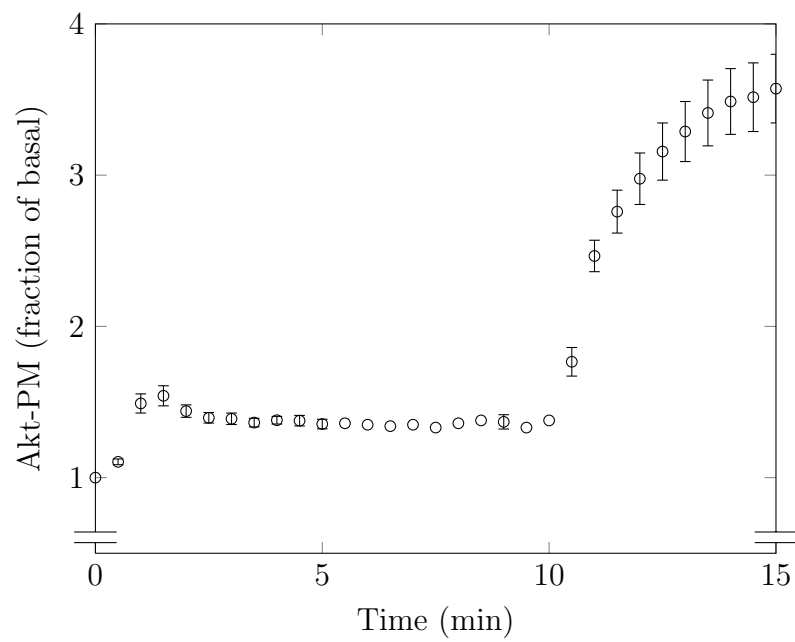


Figure 8.1: The experimental data from Norris, *et al.* [128]. The transition from basal to physiological (1 nM) insulin occurs during the first ten minutes of the time course. The transition from physiological to maximal (100 nM) insulin is from 10 to 15 minutes.

In the Norris paper, cells were first imaged for 10 minutes in the absence of insulin to establish the average fluorescence of the TIRF zone in the basal state. The cells were then stimulated with a physiological dose of insulin (1 nM) for 10 minutes, followed by a maximal dose of insulin (100 nM) for a further five minutes. The first 10 minutes after the application of 1 nM insulin will be referred to as the physiological transition and the five minutes following the application of 100 nM insulin the maximal transition.

During the physiological transition, Akt-PM undergoes a rapid increase, culminating in an overshoot before a relaxation to a higher steady state (Figure 8.1). This new equilibrium is reached within four or five minutes of the initial application of insulin.

In contrast, it is unclear from the data for the second, maximal transition whether the Akt-PM level plateaus or overshoots as the time course is short. When fitted to an exponential rise (see Section 8.2.3), however, the rate constant obtained for the maximal transition was  $0.60 \text{ min}^{-1}$  with a 95% confidence interval of (0.47, 0.72). This equates to a doubling time of approximately 1.16 minutes. Thus the maximal transition represents a slower, more sustained rise in the level of Akt-PM than the physiological transition.

## 8.2.2 The Model

The Akt Translocation model presented in Chapter 7 (with some minor modifications) was used for the parameter optimisation. In this model, the system was initially in a steady state determined by the insulin concentration, and the transition from one equilibrium to another in response to a step change in insulin was analysed. The system is equivalent to a damped harmonic oscillator with large damping. As a result, the transition from one steady state to another occurs via one of two broad modes: overshoot (undershoot) or monotonic increase (decrease). In addition, the minimal assumption that insulin affects only the rate of Akt docking at the plasma membrane was made. As will be demonstrated shortly, this assumption requires revision.

Optimising the model to the experimental data necessitated some modifications. Firstly, the Akt pools were re-normalized to match the experimental data. Secondly, a time delay following the application of insulin was added. This time delay represents the time required for the insulin signal to propagate through the upstream signalling cascade prior to the initiation of Akt translocation. The structure of the model is otherwise the same as that in Chapter 7.

A diagram of the modified model is shown in Figure 8.2. The model has three Akt pools:

- $x_1$ , cytosolic Akt;
- $x_2$ , Akt primed for docking at the plasma membrane; and
- $x_3$ , Akt docked at the plasma membrane.

Furthermore, there are seven parameters: three rate constants; three factors representing the effect of insulin on the rate constants; and the time delay. For the system in the basal steady state (that is, in the absence of insulin stimulation) the rate constants are:

- $k_1$ , the rate at which Akt enters the primed pool (the basal priming rate);
- $k_2$ , the rate at which Akt enters the TIRF zone to dock at the plasma membrane (the basal docking rate); and
- $k_3$ , the rate of recycling of Akt from the TIRF zone to the cytosol (the basal recycling rate).

The effect of insulin on each of the translocation subprocesses is represented by the positive multiplicative factors  $\alpha$ ,  $\beta$ , and  $\gamma$ , which vary with the insulin concentration. Thus, for any given insulin level, the effective docking rate is  $\alpha k_2$ ; the effective recycling rate is  $\beta k_3$ ; and the effective priming rate is  $\gamma k_1$ , as shown in Figure 8.2. The variables, parameters, and equations of the model are also listed in Table 8.1.

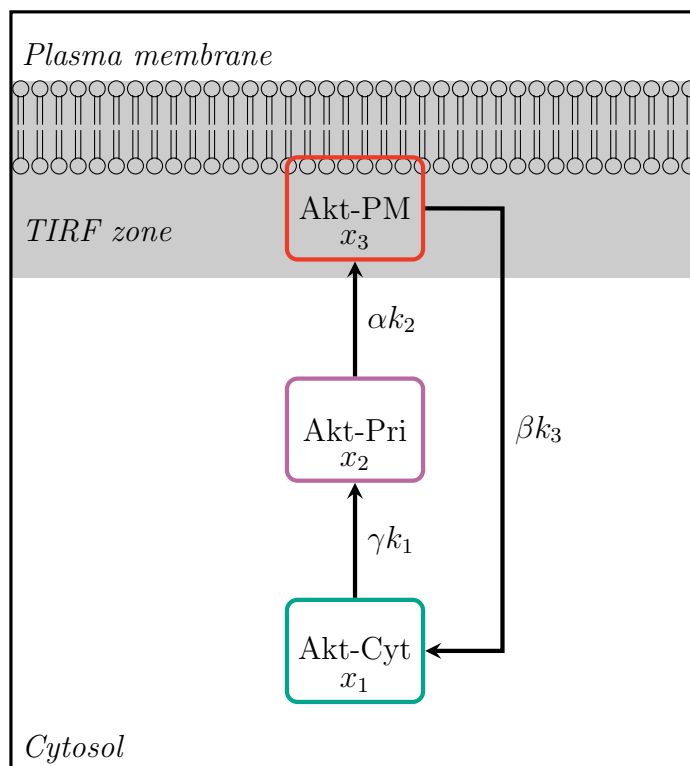


Figure 8.2: Diagram of the modified Akt Translocation model. Akt is initially synthesized in the cytosol ( $x_1$ ). It is then primed for activation ( $x_2$ ). In response to insulin, the primed Akt moves into the TIRF zone and docks at the plasma membrane ( $x_3$ ).

Table 8.1: Variables, parameters, and equations of the modified Akt Translocation model.

<b>Variables</b>	
$x_1$ :	Akt in the cytosol (Akt-Cyt)
$x_2$ :	Akt in the primed pool (Akt-Pri)
$x_3$ :	Akt docked at the PM (Akt-PM)
<b>Parameters</b>	
$k_1$ :	Basal priming rate of Akt
$k_2$ :	Basal docking rate of Akt at the plasma membrane
$k_3$ :	Basal recycling rate of Akt from the plasma membrane to the cytosol
$I(t)$ :	The insulin concentration at time $t$
$\alpha(I)$ :	The effect of insulin on the docking rate
$\beta(I)$ :	The effect of insulin on the recycling rate
$\gamma(I)$ :	The effect of insulin on the priming rate
$\Delta t$ :	The time delay
<b>Equations</b>	
$\frac{dx_1}{dt}$	$= -\gamma k_1 x_1 + \beta k_3 x_3$
$\frac{dx_2}{dt}$	$= \gamma k_1 x_1 - \alpha k_2 x_2$
$\frac{dx_3}{dt}$	$= \alpha k_2 x_2 - \beta k_3 x_3$
Note: at all times, $x_1 + x_2 + x_3 = T$ , where $T$ is total Akt (a constant).	

Akt occupies an intermediate position in the insulin signalling pathway [15]. Upstream propagation of the insulin signal causes a delay between the application of insulin and the translocation response. Even in the Akt Switch model, there were discrepancies in model output at high insulin levels due to the signalling delay (see Section 6.4). Consequently, for the parameter optimisation of the Akt Translocation model, a time delay,  $\Delta t$ , was inserted after the initial application of insulin. Thus, for the physiological transition,  $\alpha$  is represented by the step function,

$$\alpha = \begin{cases} 1 & \text{if } t < \Delta t, \\ \alpha_{phys} & \text{otherwise.} \end{cases} \quad (8.1)$$

The minimalist assumption that the docking rate is the sole point of action of the insulin signal corresponds to  $\beta = \gamma = 1$  throughout.

As shown in Chapter 7, there is a stable steady state to which the system converges. For a given insulin level,  $I$ , the steady state values of the three Akt pools— $x_1^*$ ,  $x_2^*$  and  $x_3^*$ —can be written as

$$\begin{aligned} x_1^* &= \frac{\alpha\beta k_2 k_3}{\alpha\gamma k_1 k_2 + \alpha\beta k_2 k_3 + \beta\gamma k_1 k_3} \cdot T, \\ x_2^* &= \frac{\beta\gamma k_1 k_3}{\alpha\gamma k_1 k_2 + \alpha\beta k_2 k_3 + \beta\gamma k_1 k_3} \cdot T, \\ x_3^* &= \frac{\alpha\gamma k_1 k_2}{\alpha\gamma k_1 k_2 + \alpha\beta k_2 k_3 + \beta\gamma k_1 k_3} \cdot T, \end{aligned}$$

where  $\alpha$ ,  $\beta$ , and  $\gamma$  are functions of  $I$ . In this chapter there are three levels of insulin stimulation: basal,  $I_0$ ; physiological,  $I_{phys}$ ; and maximal,  $I_{max}$ . In addition,  $\alpha$ ,  $\beta$ , and  $\gamma$  have been defined as step functions of the insulin level in a similar fashion to Equation 8.1. As will be seen later, the following values are sufficient to describe the physiological and maximal insulin transitions:

- For  $I = I_0$ ,  $\alpha = \beta = \gamma = 1$ ;
- For  $I = I_{phys}$ ,  $\alpha = \alpha_{phys}$ ,  $\beta = \gamma = 1$ ;
- For  $I = I_{max}$ ,  $\alpha = \alpha_{phys}$ ,  $\beta = \beta_{max}$ , and  $\gamma = 1$ .

Initial conditions for the transition to physiological insulin were calculated from the basal steady states. In terms of model variables, the experimental data gives the value of  $x_3$  as a fraction of  $x_3(0)$ . In order to facilitate a direct comparison with the data, the model was re-normalized so that  $x_3^* = 1$  in the basal steady state (when  $I = I_0$ ). This has the effect of re-scaling the total Akt pool so that

$$T = \frac{k_1 k_2 + k_2 k_3 + k_1 k_3}{k_1 k_2}.$$

By substituting  $\alpha = \beta = \gamma = 1$  into the relative steady states and multiplying by  $T$ , the basal initial conditions,

$$x_1(0) = \frac{k_3}{k_1}, \quad x_2(0) = \frac{k_3}{k_2}, \quad x_3(0) = 1,$$

are obtained.

### 8.2.3 Parameter Optimisation

The TagRFP-T-Akt2 time course was extracted from Fig. 1F of [128]. This data was corrected for photo-bleaching with the control data (also from Fig. 1F). Error bounds were extracted, where possible. For some values in the data set, error bounds were obscured by the graphical marker used. In this case, the error bound values were taken to be that of the data. An extended data set was created comprising the data values and the extrema of the error bounds at each time point. Parameter optimisations were performed with the MATLAB ‘fit’ function (R2019a Mathworks 2019) at the default tolerances.

### 8.2.4 Sensitivity Calculations

In metabolic control analysis, a control coefficient measures the relative change in a metabolite concentration resulting from a small relative change to some parameter, typically an enzyme concentration [138–140]. A control coefficient can be thought of as a normalized or logarithmic derivative, although a variety of names for the same or closely allied concepts appear in the literature. Typically,  $S_x^p$ , the sensitivity of the variable  $x$  with respect to the parameter  $p$ , is defined as

$$S_x^p = \lim_{\Delta p \rightarrow 0} \frac{\Delta x/x}{\Delta p/p} = \frac{\partial \ln(x)}{\partial \ln(p)} = \frac{\partial x}{\partial p} \cdot \frac{p}{x},$$

where  $\Delta x$  is a small change in the value of  $x$  resulting from  $\Delta p$ , a small change in the value of  $p$ .

As the model has an analytic solution, the sensitivities can be calculated directly. When the system is in the steady state under physiological insulin (that is, when  $I = I_{phys}$  and  $\beta = \gamma = 1$ ), the sensitivities with respect to  $\alpha$  are:

$$\begin{aligned} S_{x_1^*}^\alpha &= \frac{k_1 k_3}{\alpha k_1 k_2 + k_1 k_3 + \alpha k_2 k_3}, \\ S_{x_2^*}^\alpha &= -\frac{\alpha k_2 (k_1 + k_3)}{\alpha k_1 k_2 + k_1 k_3 + \alpha k_2 k_3}, \\ S_{x_3^*}^\alpha &= \frac{k_1 k_3}{\alpha k_1 k_2 + k_1 k_3 + \alpha k_2 k_3}. \end{aligned}$$

Note that the sign of  $S_{x_2^*}^\alpha$  is negative whilst the other two are positive (and equal). This indicates that as the value of  $\alpha$  is increased, the cytosolic and plasma membrane pools of Akt are enriched at the expense of the primed pool.

The transition to maximal insulin involves perturbations to multiple parameter values which are not necessarily small. This invalidates the taking of limits as in the standard definition of sensitivity. Instead, the relative change,

$R_n$ , which is the change in the steady state value of the  $n$ th Akt pool as a fraction of the corresponding basal steady state, may be defined. That is,

$$R_n(I) = \frac{x_n^*(I) - x_n^*(I_0)}{x_n^*(I_0)},$$

where  $x_n^*(I)$  is the steady state value of the  $n$ th Akt pool at an insulin level of  $I$ . At maximal insulin (that is, when  $\gamma = 1$ ), the relative changes are:

$$\begin{aligned} R_1 &= \frac{\alpha\beta(k_1k_2 + k_2k_3 + k_1k_3)}{\alpha k_1k_2 + \beta(\alpha k_2k_3 + k_1k_3)} - 1; \\ R_2 &= \frac{\beta(k_1k_2 + k_2k_3 + k_1k_3)}{\alpha k_1k_2 + \beta(\alpha k_2k_3 + k_1k_3)} - 1; \\ R_3 &= \frac{\alpha(k_1k_2 + k_2k_3 + k_1k_3)}{\alpha k_1k_2 + \beta(\alpha k_2k_3 + k_1k_3)} - 1. \end{aligned}$$

It can be seen that if  $\alpha$  is increased and  $\beta$  is decreased, then  $x_3^*$  increases and  $x_2^*$  decreases; whereas the change in  $x_1^*$  depends on the relative magnitudes of the changes in  $\alpha$  and  $\beta$ .

As the parameter optimisation showed that changes to  $\gamma$  are not necessary to fit the experimental data, these sensitivities and relative changes have been omitted.

## 8.3 Results

### 8.3.1 The Model Optimised to Physiological Insulin

The model was first optimised to the experimental data for the transition to physiological insulin (that is, for  $0 \leq t \leq 10$ ). The parameter values, 95% confidence intervals, and goodness of fit data obtained are given in Table 8.2. A second optimisation with  $\Delta t$  set to zero was also attempted. In theory, this should result in a more parsimonious and hence preferable model.

However, the quality of the fit was much poorer: the adjusted R-squared value was considerably lower (0.7607) and the 95% confidence intervals of all parameters included zero.

A comparison of model simulations with and without the delay and the experimental data is shown in Figure 8.3. In addition to an objective improvement in the goodness of fit, as demonstrated by an improved adjusted R-squared value, it is clear that the model with the time delay (the solid blue curve) is better able to capture the overshoot characteristics of the data, such as initial gradient, peak height, peak width, and peak timing, than the model without time delay (red, dashed curve).

Two further parameter optimisations, in which the values of  $\beta$  and  $\gamma$  rather than  $\alpha$  were individually varied in a step-wise fashion, were also attempted. The parameter values and goodness of fit data for these two parameter optimisations are given in Tables 8.3 and 8.4. These parameter sets yielded much poorer fits as they were unable to replicate the overshoot behaviour of Akt-PM. A plot of these simulations in comparison with the experimental data is shown in Figure 8.4. In summary, for the transition from basal to physiological insulin, a step change in the value of  $\alpha$  in conjunction with a time delay is sufficient to embody the experimental data.

The sensitivities and relative changes were calculated from the parameter values for the transition to physiological insulin. The sensitivities with respect to  $\alpha$  of the steady states were  $(S_{x_1^*}^\alpha, S_{x_2^*}^\alpha, S_{x_3^*}^\alpha) = (0.41, -0.60, 0.41)$ . The sensitivity captures small-scale changes in steady state behaviour in response to infinitesimal perturbations of the parameter values. In contrast, the relative change is a description of the response to larger perturbations. The relative changes calculated for the transition to physiological insulin were  $(R_1, R_2, R_3) = (0.36, -0.28, 0.36)$ . Thus, although the magnitudes differ, both descriptors predict the depletion of the primed Akt pool and the augmentation of the cytosolic and plasma membrane pools.

Table 8.2: The parameter values, 95% confidence intervals, and goodness of fit data for the optimisation to the physiological insulin data only.

<b>Parameter</b>	<b>Value</b>	<b>Confidence Interval</b>
$k_1$	0.6205 min <sup>-1</sup>	(0.3938, 0.8472)
$k_2$	0.3789 min <sup>-1</sup>	(0.05438, 0.7034)
$k_3$	2.266 min <sup>-1</sup>	(0.03915, 4.493)
$\alpha_{phys}$	1.878	(1.283, 2.472)
$\Delta t$	0.4441 min	(0.4013, 0.487)
<b>Goodness of Fit Data</b>		
Sum of squares error:		0.0049
R-squared:		0.9809
Adjusted R-squared:		0.9761
Root mean square error:		0.0175

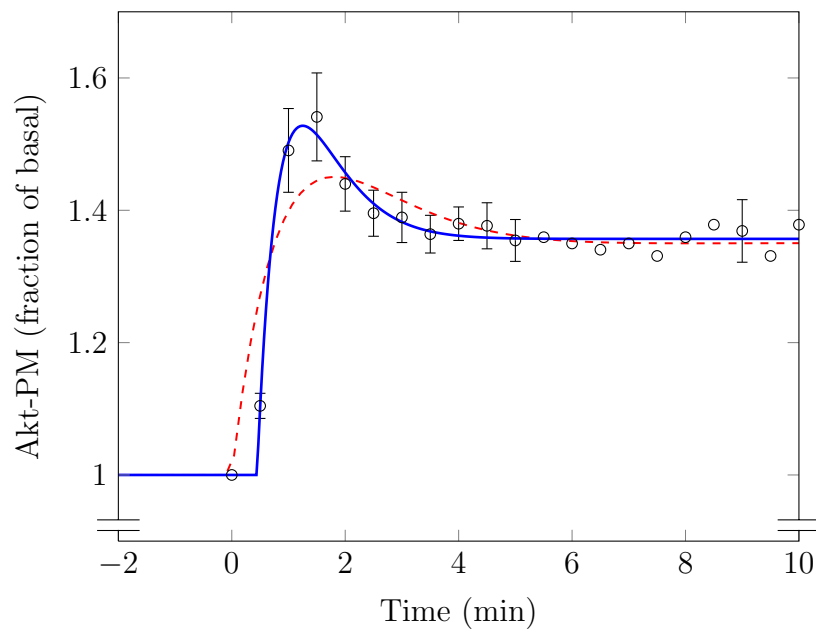


Figure 8.3: Model simulations with parameter values optimised to the experimental data (black dots) for the model with delay (solid blue curve) and the model without delay (dashed red curve).

Table 8.3: The parameter values, 95% confidence intervals, and goodness of fit data for an attempted optimisation to the physiological insulin data in which the parameter  $\beta$  was varied. Note that the 95% confidence intervals of all parameters included zero, and the goodness of fit data was worse than that for the parameter set in which  $\alpha$  was changed.

<b>Parameter</b>	<b>Value</b>	<b>Confidence Interval</b>
$k_1$	1.172 min <sup>-1</sup>	(-141.2, 143.6)
$k_2$	1.082 min <sup>-1</sup>	(-184.9, 187.1)
$k_3$	7.537 min <sup>-1</sup>	(-144.5, 159.5)
$\beta_{phys}$	0.7028	(-0.6401, 2.046)
$\Delta t$	0.4403 min	(-1.65, 2.53)
<b>Goodness of Fit Data</b>		
Sum of squares error:		0.0490
R-squared:		0.8082
Adjusted R-squared:		0.7602
Root mean square error:		0.0553

Table 8.4: The parameter values, 95% confidence intervals, and goodness of fit data for an attempted optimisation to the physiological insulin data in which the parameter  $\gamma$  was varied. Once again, the 95% confidence intervals of all parameters included zero, and the goodness of fit data was worse than that of the parameter set in which  $\alpha$  was changed.

Parameter	Value	Confidence Interval
$k_1$	8.13 min <sup>-1</sup>	(-106.9, 123.1)
$k_2$	7.133 min <sup>-1</sup>	(-281.1, 295.4)
$k_3$	8.207 min <sup>-1</sup>	(-327.2, 343.6)
$\gamma_{phys}$	7.515	(-452.3, 467.3)
$\Delta t$	0.4651 min	(-0.321, 1.251)
Goodness of Fit Data		
Sum of squares error:		0.0520
R-squared:		0.7963
Adjusted R-squared:		0.7454
Root mean square error:		0.0570

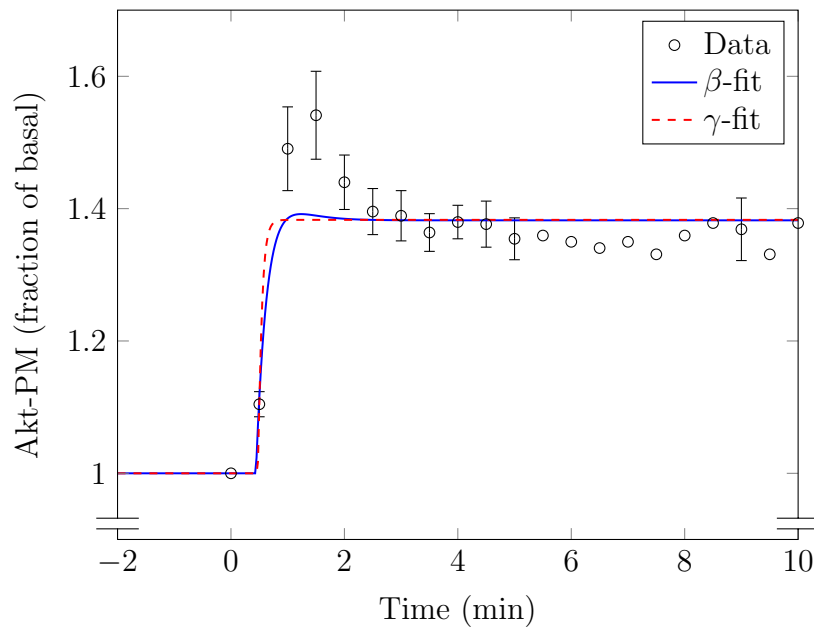


Figure 8.4: Model simulations of the parameter sets in which  $\beta$  (blue solid line) or  $\gamma$  (red, dashed line) were allowed to vary. The experimental data is also shown (black dots). Although appropriate steady state values were obtained, neither parameter set was able to reproduce the overshoot apparent in the experimental data.

### 8.3.2 The Model Optimised to Maximal Insulin

In order to identify the dominant processes operating in the translocation of Akt at both insulin concentrations, it is necessary to determine a minimal set of parameter changes that embodies the observed data for the full 15 minute time course. Figure 8.5 shows a parameter sweep of  $\alpha_{max}$  in comparison with the experimental data. In this figure, at  $t = 10$  minutes the value of  $\alpha$  was switched a second time to  $\alpha_{max} = k\alpha_{phys}$ , where  $1 \leq k \leq 5$ . Other parameters were set to the values obtained from the optimisation to physiological insulin listed in Table 8.2. It can be seen that the model cannot reproduce the data in this fashion. As shown in Chapter 7, as  $\alpha_{max}$  increases, the height of the subsequent peak also increases (Figure 7.6) but the timing decreases (Figure 7.5). Thus a slow but sustained rise as seen in the data for the transition to maximal insulin cannot be successfully fitted by merely increasing the value of  $\alpha_{max}$ .

Similarly, the parameter sweep of  $\gamma_{max}$  shown in Figure 8.6 demonstrates that a single change to this parameter is also insufficient to describe the data. In this plot, the value of  $\gamma$  (the multiplier of the priming rate) was changed at  $t = 10$  minutes from one to  $\gamma_{max}$ , where the values of  $\gamma_{max}$  were taken from a logarithmic scale between one and one million. It is evident that the subsequent maximum value of Akt-PM saturates at roughly 2.5 times the basal value, even with a million fold increase in the value of  $\gamma_{max}$ .

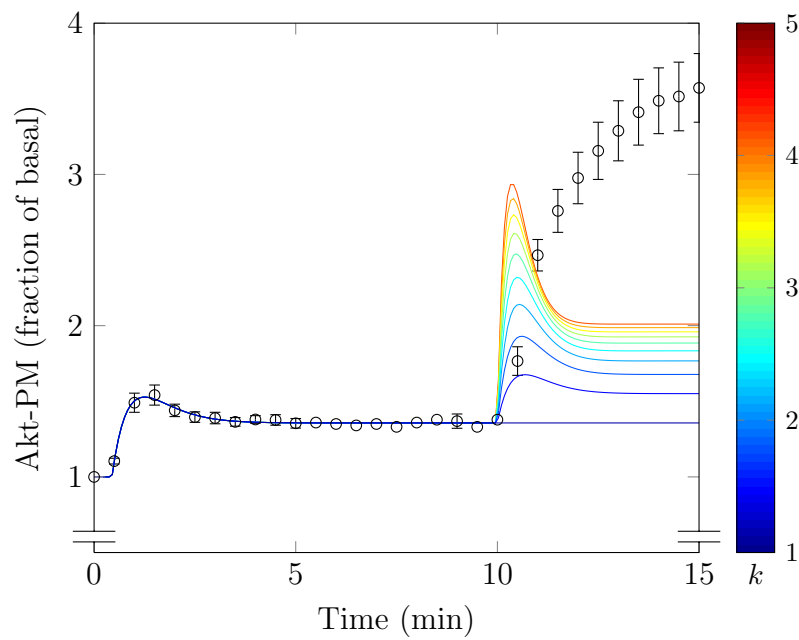


Figure 8.5: Parameter sweep of  $\alpha_{max}$ . At time  $t = 10$  min the value of  $\alpha$  was switched to  $\alpha_{max} = k\alpha_{phys}$  for  $1 \leq k \leq 5$ . The other parameters were held constant at the values listed in Table 8.2.

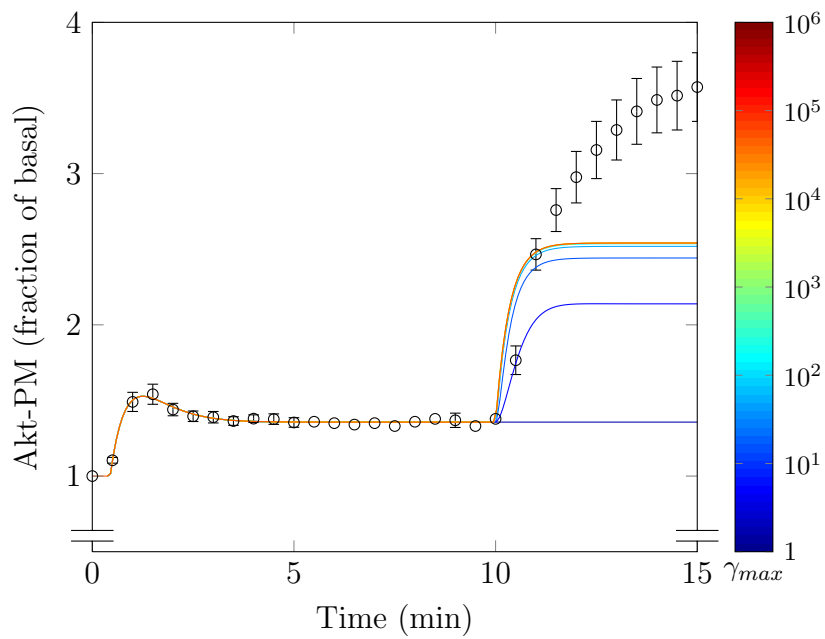


Figure 8.6: Parameter sweep of  $\gamma_{max}$ . At time  $t = 10$  min  $\gamma$  was switched from one to  $\gamma_{max}$  for  $1 \leq \gamma_{max} \leq 10^6$ . The other parameters were set to the values listed in Table 8.2 throughout the simulations.

The model could represent the observed data, however, if the condition that  $\beta = 1$  following the application of maximal insulin was relaxed. Recall that the insulin dependence of the model is embodied by changes to the multipliers  $\alpha$ ,  $\beta$ , and  $\gamma$  of the rates  $k_1$ ,  $k_2$ , and  $k_3$ , respectively (which take single values throughout the time course). For the optimisation to the full data set,  $\alpha$  and  $\beta$  were changed at two different time points. At time  $t = \Delta t_\alpha$  (after the application of 1 nM insulin),  $\alpha$  was switched to  $\alpha_{phys}$ , where  $\alpha_{phys} > 1$ . At time  $t = 10 + \Delta t_\beta$  (following the application of 100 nM insulin),  $\beta$  was switched to  $\beta_{max}$ , where  $\beta_{max} < 1$ ,  $\alpha$  being maintained at  $\alpha_{phys}$ . Furthermore, three different scenarios for the second time delay were optimised to the data: in the first,  $\Delta t_\alpha$  and  $\Delta t_\beta$  were equal (Table 8.5); in the second,  $\Delta t_\alpha$  and  $\Delta t_\beta$  were allowed to differ (Table 8.6); and in the third,  $\Delta t_\beta = 0$  (Table 8.7).

Figure 8.7 shows simulations for all three parameter sets in comparison with the experimental data. The blue curve is the parameter set with equal time delays; the red curve has differing time delays; and the cyan curve has a second time delay of zero. The inset shows all three simulations in comparison with the simulation from the parameter set optimised to the physiological insulin data only (black dashed line) in greater detail.

The relative changes for the transition to maximal insulin were calculated for the three parameter sets. The relative changes of the steady states,  $(R_1, R_2, R_3)$ , were  $(0.14, -0.38, 2.44)$  for the parameter set with equal time delays;  $(0.025, -0.46, 2.48)$  for differing delays; and  $(-0.23, -0.64, 2.53)$  for the second delay set to zero. Note that  $R_1$  is positive for the parameter set with equal delays; close to zero for differing delays; and negative for the second delay set to zero. This implies that the steady state cytosolic pool of Akt increases for the parameter set with equal delays; changes little, if at all, for differing delays; and decreases for the second delay set to zero. For Sensitivities for this transition were not calculated as there were large changes to multiple parameter values.

Table 8.5: The parameter values, 95% confidence intervals, and goodness of fit data for the parameter set with equal time delays. At time  $t = \Delta t$ , the value of  $\alpha$  was increased from one to  $\alpha_{phys}$ ; and at time  $t = 10 + \Delta t$ , the value of  $\beta$  was decreased from one to  $\beta_{max}$ . Other parameters took the same values throughout.

Parameter	Value	Confidence Interval
$k_1$	0.3073 min <sup>-1</sup>	(0.06667, 0.5479)
$k_2$	0.2442 min <sup>-1</sup>	(0.01424, 0.4741)
$k_3$	2.239 min <sup>-1</sup>	(1.968, 2.51)
$\alpha_{phys}$	1.845	(1.431, 2.258)
$\beta_{max}$	0.3324	(0.2874, 0.3774)
$\Delta t$	0.4296 min	(0.3605, 0.4986)
<b>Goodness of Fit Data</b>		
Sum of squares error:		0.2265
R-squared:		0.9899
Adjusted R-squared:		0.9879
Root mean square error:		0.0952

Table 8.6: The parameter values, 95% confidence intervals, and goodness of fit data for the parameter set with differing time delays. Note that the 95% confidence interval of  $\Delta t_\beta$  includes zero.

Parameter	Value	Confidence Interval
$k_1$	0.3885 min <sup>-1</sup>	(0.1811, 0.5959)
$k_2$	0.2749 min <sup>-1</sup>	(0.08634, 0.4635)
$k_3$	1.532 min <sup>-1</sup>	(1.086, 1.978)
$\alpha_{phys}$	1.905	(1.532, 2.279)
$\beta_{max}$	0.2947	(0.2113, 0.3781)
$\Delta t_\alpha$	0.4373 min	(0.3932, 0.4814)
$\Delta t_\beta$	0.1111 min	(-0.8928, 1.115)
Goodness of Fit Data		
Sum of squares error:		0.0527
R-squared:		0.9977
Adjusted R-squared:		0.9971
Root mean square error:		0.0469

Table 8.7: The parameter values, 95% confidence intervals, and goodness of fit data for the parameter set with  $\Delta t_\beta = 0$ .

<b>Parameter</b>	<b>Value</b>	<b>Confidence Interval</b>
$k_1$	0.5077 min <sup>-1</sup>	(0.4301, 0.5854)
$k_2$	0.381 min <sup>-1</sup>	(0.3412, 0.4208)
$k_3$	1.195 min <sup>-1</sup>	(1.015, 1.376)
$\alpha_{phys}$	2.143	(2.057, 2.228)
$\beta_{max}$	0.2194	(0.1846, 0.2542)
$\Delta t_\alpha$	0.43 min	(0.4083, 0.4517)
<b>Goodness of Fit Data</b>		
Sum of squares error:		0.0534
R-squared:		0.9976
Adjusted R-squared:		0.9972
Root mean square error:		0.0462

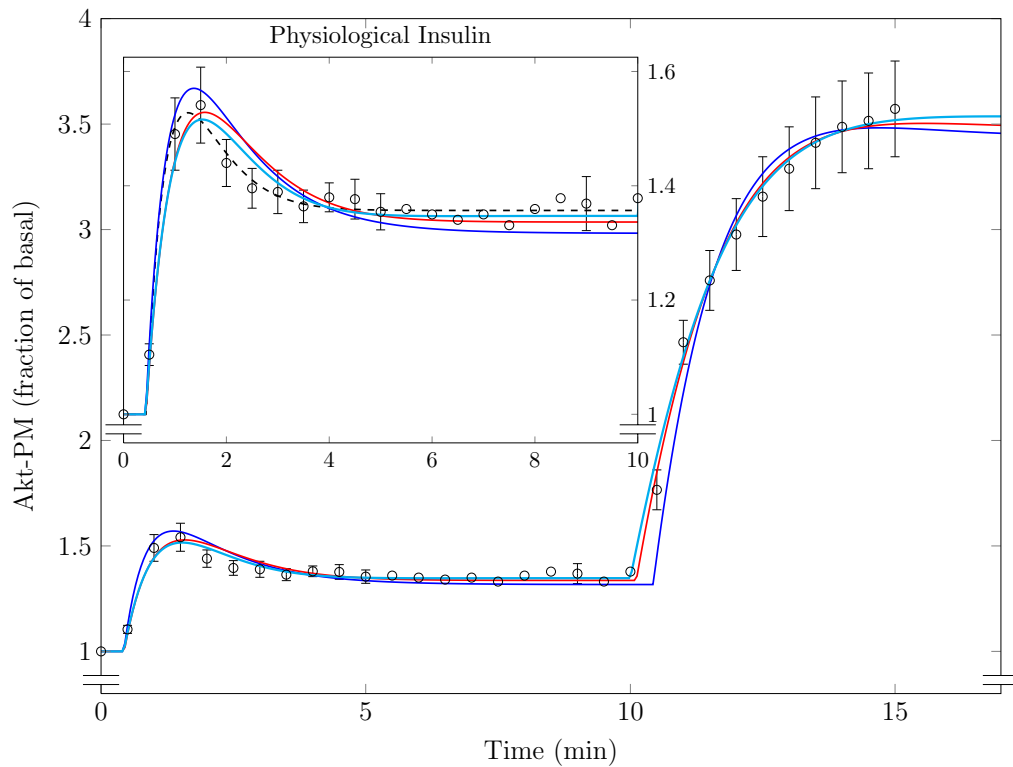


Figure 8.7: Model simulations with parameter values optimised to the full time course in comparison with the experimental data (black dots). In this plot, the value of  $\alpha$  was varied with a time delay of  $\Delta t_\alpha$  after  $t = 0$ . The value of  $\beta$  was also varied with a time delay of  $\Delta t_\beta$  after  $t = 10$ . For the blue curve,  $\Delta t_\alpha$  and  $\Delta t_\beta$  were equal; for the red curve,  $\Delta t_\alpha$  and  $\Delta t_\beta$  were allowed to differ; and for the cyan curve,  $\Delta t_\beta$  was set to zero. The inset shows all three simulations in comparison with the simulation using the physiological insulin only parameter set (dashed black curve) in greater detail.

## 8.4 Discussion

The Akt Translocation model has been successfully optimised to the experimental data for the transition from basal to physiological insulin. A step increase in the effective docking rate of Akt at the plasma membrane (that is,  $\alpha k_2$ ) that occurs after a time delay of approximately 0.4 min constitutes the minimal change required to embody the experimental data. This minimal encoding suggests that, for the transition to physiological insulin at least, plasma membrane docking is the rate limiting step. The delay may be due to the experimental protocol, as the physiological level of insulin may take time to reach and activate the insulin receptors. However, as noted in Chapter 6, similar discrepancies were seen when the Akt Switch model was optimised to data from a different experimental protocol. Furthermore, these discrepancies were more noticeable at higher insulin levels, thus it is likely that the delay represents the timing of the insulin signalling system itself, rather than differential rates of diffusion due to changes in the insulin concentration.

It is known that Akt occupies an intermediate position in the insulin signalling pathway. Components of the pathway upstream from Akt include, *inter alia*, the insulin receptor, IRS1, PI3K, and PIP<sub>3</sub> [15]. Thus it is reasonable to assume that the propagation of the insulin signal through the upstream cascade results in a delay between the application of insulin and the upregulation of Akt translocation. The improvement in the fit obtained with the model with the time delay (see Figure 8.3) supports this assumption.

The data shows a substantial increase in Akt in the TIRF zone following the application of 100 nM insulin. At any given time, the size of the Akt-PM pool is controlled by the balance of the effective docking rate ( $\alpha k_2$ ) and the effective recycling rate ( $\beta k_3$ ). As demonstrated in Figure 8.5, it is not possible to replicate the transition to maximal insulin simply with an additional increase in the effective docking rate.

It is evident from Figure 8.5 that both the experimental data and the model simulation attain a quasi-steady state within five minutes of the application

of a physiological level of insulin. In addition, a calculation of either the sensitivities with respect to  $\alpha$  (the insulin effect on the docking rate) or the relative changes of the steady state values shows that as  $\alpha$  is increased, the equilibrium distribution of Akt amongst the three pools changes, resulting in a marked decrease in the primed Akt pool. This new, insulin-stimulated steady state forms the initial state from which the transition to maximal insulin occurs.

One hypothesis to explain the slow rise seen in the data for the transition to maximal insulin is the depletion of the primed pool. Depletion would necessitate replenishment of the primed pool from the cytosolic Akt before the system could respond to further increases in insulin. In the steady state under physiological insulin, Akt enters the primed pool from the cytosol at the basal priming rate,  $k_1$ , and exits the primed pool by docking at the plasma membrane at the effective docking rate,  $\alpha k_2$ . In all parameter sets obtained,  $k_1$  is less than  $\alpha k_2$ . This implies that replenishment of the primed pool is relatively slow. However, as can be seen from the parameter sweep of  $\alpha_{max}$  in Figure 8.5, the model is still able to respond with a sustained increase in Akt-PM (indeed, an overshoot), even from the steady state under physiological insulin. It is the shape of the response—initial gradient, peak timing, and other characteristics—that cause the mismatch between the simulation and the experimental data. As the optimised model clearly has sufficient Akt in the primed pool for a rapid response, the depletion hypothesis does not explain the observed behaviour.

In contrast, the full time course data can be closely replicated by the model if the effective recycling rate—the rate at which Akt leaves the plasma membrane to return to the cytosol—is decreased following the application of maximal insulin (Figure 8.7). All three simulations shown in this figure involved a decrease in the effective recycling rate of roughly 70 to 80 percent (see Tables 8.5, 8.6, and 8.7). This may be referred to as the retention hypothesis, since it indicates that docked Akt is retained at the plasma membrane for a longer period of time.

Recent literature concerning Akt regulation suggests that there are two predominant models of events following the activation of Akt at the plasma membrane [18, 141]. The first is the classical or diffusion model, in which pAkt is locked into an active conformation by double phosphorylation and then diffuses to various compartments within the cell. More recently, a membrane-bound model has been suggested [142]. In the membrane-bound model, pAkt remains catalytically active only while it is closely associated with the membrane lipids PIP<sub>3</sub> and PIP<sub>2</sub>. Dissociation from membranes enriched with such lipids results in rapid dephosphorylation and consequent loss of activity.

The membrane retention hypothesis suggested by the parameter optimisation is consistent with either model of post-activation events. In the case of the classical model, it could indicate a prolonged tethering of Akt at the plasma membrane that occurs under maximal insulin conditions. Alternately, in the membrane-bound model, it could result from a differential sorting of pAkt into membrane-bound compartments that are then targeted to various sites in the cell. As the Akt Translocation model does not track the phosphorylation state, both the basal recycling rate ( $k_3$ ) and the effective recycling rate ( $\beta k_3$ ) represent a weighted sum of the return of activated and unactivated Akt from the plasma membrane to the cell interior. If the recycling rate is affected by the phosphorylation state, a more comprehensive mathematical model of Akt activation—one that tracks both translation and phosphorylation—is required to elucidate possible mechanisms.

Whilst the parameter optimisation of the Akt Translocation model in its current form does not distinguish between the rival post-activation scenarios, it does strongly suggest a change in the dominant processes regulating system behaviour at maximal insulin. This may be termed the “dimmer switch model” of Akt translocation. A dimmer switch is commonly used to flexibly control the brightness of domestic lighting. Firstly, the dimmer switch must be turned on before the circuit can produce a signal at all. The signal amplitude is then regulated by the dimmer in a separate, continuous process. In

the case of Akt translocation, the initial switch regulates the rate of release of Akt from the primed pool, after which it enters the TIRF zone. This is triggered at a comparatively low level of insulin and essentially functions as an on/off switch. The secondary, dimmer regulation, however, is determined by other processes that occur once Akt is docked at the plasma membrane. In comparison with the on/off behaviour of the initial switch, these processes exhibit a markedly different dose-response relationship to the insulin concentration. Their overall effect is to retain Akt within the TIRF zone, particularly at higher levels of insulin.

Further support for the dimmer switch model is provided by the relative lengths of the time delays found in the optimisation to the full time course data (Figure 8.7). It should be noted that the time delay potentially consists of two components: a signalling delay, caused by biochemical changes to upstream components; and a translocation delay, brought about by the physical movement of Akt itself. Presumably, the signalling delay is much shorter than the translocation delay. Indeed, it is possible that the signalling delay is not detectable given the time-resolution of the current data. For the transition to physiological insulin, the time delay is comparatively long (approximately 0.4 min in all parameter sets). In contrast, the best fits to the data for the transition to maximal insulin involved a short or non-existent time delay (the red and cyan curves in Figure 8.7). This suggests that the first delay incorporates both a signalling and a translocation delay; whereas the second delay is a signalling delay only.

The dimmer switch model of Akt translocation could be further refined should appropriate experimental data become available. With the current experimental data terminating at 15 minutes, it is not clear whether Akt at the plasma membrane has reached a plateau or is still increasing. Figure 8.7 shows simulations from the three parameter sets continued on for a further two minutes after the experimental data ends. The cyan curve (in which the second delay is zero) appears to plateau, but the red and blue curves (differing and equal delays) exhibit small overshoots. Judged in terms of the

adjusted R-squared value, the cyan and red curves are a (slightly) better fit to the experimental data than the blue. In addition, the cyan curve is a good approximation for the physiological transition, both for the overshoot and the steady state values. Of the three parameter sets, it compares most favourably with the simulation from the optimisation to the physiological insulin data only (see inset, Figure 8.7).

However, the three parameter sets have different implications for the steady state values of the model at maximal insulin. A calculation of the relative changes shows that the direction of change (increase or decrease) for the cytosolic Akt pool differs between the parameter sets: positive for the parameter set with equal time delays (0.14); small but positive for differing time delays (0.025); and negative for the zero second time delay ( $-0.23$ ). In Chapter 6 it was hypothesized that the cycling of Akt and pAkt between cytosol and plasma membrane effectively splits the downstream insulin signal into two branches. One is a fast acting, plasma membrane-bound branch, that is mostly associated with the metabolic functions of Akt; the second is a slower, more sustained, cytosolic branch that is associated predominantly with the mitogenic functions of Akt. It is possible that a change in the steady state values of the plasma membrane and the cytosolic pools of Akt could have differential effects on the two branches of down-stream signalling. A longer time course under the current experimental protocol would permit a parameter optimisation that distinguishes more clearly between the three parameter sets by a more accurate calculation of steady state values at maximal insulin.

Data from a more detailed range of insulin concentrations would be useful for fine-tuning the model. In particular, experimental data for a transition directly from basal to maximal insulin would elucidate the nature of the time delay quantified by the parameter optimisation. Furthermore, in the current model,  $\alpha$  and  $\beta$  are both step functions of the insulin input, as greater detail was not justified by the existing experimental data. Should further data become available, the step functions could be replaced with

mathematically smoother (and more biologically plausible) functional forms, thus determining the dose response of the rates in the system.

## 8.5 Summary

From the parameter optimisation of the Akt Translocation model, a time delay of approximately 0.4 min between the initial application of insulin and the translocation of Akt in 3T3-L1 adipocytes was quantified. This places a time constraint on the intermediate processes, specifically those lying between the insulin receptor and the translocation of Akt. Interestingly, further time delays do not need to be invoked to explain the translocation response to subsequent applications of insulin.

This investigation indicates that the dominant processes acting in the translocation of Akt differ with the insulin dose. In the case of physiological insulin, it is sufficient for the system to regulate the release of Akt directly to the plasma membrane in response to the insulin signal. However, at higher levels of insulin, further changes in the rate of release are unable to describe the system behaviour. Under these conditions, regulation of the recycling of Akt from the plasma membrane to the cytosol is also required.

The very different modalities of regulation observed in the physiological and maximal insulin states reinforce the idea that the dynamic behaviour at maximal insulin cannot be directly extrapolated to that at the physiological level.

The optimisation of the Akt Translocation model to data has allowed the quantification of the timing of upstream signalling. Extending the model to include phosphorylation will further elucidate the downstream signalling pathway.



## **Part III**

# **Discussion, Conclusion, Future Work**



# Chapter 9

## Discussion

Akt is a pivotal crosstalk node mediating between multiple signalling pathways within the mammalian cell. Known to play a central role in cell fate decisions (growth, proliferation, and anti-apoptosis), Akt also functions as a key regulator of glucose transport in response to insulin. The activation of only a small percent of the Akt in insulin-sensitive cells results in maximal translocation of GLUT4 to the plasma membrane, enabling the diffusion of glucose into the cell. Since glucose transport into the cell is rate-limiting for glucose metabolism [15, 39], Akt constitutes a vital link coordinating resource intensive processes, such as growth and proliferation, with cellular metabolism.

As the dysregulation of Akt is associated with numerous “diseases of affluence,” such as diabetes and cancer, it has drawn considerable attention from the research community, including mathematical modellers. Many models featuring Akt in a variety of signalling pathways and cell types have appeared in the literature (see Section 3.4). However, the treatment of Akt translocation and activation within these models has, with a few exceptions, been somewhat cursory. This is, at least in part, the result of limitations to the current understanding of the biological processes involved.

However, it is clear that the signalling specificity of Akt is driven both by its biochemical state and its spatial distribution within the cell. Nonetheless, few of the mathematical models developed to date have addressed this important aspect of Akt signalling. The Akt Switch model in Chapter 6 constituted an initial investigation into the interplay between the translocation and phosphorylation subprocesses in the activation of Akt. The model employed two spatial pools—at the plasma membrane and in the cytosol—and tracked the phosphorylation state of Akt in both locations (see Figure 6.2). The result was a simple, linear, deterministic, four-compartment ODE model that embodied the main features of Akt activation. This model had an analytic solution, was computationally tractable, and produced output consistent with the main features of the existing experimental data.

Notwithstanding its inherent simplicity, the Akt Switch model provided significant insight into Akt activation. Firstly, the model demonstrated that some of the apparent anomalies of Akt signalling could be explained by distinguishing between the roles of translocation and phosphorylation in the activation of Akt. In particular, the widely reported overshoot of pAkt in the initial stages of signalling could be explained if these subprocesses occur on time scales differing by several orders of magnitude. In addition, translocation was identified as the slower, rate-limiting step (Table 6.3). This is a biologically plausible result, as translocation involves the physical movement of components within the cell, whereas phosphorylation is a chemical reaction taking place *in situ*.

Secondly, the explicit inclusion of two cellular locations in the model (cytosol and plasma membrane) enabled different modalities of downstream regulation. In effect, the movement of Akt and pAkt between cytosol and plasma membrane splits the downstream signal into a fast acting, plasma membrane-bound branch and a slower, more sustained, cytosolic branch of signalling. In the optimised Akt Switch model, these two signalling branches exhibited distinct differences in the initial rate, degree of overshoot, and steady state values of pAkt under various levels of insulin stimulation (Figure 6.8). More-

---

over, this differential regulation was achieved without the need to invoke complex feedback mechanisms.

However, as with all mathematical models, the Akt Switch model had significant limitations. As seen in Figure 6.7, there was a noticeable discrepancy between the model output and the experimental data in the first few minutes of the simulation. This discrepancy was particularly obvious at the higher (100 nM) insulin concentration, and is indicative of a timing delay in the activation process, most probably caused by a delay in the translocation of Akt. Nonetheless, the addition of a further parameter in the form of a timing delay could not be justified due to the scarcity of the experimental data (see Section 6.3.3). More importantly, TIRF microscopy data published after the development of the Akt Switch model demonstrated that the translocation process itself manifests overshoot, quite apart from the phosphorylation state of Akt [128].

Consequently, the Akt Translocation model was devised in order to investigate this subprocess further (Chapter 7). As overshoot was evident in the translocation process itself, an ODE model with three distinct Akt pools was developed. The three pools represented Akt within the cytosol, Akt primed for docking at the plasma membrane, and Akt docked at the plasma membrane (see Figure 7.1). As the model did not track the phosphorylation state of Akt, all three pools potentially contained both phosphorylated and un-phosphorylated Akt.

Preliminary mathematical analysis of the Akt Translocation model was carried out in Section 7.3.1. Firstly, the model was non-dimensionalised (that is, re-written in terms of relative rates). This resulted in a slightly simpler formulation, which was then shown to be mathematically equivalent to the harmonic oscillator equation (Section 7.3.1). This is a well-studied and well-understood differential equation which provided a useful analytical framework for understanding the system. Both the steady state and transient behaviours of the model over the entire parameter space were elucidated, and it was shown the model is always heavily damped. This means that the

observable output of the model can be classified as either overshoot (undershoot) or monotonic increase (decrease), only. Conditions for overshoot—a biologically significant feature of Akt translocation—were also determined.

In addition, important downstream signalling metrics (peak height, peak timing, and initial gradient of Akt-PM) as functions of the insulin concentration were analysed in Section 7.3.3. This revealed an inherent hysteresis in the behaviour of the model arising from the initial conditions. Hysteresis is potentially significant for downstream signalling, and will undoubtedly be an important theme in any future investigation of the behaviour of the model under pulsatile insulin stimulation (see Chapter 10).

Throughout the analysis of the Akt Translocation model, it was assumed that the insulin signal impinges on the system by increasing the docking rate of Akt. That is to say, the fraction of Akt at the plasma membrane increases in response to insulin because Akt enters the plasma membrane pool at a faster rate, rather than leaving at a slower rate. However, optimisation of the Akt Translocation model to TIRF microscopy data from 3T3-L1 adipocytes under insulin stimulation at both physiological (1 nM) and very high (100 nM) concentrations [128] showed that this is not necessarily so.

As an outcome of the parameter optimisation detailed in Chapter 8, the time delay between the application of insulin and the Akt translocation response noted in Chapter 6 was quantified. For physiological insulin, the delay was approximately 0.4 min (Table 8.2). This is a significant result, as it places limitations on the timing of signalling events upstream from Akt in the insulin signalling pathway. Intriguingly, the transition from physiological insulin to higher stimuli did not incur a further delay.

These results also suggest that the dominant processes regulating the Akt-PM fraction differ with the insulin dose. At the physiological level, the rate-limiting step was the release of Akt to the plasma membrane in response to the insulin signal, consistent with the mathematical analysis in Chapter 7. At higher levels, in contrast, further changes to the rate of release alone were

unable to describe the system behaviour (Figure 8.5). Under these conditions, a decrease in the rate of recycling of Akt from the plasma membrane to the cytosol was needed in order to reproduce the experimental data (Figure 8.7). This suggests that at higher insulin levels, other processes come into play that prolong the retention of docked Akt at the plasma membrane.

Broadly speaking, views on post-activation events in the Akt cycle fall into two major camps. The classical view holds that activated Akt leaves the plasma membrane following phosphorylation and diffuses to its many substrates which are found throughout the cell. In the membrane-bound view, however, pAkt retains its activated state only as long as it is tightly associated with lipid membranes such as PIP<sub>2</sub> and PIP<sub>3</sub>. This would require the post-activation movement of pAkt through the cell to occur via some sort of vesicle transport mechanism. Unfortunately, the Akt Translocation model in its current form cannot cast any light on this interesting question, as the behaviour of the model is consistent with either explanation. This is, in part, due to the fact that the phosphorylation state of Akt is not explicitly included in the model.

Accordingly, an obvious next step in the study of Akt activation is the development of a model that tracks both the location and biochemical state of all Akt in the cell. One such model (amongst other things) is suggested as future work in Chapter 10. It is hoped that the development and validation of this model will lead to further insight into this important signalling node.



# Chapter 10

## Future Work

The regulation of Akt translocation and activation remains a significant, if only partially understood, portion of the insulin signalling network. The following are some potentially fruitful areas of investigation arising from the current work.

The first is the response of the insulin signalling pathway to pulsatile or periodic insulin inputs. It is known that *in vivo* insulin secretion is periodic, with oscillations that occur on a number of different timescales: rapid (5-15 minutes); ultradian (1-2 hours); or circadian (24 hours) [4]. The pulsatile release of insulin is believed to be necessary for the maintenance of normal glucose homeostasis [125]; and dysregulation of pulsatile secretion, particularly in the high frequency modes, is an early development in pre-diabetes [127]. However, very little, if any, experimental work has been performed *in vitro* on the response of the insulin signalling pathway to periodic stimulation, as it is difficult to vary the insulin concentration in a periodic fashion under standard ‘wet lab’ conditions. In contrast, the system response to periodic forcing of the insulin signalling pathway or one of its subcomponents, such as Akt, can be readily studied *in silico*. There are a plethora of mathematical methods and techniques in the areas of control system engineering and sig-

nal analysis, in particular, that could be profitably brought to bear on this interesting question.

The second is the embedding of a mathematical model of Akt activation—either the extant Akt Switch model or the Akt Activation model proposed later in this chapter—in a larger model of the insulin signalling pathway. An obvious candidate is the Sedaghat model, but there are numerous other models for the various components of the insulin signalling pathway, some of which have been discussed in Chapter 3. There are two facets to this task which can be pursued independently: the link with the upstream signalling network, between the insulin receptor and the formation of  $\text{PIP}_3$ ; and the downstream link between Akt activation and GLUT4 translocation.

The parameter optimisation of the Akt Translocation model recounted in Chapter 8 provided an estimate of the time delay between the application of insulin and the subsequent translocation of Akt. This places an important constraint on the timing of signalling events between the insulin receptor and Akt, and should inform future attempts to model the upstream signalling pathway. Similarly, it can be expected that the development and validation of models connecting Akt activation to that of its numerous substrates will provide further insight into the downstream signalling pathway. With such a model, the different regulatory modalities afforded by the two ‘arms’ of Akt signalling—one at the plasma membrane and one in the cytosol—could be further investigated. Prior to this, however, it is clear that a more detailed treatment of the role of phosphorylation in Akt activation is necessary.

Currently, the future task of highest priority is the development, optimisation, and validation of a mathematical model that incorporates both the physical movement of Akt and changes to its phosphorylation state. A schematic diagram of one such model—the Akt Activation model—is given in Figure 10.1. The variables, parameters and equations of the model are listed in Table 10.1, and MATLAB code is given in Appendix A.4.

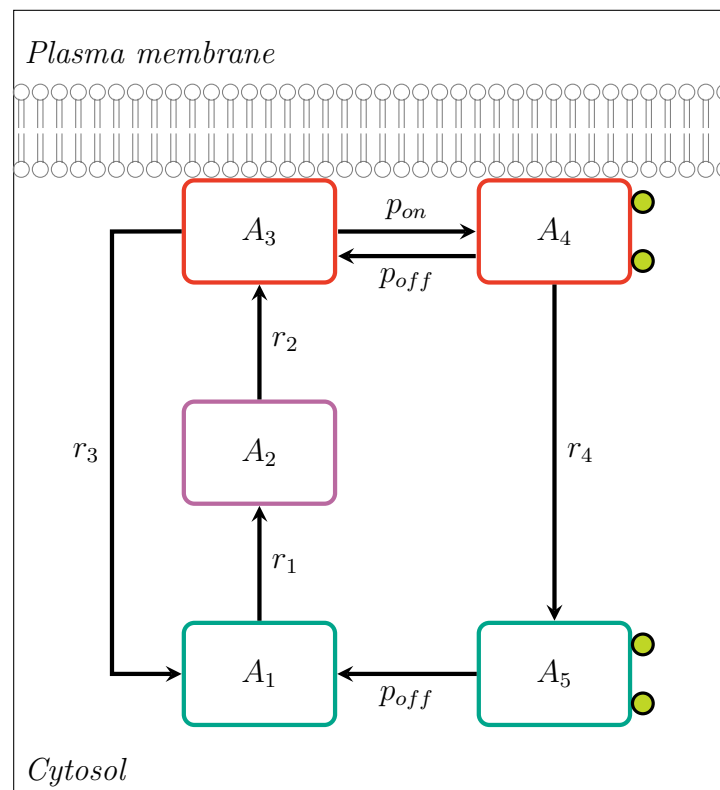


Figure 10.1: Diagram of the Akt Activation model. Unactivated Akt is initially synthesized in the cytosol ( $A_1$ ). It enters the primed pool ( $A_2$ ) and then docks at the plasma membrane ( $A_3$ ). At the plasma membrane, the Akt is activated by phosphorylation ( $A_4$ ), and is redistributed in the activated conformation to the cytosol ( $A_5$ ).

Table 10.1: Variables, parameters, and equations of the Akt Activation model.

<b>Variables</b>	
$A_1$ :	Unactivated Akt in the cytosol
$A_2$ :	Unactivated Akt in the primed pool
$A_3$ :	Unactivated Akt docked at the plasma membrane
$A_4$ :	Activated Akt (pAkt) docked at the plasma membrane
$A_5$ :	Activated Akt (pAkt) in the cytosol
<b>Parameters</b>	
$r_1$ :	Rate of transition into the primed state
$r_2$ :	Rate of docking of Akt at the plasma membrane
$r_3$ :	Rate of recycling of Akt from plasma membrane to cytosol
$r_4$ :	Rate of recycling of pAkt from plasma membrane to cytosol
$p_{on}$ :	Rate of phosphorylation of Akt
$p_{off}$ :	Rate of dephosphorylation of pAkt
<b>Equations</b>	
$\frac{dA_1}{dt}$	$= r_3A_3 + p_{off}A_5 - r_1A_1$
$\frac{dA_2}{dt}$	$= r_1A_1 - r_2A_2$
$\frac{dA_3}{dt}$	$= r_2A_2 - (r_3 + k_{on})A_3 + p_{off}A_4$
$\frac{dA_4}{dt}$	$= p_{on}A_3 - (p_{off} + r_4)A_4$
$\frac{dA_5}{dt}$	$= r_4A_4 - p_{off}A_5$
Note:	at all times, $\sum_{i=1}^5 A_i = 100$ (percentages).

---

The Akt Activation model is the Akt Translocation model with added pools representing the phosphorylation state of Akt. It is assumed that the Akt is dephosphorylated before entering the primed pool, so there are only two phosphorylated pools: one in the cytosol and one at the plasma membrane. This results in a total of five state variables:  $A_1$ , unactivated Akt in the cytosol;  $A_2$ , Akt primed for docking at the plasma membrane;  $A_3$ , unactivated Akt docked at the plasma membrane;  $A_4$ , activated Akt at the plasma membrane; and  $A_5$ , activated Akt in the cytosol. As with the previous model, it is assumed that total Akt is conserved. In addition, the model has six rate constants:  $r_1$ , the rate of transition of Akt into the primed pool (priming rate);  $r_2$ , the rate of Akt docking at the plasma membrane (docking rate);  $r_3$ , the rate of Akt recycling from plasma membrane to cytosol (recycling rate of Akt);  $r_4$ , the rate of pAkt recycling from plasma membrane to cytosol (recycling rate of pAkt);  $p_{on}$ , the phosphorylation rate of Akt; and  $p_{off}$ , the dephosphorylation rate of pAkt.

Figure 10.2 shows output from a simulation of the Akt Activation model. All three curves in this plot represent Akt docked at the plasma membrane: the red curve is unphosphorylated Akt ( $A_3$ ); the blue curve is phosphorylated Akt ( $A_4$ ); and the magenta curve is total Akt ( $A_3 + A_4$ ). Thus the magenta curve corresponds to the variable  $x_3$  in the Akt Translocation model. The parameter values used for this simulation were:  $r_1 = 0.6205$ ;  $r_2 = 0.3789$ ;  $r_3 = 2.266$ ;  $r_4 = 2.266$ ;  $p_{on} = 0.6$ ; and  $p_{off} = 0.06$ . These parameter values were, at best, educated guesses and have not yet been optimised to experimental data.

There are a number of simplifications of the model structure that could be considered. For example, in the current model, it is tacitly assumed that dephosphorylation occurs at the same rate, irrespective of location. This is not necessarily so. Indeed, it may not be possible to source appropriate experimental data to quantify the value of  $p_{off}$  at the plasma membrane. In that case, both phosphorylation and dephosphorylation at the plasma membrane could be replaced with a single forward reaction that occurs at

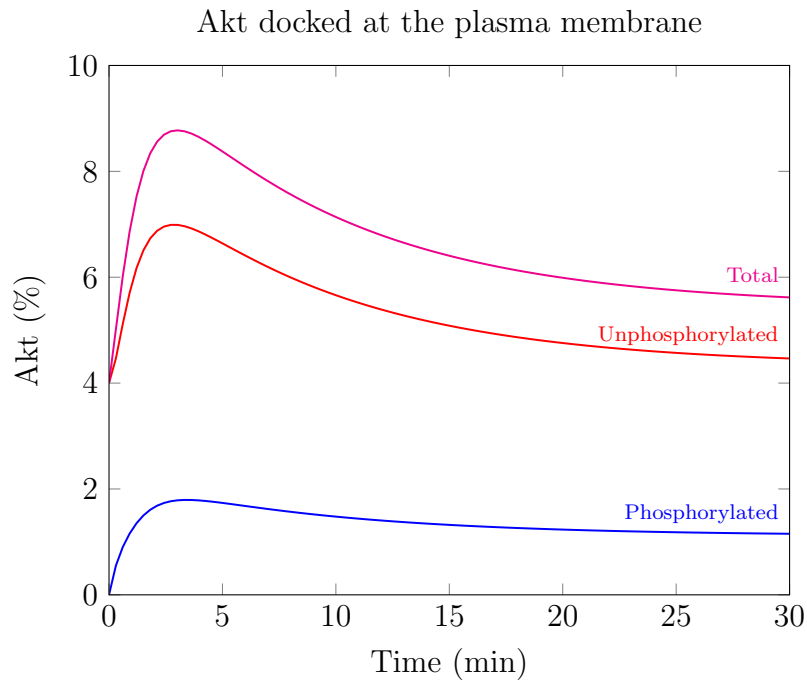


Figure 10.2: Model simulation of the Akt activation model. The red curve is the level of unphosphorylated Akt docked at the plasma membrane ( $A_3$ ); the blue curve is the phosphorylated Akt at the plasma membrane ( $A_4$ ); and the magenta curve is the total Akt docked at the plasma membrane ( $A_3 + A_4$ ). Parameter values were:  $r_1 = 0.6205$ ;  $r_2 = 0.3789$ ;  $r_3 = 2.266$ ;  $r_4 = 2.266$ ;  $p_{on} = 0.6$ ; and  $p_{off} = 0.06$ . Note that these values were hand-picked and have not been optimised to data.

the effective phosphorylation rate,  $p_{eff} = p_{on} - p_{off}$ . This would permit more tightly constrained data fitting and more straightforward interpretation of results.

One of the most exciting outcomes of the Akt Activation model is the opportunity to test rival scenarios concerning post-activation events against experimental data. Parameter optimisation of the model could be used to investigate the membrane retention hypothesis, and post-activation events in the Akt cycle more generally. For instance, in the parameter set used for Figure 10.2, the recycling rate of Akt ( $r_3$ ) and pAkt ( $r_4$ ) were equal. This could be made a hard constraint in the data fitting. Alternately,  $r_3$  and  $r_4$  could be allowed to differ, or  $r_3$  could be set to zero.

Finally, the differing signalling modalities emanating from pAkt, either at the plasma membrane or in the cytosolic pool, could be explored. By linking the Akt Activation model to the downstream substrates of Akt, interesting questions concerning the regulation of the downstream insulin signalling pathway could be explored.



# Chapter 11

## Conclusion

Akt is a protein kinase that regulates numerous processes in the cell, including cell growth and division, anti-apoptosis, and glucose metabolism. The abnormal regulation of Akt is implicated in many diseases, such as cancer, cardiovascular disease, and type two diabetes.

Akt is synthesized inside the cell in an inert state. Under the influence of insulin, it moves to the plasma membrane to be activated by phosphorylation. However, activated Akt (pAkt) is also found in many other locations, including the cytoplasm, the mitochondrial membrane, and the nucleus: the spatial distribution of pAkt within the cell is an important determinant of downstream regulation. However, this aspect of Akt signalling has received scant treatment in the existing mathematical modelling literature.

The Akt Switch model was a simple, linear, four-compartment ordinary differential equation (ODE) model of Akt activation that tracked both the biochemical state and the physical location of Akt. Computationally tractable and readily analysed, it elucidated some of the apparent anomalies of Akt signalling. In particular, it enabled the differential regulation of downstream substrates via the two branches of Akt signalling (plasma membrane-bound and cytosolic), without the need for complex feedback mechanisms.

However, the Akt Switch model had some limitations, including an initial discrepancy between the model output and the experimental data. Furthermore, overshoot in the Akt Switch model resulted from the interaction between the different timescales of translation and phosphorylation, whereas subsequently published TIRF microscopy work clearly demonstrated the presence of overshoot in the translocation process itself.

As a consequence, the Akt Translocation model was developed to investigate the translocation of Akt in response to insulin *in vitro*. It was a simple, deterministic, three-compartment ODE model that could reproduce the salient features of Akt translocation, such as a significant overshoot in the plasma membrane-bound Akt fraction (Akt-PM) in the early stages of simulation. Analysis of the model showed that it behaves as a heavily damped harmonic oscillator with solution curves that either increase monotonically or overshoot. Further analysis also demonstrated that the model exhibits a distinct hysteresis arising from the initial state of the system.

Optimisation of the model to the TIRF microscopy data yielded further insights. A time delay of approximately 0.4 min between the application of insulin and the Akt response was established for the transition from basal to physiological insulin. However, no delay was required for a further transition to maximal insulin. In addition, it was apparent that the processes regulating the size of the Akt-PM pool vary with the insulin level. For physiological insulin, the rate limiting step was the release of Akt to the plasma membrane. At high insulin levels, however, the additional down-regulation of Akt recycling away from the plasma membrane was also necessary to explain the data.

Akt is a vital part of insulin signalling and glucose metabolism. The models developed in this thesis provide a solid foundation for the further elucidation of this critical crosstalk node.

# Appendices



# Appendix A

## MATLAB

### A.1 Receptor State Space Model

```
function RSSM
% Simulates the Receptor state space model with the
% Sedaghat downstream subsystem.
clear all

function output=RSSM_ODE(t,X)
% Insulin pulse (15 min)
if t<15
    y1=X(1)*1e-9;
else y1=0;
end

% Receptor state space model
y2=X(2);    % unbound surface insulin receptors
y3=X(3);    % activated insulin receptors (x4+x5) from old model

% Downstream Sedaghat model
x9=X(4);    % unphosphorylated IRS-1
x10=X(5);   % tyrosine phosphorylated IRS-1
```

---

```

x11=X(6);      % unactivated PI3 kinase
x12=X(7);      % tyrosine phosphorylated IRS-1/PI3 kinase complex
x13=X(8);      % PI(3,4,5)P_3
x14=X(9);      % PI(4,5)P_2
x15=X(10);     % PI(3,4)P_2
x16=X(11);     % unactivated akt
x17=X(12);     % activated akt
x18=X(13);     % unactivated PKC-zeta
x19=X(14);     % activated PKC-zeta
x20=X(15);     % intracellllular GLUT4
x21=X(16);     % cell surface GLUT4

% Parameters
% Receptor state space model
r1=6e7;
rm1=0.202;
PTP=1;

% Downstream Sedaghat
k7=4.16;
km7=(2.5/7.45)*4.16;
k8=5.00e-15/(7.45e-13*9.5e-14)*10.0;
km8=10.0;
IRp=8.97e-13;

k9=(1.39-(0.31/99.4)*(94/3.1)*1.39)*(x12/5.0e-15)+...
    (0.31/99.4)*(94/3.1)*1.39;
km9=(94/3.1)*1.39;
k10=2.77*(3.1/2.9);
km10=2.77;
PTEN=1;
SHIP=1;

k11=0.1*6.93*((x13-0.31)/2.79);
km11=6.93;
k12=0.1*6.93*((x13-0.31)/2.79);
km12=6.93;
k13=(4/96)*0.167;
km13=0.167;

```

```

k13p=(40/60-4/96)*0.167*min((0.2*x17+0.8*x19)/(100/11),1);
k14=96*0.001155;
km14=0.001155;

% Differential equations
% Receptor state space model
dy1dt=0;
dy2dt=rml*y3-r1*y1*y2;
dy3dt=r1*y1*y2-rml*y3;

% Downstream Sedaghat
dx9dt=km7*PTP*x10 - k7*x9*y3/IRp;
dx10dt=k7*x9*y3/IRp + km8*x12 - (km7*PTP + k8*x11)*x10;
dx11dt=km8*x12 - k8*x10*x11;
dx12dt=k8*x10*x11 - km8*x12;
dx13dt=k9*x14 + k10*x15 - (km9*PTEN + km10*SHIP)*x13;
dx14dt=km9*PTEN*x13 - k9*x14;
dx15dt=km10*SHIP*x13 - k10*x15;
dx16dt=km11*x17 - k11*x16;
dx17dt=k11*x16 - km11*x17;
dx18dt=km12*x19 - k12*x18;
dx19dt=k12*x18 - km12*x19;
dx20dt=km13*x21 - (k13 + k13p)*x20 + k14 - km14*x20;
dx21dt=(k13+k13p)*x20 - km13*x21;

%result
output=[dy1dt;dy2dt;dy3dt;dx9dt;dx10dt;
        dx11dt;dx12dt;dx13dt;dx14dt;dx15dt;
        dx16dt;dx17dt;dx18dt;dx19dt;dx20dt;dx21dt];
end

% Insulin input in nM
Ins=100;

% Initial conditions
ICs=[9e-13,0,1e-12,0,1e-13,0,0.31,99.4,0.29,100,0,100,0,96,4];

% Model simulation
options=odeset('InitialStep',0.0001,'RelTol',1e-9,'AbsTol',1e-15);

```

```

sol=ode45(@RSSM_ODE,[0,60],[Ins,ICs],options);

% Plot of GLUT4-PM
tint=linspace(0,60,100);
P=deval(sol,tint);
plot(tint,P(16,:))
ylim([0 40])
xlabel('Time (min)')
ylabel('GLUT4 Expression (PM)')
end

```

## A.2 Akt Switch Model

```

function AktSwitch
% Simulates the Akt Switch model at 1 nM insulin
clear all

function output= AktSwitch_ODE(t,x)
% Variables
Ac=x(1); % Akt_Cyt
Pc=x(2); % pAkt_Cyt
Ap=x(3); % Akt_PM
Pp=x(4); % pAkt_PM

% Parameter values for 1 nM insulin
alpha=0.014;
beta=2.2;
k_in=0.55;
k_off=0.35;
k_out=alpha*k_in;
k_on=beta*k_off;

% Differential equations
dAc_dt=k_off*Pc - k_out*Ac + k_in*Ap;
dPc_dt=k_in*Pp - (k_off+k_out)*Pc;
dAp_dt=k_off*Pp + k_out*Ac - (k_on+k_in)*Ap;
dPp_dt=k_on*Ap + k_out*Pc - (k_in+k_off)*Pp;

```

```
output=[dAc_dt;dPc_dt;dAp_dt;dPp_dt];
end

% Initial conditions
AC0=0.95;
PC0=0;
AP0=0.05;
PP0=0;

% Model simulation
options=odeset('InitialStep',0.0001,'RelTol',1e-9,'AbsTol',1e-15);
sol=ode15s(@AktSwitch_ODE,[0 30],[AC0 PC0 AP0 PP0],options);

% Plot model output
t=linspace(0,30,200); %timepoints for plotting output
Q=deval(sol,t);      %Finds solution at time points in data
plot(t,Q(4,:))
xlabel('Time (min)')
ylabel('pAkt-PM')
end
```

### A.3 Akt Translocation Model

```
function AktTranslocation
% Simulates the Akt translocation model at 1 nM insulin
clear all

% Parameters for 1 nM insulin
k1=0.6205;
k2=0.3789;
k3=2.266;

function output= AktTrans_ODE(t,y)
% Variables
X1=y(1);    %Akt-Cyt
X2=y(2);    %Akt-Pri
```

```
X3=y(3);      %Akt-PM

% Step change in alpha
if t<0.4441
    Alpha=1;
else Alpha=1.878;
end

% Differential equations
dx1_dt=-k1*X1 + k3*X3;
dx2_dt=k1*X1-k2*Alpha*X2;
dx3_dt=Alpha*k2*X2-k3*X3;

output=[dx1_dt;dx2_dt;dx3_dt];
end

% Initial Conditions
ICs=[k3/k1,k3/k2,1];

% Model simulation
options=odeset('InitialStep',0.0001,'RelTol',1e-9,'AbsTol',1e-15);
sol=ode45(@AktTrans_ODE,[-5 15],ICs,options);

% Plot output
tint=linspace(-5,15,200);      %timepoints for plotting
Q=deval(sol,tint);

plot(tint,Q(3,:))
ylim([0.8 1.6])
ylabel('Akt-PM')
xlabel('time (min)')
end
```

## A.4 Akt Activation Model

```
function ActModel
% Simulates the Akt Activation model

clear all

%Parameter values
r1=0.6205; %Priming rate
r2=0.3789; %Docking rate of Akt
r3=2.266; %Recycling rate of Akt
r4=2.266; %Recycling rate of pAkt
pon=0.6; %Phosphorylation rate
poff=0.06; %Dephosphorylation rate

function output=ActMod_ODE(t,y)
% Variables
A1=y(1); %Akt-Cyt
A2=y(2); %Akt-Pri
A3=y(3); %Akt-PM
A4=y(4); %pAkt-PM
A5=y(5); %pAkt-Cyt

% Differential equations
dA1_dt=r3*A3+poff*A5-r1*A1;
dA2_dt=r1*A1-r2*A2;
dA3_dt=r2*A2-(r3+pon)*A3+poff*A4;
dA4_dt=pon*A3-(poff+r4)*A4;
dA5_dt=r4*A4-poff*A5;

output=[dA1_dt;dA2_dt;dA3_dt;dA4_dt;dA5_dt];
end

% Initial Conditions
ICs=[64,32,4,0,0]; %percentages

% Model simulation
options=odeset('InitialStep',0.0001,'RelTol',1e-9,'AbsTol',1e-15);
```

```
sol=ode45(@ActMod_ODE,[0 30],ICs,options);

% Plot output
tint=linspace(0,30,200);    %timepoints for plotting
Q=deval(sol,tint);
plot(tint,Q(3,:))
ylabel('Akt-PM')
xlabel('time (min)')
end
```

# Bibliography

- [1] AR Saltiel and CR Kahn. Insulin signalling and the regulation of glucose and lipid metabolism. *Nature*, 414(6865):799–806, 2001.
- [2] R Muniyappa, H Chen, M Montagnani, A Sherman, and MJ Quon. Endothelial dysfunction due to selective insulin resistance in vascular endothelium: insights from mechanistic modeling. *American journal of physiology. Endocrinology and metabolism*, Available online 10 August 2020.
- [3] DF Steiner and DE James. Cellular and molecular biology of the beta cell. *Diabetologia*, 35(2):S41–S48, 1992.
- [4] CB Landersdorfer and WJ Jusko. Pharmacokinetic/pharmacodynamic modelling in diabetes mellitus. *Clinical Pharmacokinetics*, 47(7):417–448, 2008.
- [5] MG Pedersen, R Bertram, and A Sherman. Intra-and inter-islet synchronization of metabolically driven insulin secretion. *Biophysical Journal*, 89(1):107–119, 2005.
- [6] O Schmitz, J Rungby, L Edge, and CB Juhl. On high-frequency insulin oscillations. *Ageing Research Reviews*, 7(4):301–305, 2008.
- [7] GD Holman and M Kasuga. From receptor to transporter: insulin signalling to glucose transport. *Diabetologia*, 40(9):991–1003, 1997.

- 
- [8] RM Shymko, E Dumont, P De Meyts, and JE Dumont. Timing-dependence of insulin-receptor mitogenic versus metabolic signalling: a plausible model based on coincidence of hormone and effector binding. *Biochemical Journal*, 339(3):675, 1999.
- [9] AR Saltiel and JE Pessin. Insulin signaling pathways in time and space. *Trends in Cell Biology*, 12(2):65–71, 2002.
- [10] H Kubota, R Noguchi, Y Toyoshima, Y Ozaki, S Uda, K Watanabe, W Ogawa, and S Kuroda. Temporal coding of insulin action through multiplexing of the Akt pathway. *Molecular Cell*, 2012.
- [11] P De Meyts. Insulin and its receptor: structure, function and evolution. *BioEssays*, 26(12):1351–1362, 2004.
- [12] CM Taniguchi, B Emanuelli, and CR Kahn. Critical nodes in signalling pathways: Insights into insulin action. *Nature Reviews Molecular Cell Biology*, 7(2):85–96, 2006.
- [13] K Lindmo and H Stenmark. Regulation of membrane traffic by phosphoinositide 3-kinases. *Journal of Cell Science*, 119(4):605, 2006.
- [14] S Fröjdö, H Vidal, and L Pirola. Alterations of insulin signaling in type 2 diabetes: A review of the current evidence from humans. *BBA - Molecular Basis of Disease*, 1792(2):83–92, 2009.
- [15] AF Rowland, DJ Fazakerley, and DE James. Mapping insulin/GLUT4 circuitry. *Traffic*, 12(6):672–681, 2011.
- [16] E Gonzalez and TE McGraw. Insulin signaling diverges into Akt-dependent and-independent signals to regulate the recruitment/docking and the fusion of GLUT4 vesicles to the plasma membrane. *Molecular Biology of the Cell*, 17(10):4484–4493, 2006.
- [17] Y Ng, G Ramm, JG Burchfield, ACF Coster, J Stöckli, and DE James. Cluster analysis of insulin action in adipocytes reveals a key role for Akt at the plasma membrane. *Journal of Biological Chemistry*, 285(4):2245–2257, 2010.

- [18] MG Sugiyama, GD Fairn, and CN Antonescu. Akt-ing up just about everywhere: Compartment-specific Akt activation and function in receptor tyrosine kinase signaling. *Frontiers in Cell and Developmental Biology*, 7:70, 2019.
- [19] A Toker and S Marmiroli. Signaling specificity in the Akt pathway in biology and disease. *Advances in Biological Regulation*, 55:28–38, 2014.
- [20] K Won, BK Kim, G Han, K Lee, Y Jung, H Kim, KB Song, K Chung, and M Won. NSC126188 induces apoptosis of prostate cancer PC-3 cells through inhibition of Akt membrane translocation, FoxO3a activation, and RhoB transcription. *Apoptosis*, 19(1):179–190, 2014.
- [21] Y Zhao, Y Lin, H Zhang, A Mañas, W Tang, Y Zhang, D Wu, A Lin, and J Xiang. Ubl4A is required for insulin-induced Akt plasma membrane translocation through promotion of Arp2/3-dependent actin branching. *Proceedings of the National Academy of Sciences*, 112(31):9644–9649, 2015.
- [22] A Bellacosa, CC Kumar, A Di Cristofano, and JR Testa. Activation of AKT kinases in cancer: implications for therapeutic targeting. *Advances in Cancer Research*, 94:29–86, 2005.
- [23] A Di Cristofano and PP Pandolfi. The multiple roles of PTEN in tumor suppression. *Cell*, 100(4):387–390, 2000.
- [24] I Hers, EE Vincent, and JM Tavaré. Akt signalling in health and disease. *Cellular Signalling*, 23(10):1515–1527, 2011.
- [25] A Tsuchiya, T Kanno, and T Nishizaki. PI3 kinase directly phosphorylates Akt1/2 at Ser473/474 in the insulin signal transduction pathway. *Journal of Endocrinology*, 220(1):49–59, 2014.
- [26] MM Hill, SF Clark, DF Tucker, MJ Birnbaum, DE James, and SL Macaulay. A role for protein kinase B  $\beta$ /Akt2 in insulin-stimulated GLUT4 translocation in adipocytes. *Molecular and Cellular Biology*, 19(11):7771–7781, 1999.

- [27] Q Wang, R Somwar, PJ Bilan, Z Liu, J Jin, JR Woodgett, and A Klip. Protein kinase B/Akt participates in GLUT4 translocation by insulin in L6 myoblasts. *Molecular and Cellular Biology*, 19(6):4008–4018, 1999.
- [28] Y Ng, G Ramm, JA Lopez, and DE James. Rapid activation of Akt2 is sufficient to stimulate GLUT4 translocation in 3T3-L1 adipocytes. *Cell Metabolism*, 7(4):348–356, 2008.
- [29] S Tan, Y Ng, CC Meoli, A Kumar, P Khoo, DJ Fazakerley, JR Junutula, S Vali, DE James, and J Stöckli. Amplification and demultiplexing in insulin-regulated Akt protein kinase pathway in adipocytes. *Journal of Biological Chemistry*, 287(9):6128–6138, 2012.
- [30] V Calleja, D Alcor, MI Laguerre, J Park, B Vojnovic, BA Hemmings, J Downward, PJ Parker, and B Larijani. Intramolecular and intermolecular interactions of protein kinase B define its activation in vivo. *PLoS Biology*, 5(4):e95, 2007.
- [31] E Gonzalez and TE McGraw. The Akt kinases. *Cell Cycle*, 8(16):2502–2508, 2009.
- [32] RC Hresko and M Mueckler. mTOR·RICTOR is the Ser473 kinase for Akt/protein kinase B in 3T3-L1 adipocytes. *Journal of Biological Chemistry*, 280(49):40406, 2005.
- [33] DD Sarbassov, DA Guertin, SM Ali, and DM Sabatini. Phosphorylation and regulation of Akt/PKB by the rictor-mTOR complex. *Science*, 307(5712):1098–1101, 2005.
- [34] AL Kearney, KC Cooke, DM Norris, A Zadoorian, JR Krycer, DJ Fazakerley, JG Burchfield, and DE James. Serine 474 phosphorylation is essential for maximal Akt2 kinase activity in adipocytes. *Journal of Biological Chemistry*, pages jbc–RA119, 2019.
- [35] DR Alessi, M Andjelkovic, B Caudwell, P Cron, N Morrice, P Cohen, and BA Hemmings. Mechanism of activation of protein kinase B by insulin and IGF-1. *The EMBO Journal*, 15(23):6541, 1996.

- [36] SJ Humphrey, G Yang, P Yang, DJ Fazakerley, J Stöckli, JY Yang, and DE James. Dynamic adipocyte phosphoproteome reveals that Akt directly regulates mTORC2. *Cell Metabolism*, 17(6):1009–1020, 2013.
- [37] M Andjelkovic, DR Alessi, R Meier, A Fernandez, NJC Lamb, M Frech, P Cron, P Cohen, JM Lucocq, and BA Hemmings. Role of translocation in the activation and function of protein kinase B. *Journal of Biological Chemistry*, 272(50):31515–31524, 1997.
- [38] MT Kunkel, Q Ni, RY Tsien, J Zhang, and AC Newton. Spatio-temporal dynamics of protein kinase B/Akt signaling revealed by a genetically encoded fluorescent reporter. *Journal of Biological Chemistry*, 280(7):5581–5587, 2005.
- [39] GD Holman and SW Cushman. Subcellular trafficking of GLUT4 in insulin target cells. In *Seminars in Cell & Developmental Biology*, volume 7, pages 259–268. Elsevier, 1996.
- [40] JW Slot, HJ Geuze, S Gigengack, DE James, and GE Lienhard. Translocation of the glucose transporter GLUT4 in cardiac myocytes of the rat. *Proceedings of the National Academy of Sciences*, 88(17):7815–7819, 1991.
- [41] R Govers, ACF Coster, and DE James. Insulin increases cell surface GLUT4 levels by dose dependently discharging GLUT4 into a cell surface recycling pathway. *Molecular and Cellular Biology*, 24(14):6456–6466, 2004.
- [42] PD Brewer, I Romenskaia, MA Kanow, and CC Mastick. Loss of AS160 Akt substrate causes Glut4 protein to accumulate in compartments that are primed for fusion in basal adipocytes. *Journal of Biological Chemistry*, 286(30):26287–26297, 2011.
- [43] PD Brewer, EN Habtemichael, I Romenskaia, CC Mastick, and ACF Coster. Insulin-regulated Glut4 translocation: Membrane protein trafficking with six distinctive steps. *Journal of Biological Chemistry*, 289:jbcm114, 2014.

- 
- [44] J Stöckli, DJ Fazakerley, and DE James. GLUT4 exocytosis. *Journal of Cell Science*, 124(24):4147–4159, 2011.
- [45] AR Sedaghat, A Sherman, and MJ Quon. A mathematical model of metabolic insulin signaling pathways. *American Journal of Physiology-Endocrinology And Metabolism*, 283(5):1084–1101, 2002.
- [46] YH Chew, YL Shia, CT Lee, FAA Majid, LS Chua, MR Sarmidi, and RA Aziz. Modeling of glucose regulation and insulin-signaling pathways. *Molecular and Cellular Endocrinology*, 303(1-2):13–24, 2009.
- [47] C Luni and FJ Doyle III. Robust multi-drug therapy design and application to insulin resistance in type 2 diabetes. *International Journal of Robust and Nonlinear Control*, 21(15):1730–1741, 2011.
- [48] R Pattaranit and HA van den Berg. Mathematical models of energy homeostasis. *Journal of The Royal Society Interface*, 5(27):1119, 2008.
- [49] BJ Goldstein, P Li, W Ding, F Ahmad, and W Zhang. Regulation of insulin action by protein tyrosine phosphatases. *Vitamins & Hormones*, 54:67–96, 1998.
- [50] W Liu, CC Hsin, and F Tang. A molecular mathematical model of glucose mobilization and uptake. *Mathematical Biosciences*, 221(2):121–129, 2009.
- [51] E Magrofuoco, N Elvassore, and FJ Doyle. Theoretical analysis of insulin-dependent glucose uptake heterogeneity in 3D bioreactor cell culture. *Biotechnology Progress*, 28(3):833–845, 2012.
- [52] PW Bates, Y Liang, and AW Shingleton. Growth regulation and the insulin signaling pathway. *Networks and Heterogeneous Media*, 8(1):65–78, 2013.
- [53] GR Smith and DP Shanley. Computational modelling of the regulation of insulin signalling by oxidative stress. *BMC Systems Biology*, 7(1):41, 2013.

- [54] C Huang, M Wu, J Du, D Liu, and C Chan. Systematic modeling for the insulin signaling network mediated by IRS-1 and IRS-2. *Journal of Theoretical Biology*, 355:40–52, 2014.
- [55] E Ulfhielm. Modeling of metabolic insulin signaling in adipocytes. Master’s thesis, Linköpings University, 2006.
- [56] DP Brazil and BA Hemmings. Ten years of protein kinase B signalling: a hard Akt to follow. *Trends in Biochemical Sciences*, 26(11):657–664, 2001.
- [57] CK Ho, L Rahib, JC Liao, G Sriram, and KM Dipple. Mathematical modeling of the insulin signal transduction pathway for prediction of insulin sensitivity from expression data. *Molecular Genetics and Metabolism*, 114(1):66–72, 2015.
- [58] RH Jones, PH Sönksen, MA Boroujerdi, and ER Carson. Number and affinity of insulin receptors in intact human subjects. *Diabetologia*, 27(2):207–211, 1984.
- [59] R Hovorka, JK Powrie, GD Smith, ER Carson, PH Sonksen, and RH Jones. A non-linear model of insulin kinetics. In *Medical Informatics Europe 1991*, pages 597–601. Springer, 1991.
- [60] R Hovorka, JK Powrie, GD Smith, PH Sonksen, ER Carson, and RH Jones. Five-compartment model of insulin kinetics and its use to investigate action of chloroquine in NIDDM. *American Journal of Physiology-Endocrinology And Metabolism*, 265(1):E162–E175, 1993.
- [61] MJ Quon and LA Campfield. A mathematical model and computer simulation study of insulin receptor regulation. *Journal of Theoretical Biology*, 150(1):59, 1991.
- [62] MJ Quon. Advances in kinetic analysis of insulin-stimulated GLUT-4 translocation in adipose cells. *American Journal of Physiology- Endocrinology And Metabolism*, 266(1):144–150, 1994.

- [63] S Wanant and MJ Quon. Insulin receptor binding kinetics: modeling and simulation studies. *Journal of Theoretical Biology*, 205(3):355–364, 2000.
- [64] VV Kiselyov, S Versteyhe, L Gauguin, and P De Meyts. Harmonic oscillator model of the insulin and IGF1 receptors’ allosteric binding and activation. *Molecular Systems Biology*, 5(1), 2009.
- [65] C Luni, KR Sanft, LR Petzold, and FJ Doyle III. Modelling of detailed insulin receptor kinetics affects sensitivity and noise in the downstream signalling pathway. *IFAC Proceedings Volumes*, 43(5):326–331, 2010.
- [66] SS Hori, IJ Kurland, and JJ DiStefano. Role of endosomal trafficking dynamics on the regulation of hepatic insulin receptor activity: models for Fao cells. *Annals of Biomedical Engineering*, 34(5):879–892, 2006.
- [67] JM Backer, CR Kahn, and MF White. Tyrosine phosphorylation of the insulin receptor during insulin-stimulated internalization in rat hepatoma cells. *Journal of Biological Chemistry*, 264(3):1694–1701, 1989.
- [68] M Koschorreck and ED Gilles. Mathematical modeling and analysis of insulin clearance in vivo. *BMC Systems Biology*, 2(1):43, 2008.
- [69] CW Gray. Sensitivity analysis of the insulin signalling pathway for glucose transport. Master’s thesis, University of New South Wales, 2013.
- [70] L Ljung. *System Identification: Theory for the User*. Prentice-Hall, Englewood Cliffs, NJ, 2nd edition, 1999.
- [71] G Cedersund, J Roll, E Ulfhielm, A Danielsson, H Tidefelt, and P Strålfors. Model-based hypothesis testing of key mechanisms in initial phase of insulin signaling. *PLoS Computational Biology*, 4(6), 2008.
- [72] C Brännmark, R Palmér, ST Glad, G Cedersund, and P Strålfors. Mass and information feedbacks through receptor endocytosis govern insulin signaling as revealed using a parameter-free modeling framework. *Journal of Biological Chemistry*, 285(26):20171, 2010.

- [73] AJ Jezewski, JJ Larson, B Wysocki, PH Davis, and T Wysocki. A novel method for simulating insulin mediated GLUT4 translocation. *Biotechnology and Bioengineering*, 111(12):2454–2465, 2014.
- [74] S Mathew, S Sundararaj, H Mamiya, and I Banerjee. Regulatory interactions maintaining self-renewal of human embryonic stem cells as revealed through a systems analysis of PI3K/Akt pathway. *Bioinformatics*, pages 2334–2342, 2014.
- [75] S Mathew and I Banerjee. Quantitative analysis of robustness of dynamic response and signal transfer in insulin mediated PI3K/Akt pathway. *Computers & Chemical Engineering*, 71:715–727, 2014.
- [76] HF Nijhout and V Callier. A new mathematical approach for qualitative modeling of the insulin-TOR-MAPK network. *Frontiers in Physiology*, 4, 2013.
- [77] S Nayak, JK Siddiqui, and JD Varner. Modelling and analysis of an ensemble of eukaryotic translation initiation models. *Systems Biology, IET*, 5(1):2–14, 2011.
- [78] M Hatakeyama, S Kimura, T Naka, T Kawasaki, N Yumoto, M Ichikawa, J Kim, K Saito, M Saeki, M Shirouzu, S Yokoyama, and A Konagaya. A computational model on the modulation of mitogen-activated protein kinase (MAPK) and Akt pathways in heregulin-induced ErbB signalling. *Biochemical Journal*, 373:451–463, 2003.
- [79] E Mosca, R Alfieri, C Maj, A Bevilacqua, G Canti, and L Milanesi. Computational modeling of the metabolic states regulated by the kinase Akt. *Frontiers in Physiology*, 3:418–418, 2011.
- [80] CS Park, IC Schneider, and JM Haugh. Kinetic analysis of platelet-derived growth factor receptor/phosphoinositide 3-kinase/Akt signaling in fibroblasts. *Journal of Biological Chemistry*, 278(39):37064–37072, 2003.

- [81] RJ Romanelli, AP LeBeau, CG Fulmer, DA Lazzarino, A Hochberg, and TL Wood. Insulin-like growth factor type-I receptor internalization and recycling mediate the sustained phosphorylation of Akt. *Journal of Biological Chemistry*, 282(31):22513–22524, 2007.
- [82] WH Tan, AS Popel, and F Mac Gabhann. Computational model of Gab1/2-dependent VEGFR2 pathway to Akt activation. *PloS One*, 8(6):e67438, 2013.
- [83] P Dalle Pezze, AG Sonntag, A Thien, MT Prentzell, M Godel, S Fischer, E Neumann-Haefelin, TB Huber, R Baumeister, DP Shanley, et al. A dynamic network model of mTOR signaling reveals TSC-independent mTORC2 regulation. *Science Signalling*, 5(217):ra25, 2012.
- [84] TH Nim, L Luo, JK White, M Clément, and L Tucker-Kellogg. Non-canonical Activation of Akt in Serum-Stimulated Fibroblasts, Revealed by Comparative Modeling of Pathway Dynamics. *PLoS Computational Biology*, 11(11):e1004505, 2015.
- [85] T Tian and F Wu. Robustness analysis of the PI3K/AktT cell signaling module. *Cancer*, 3:4, 2013.
- [86] L Giri, VK Mutalik, and KV Venkatesh. A steady state analysis indicates that negative feedback regulation of ptp 1 b by Akt elicits bistability in insulin-stimulated GLUT4 translocation. *Theoretical Biology and Medical Modelling*, 1(1):2, 2004.
- [87] Guanyu Wang. Singularity analysis of the AKT signaling pathway reveals connections between cancer and metabolic diseases. *Physical Biology*, 7(4):046015, 2010.
- [88] Dana Faratian, Alexey Goltsov, Galina Lebedeva, Anatoly Sorokin, Stuart Moodie, Peter Mullen, Charlene Kay, In Hwa Um, Simon Langdon, Igor Goryanin, et al. Systems biology reveals new strategies for personalizing cancer medicine and confirms the role of pten in resistance to trastuzumab. *Cancer Research*, 69(16):6713–6720, 2009.

- [89] Alexey Goltsov, Dana Faratian, Simon P Langdon, James Bown, Igor Goryanin, and David J Harrison. Compensatory effects in the pi3k/pten/akt signaling network following receptor tyrosine kinase inhibition. *Cellular Signalling*, 23(2):407–416, 2011.
- [90] Alexey Goltsov, Dana Faratian, Simon P Langdon, Peter Mullen, David J Harrison, and James Bown. Features of the reversible sensitivity-resistance transition in pi3k/pten/akt signalling network after her2 inhibition. *Cellular Signalling*, 24(2):493–504, 2012.
- [91] Y Arkun. Dynamic Modeling and Analysis of the Cross-Talk between Insulin/AKT and MAPK/ERK Signaling Pathways. *PloS one*, 11(3):e0149684, 2016.
- [92] SM Babar, EJ Song, E Oh, and YS Yoo. Kinetic analysis of the MAPK and PI3K/Akt signaling pathways. *Molecules and Cells*, 25(3):397–406, 2008.
- [93] N Borisov, E Aksamitiene, A Kiyatkin, S Legewie, J Berkhout, T Maiwald, NP Kaimachnikov, J Timmer, JB Hoek, and BN Kholodenko. Systems-level interactions between insulin–EGF networks amplify mitogenic signaling. *Molecular Systems Biology*, 5(1):256, 2009.
- [94] R Zielinski, PF Przytycki, J Zheng, D Zhang, TM Przytycka, and J Capala. The crosstalk between EGF, IGF, and insulin cell signaling pathways – computational and experimental analysis. *BMC Systems Biology*, 3(1):88, 2009.
- [95] PKU Vinod and KV Venkatesh. Quantification of the effect of amino acids on an integrated mTOR and insulin signaling pathway. *Molecular BioSystems*, 5(10):1163–1173, 2009.
- [96] A Bertuzzi, F Conte, G Mingrone, F Papa, S Salinari, and C Sinisgalli. Insulin signaling in insulin resistance states and cancer: A modeling analysis. *PloS one*, 11(5):e0154415, 2016.

- 
- [97] B Di Camillo, A Carlon, F Eduati, and GM Toffolo. A rule-based model of insulin signalling pathway. *BMC Systems Biology*, 10(1):1, 2016.
- [98] CW Gray and ACF Coster. Crosstalk in transition: The translocation of Akt. *Journal of Mathematical Biology*, 78(4):919–942, 2019.
- [99] SH Strogatz. *Nonlinear Dynamics and Chaos: With Applications to Physics, Biology, Chemistry, and Engineering*. Perseus Books, 2001.
- [100] NAW van Riel. Dynamic modelling and analysis of biochemical networks: mechanism-based models and model-based experiments. *Briefings in Bioinformatics*, 7(4):364, 2006.
- [101] KH Cho, SY Shin, W Kolch, and O Wolkenhauer. Experimental design in systems biology, based on parameter sensitivity analysis using a Monte Carlo method: A case study for the TNF $\alpha$ -mediated NF- $\kappa$ B signal transduction pathway. *Simulation*, 79(12):726–739, 2003.
- [102] Y Zhang and A Rundell. Comparative study of parameter sensitivity analyses of the TCR-activated Erk-MAPK signalling pathway. *IEE Proceedings - Systems Biology*, 153(4):201–211, 2006.
- [103] E Balsa-Canto, A Alonso, and J Banga. An iterative identification procedure for dynamic modeling of biochemical networks. *BMC Systems Biology*, 4(1):11, 2010.
- [104] C Cosentino and D Bates. *Feedback control in systems biology*. CRC Press, 2011.
- [105] BP Ingalls. *Mathematical modeling in systems biology: an introduction*. MIT press, 2013.
- [106] PA Iglesias and BP Ingalls. *Control theory and systems biology*. MIT Press, 2010.

- [107] Z Zi, KH Cho, MH Sung, X Xia, J Zheng, and Z Sun. In silico identification of the key components and steps in IFN- $\gamma$  induced JAK-STAT signaling pathway. *FEBS letters*, 579(5):1101–1108, 2005.
- [108] AF Emery and AV Nenarokomov. Optimal experiment design. *Measurement Science and Technology*, 9:864, 1998.
- [109] CB Moler. *Numerical Computing with MATLAB*. Society for Industrial Mathematics, 2004.
- [110] EM Akirav, O Chan, K Inouye, MC Riddell, SG Matthews, and M Vranic. Partial leptin restoration increases hypothalamic-pituitary-adrenal activity while diminishing weight loss and hyperphagia in streptozotocin diabetic rats. *Metabolism*, 53(12):1558–1564, 2004.
- [111] H Satoh, MTA Nguyen, M Trujillo, T Imamura, I Usui, PE Scherer, and JM Olefsky. Adenovirus-mediated adiponectin expression augments skeletal muscle insulin sensitivity in male Wistar rats. *Diabetes*, 54(5):1304–1313, 2005.
- [112] CW Gray and ACF Coster. A receptor state space model of the insulin signalling system in glucose transport. *Mathematical Medicine and Biology: A Journal of the IMA*, 32(4):457–473, 2015.
- [113] AD Kohn, SA Summers, MJ Birnbaum, and RA Roth. Expression of a constitutively active Akt Ser/Thr kinase in 3T3-L1 adipocytes stimulates glucose uptake and glucose transporter 4 translocation. *Journal of Biological Chemistry*, 271(49):31372–31378, 1996.
- [114] KL Hoehn, C Hohnen-Behrens, A Cederberg, LE Wu, N Turner, T Yuasa, Y Ebina, and DE James. IRS1-independent defects define major nodes of insulin resistance. *Cell Metabolism*, 7(5):421–433, 2008.
- [115] CW Gray and ACF Coster. The Akt switch model: is location sufficient? *Journal of Theoretical Biology*, 398:103–111, 2016.

- [116] R Meyer, LA DAlessandro, S Kar, B Kramer, B She, D Kaschek, B Hahn, D Wrangborg, J Karlsson, M Kvarnstrom, et al. Heterogeneous kinetics of AKT signaling in individual cells are accounted for by variable protein concentration. *Frontiers in Physiology*, 3:451, 2012.
- [117] E Gonzalez and TE McGraw. Insulin-modulated Akt subcellular localization determines Akt isoform-specific signaling. *Proceedings of the National Academy of Sciences*, 106(17):7004–7009, 2009.
- [118] T Gao, F Furnari, and AC Newton. PHLPP: a phosphatase that directly dephosphorylates Akt, promotes apoptosis, and suppresses tumor growth. *Molecular Cell*, 18(1):13–24, 2005.
- [119] S Stratford, D Dewald, and S Summers. Ceramide dissociates 3'-phosphoinositide production from pleckstrin homology domain translocation. *Journal of Biochemistry*, 354:359–368, 2001.
- [120] JA Chavez and SA Summers. A ceramide-centric view of insulin resistance. *Cell Metabolism*, 15(5):585–594, 2012.
- [121] E Carvalho, B Eliasson, C Wesslau, and U Smith. Impaired phosphorylation and insulin-stimulated translocation to the plasma membrane of protein kinase B/Akt in adipocytes from Type II diabetic subjects. *Diabetologia*, 43(9):1107–1115, 2000.
- [122] RP Erickson, Z Jia, SP Gross, and CC Yu. How molecular motors are arranged on a cargo is important for vesicular transport. *PLoS Computational Biology*, 7(5):e1002032–e1002032, 2011.
- [123] R Lipowsky, Y Chai, Sn Klumpp, S Liepelt, and MJI Müller. Molecular motor traffic: From biological nanomachines to macroscopic transport. *Physica A: Statistical Mechanics and its Applications*, 372(1):34–51, 2006.
- [124] HC Chen and RV Farese. Determination of adipocyte size by computer image analysis. *Journal of Lipid Research*, 43(6):986–989, 2002.

- [125] R Bertram, A Sherman, and LS Satin. Electrical bursting, calcium oscillations, and synchronization of pancreatic islets. *Advances in Experimental Medicine and Biology*, 654:261–279, 2010.
- [126] AV Matveyenko, D Liuwantara, T Gurlo, D Kirakossian, C Dalla Man, C Cobelli, MF White, KD Copps, E Volpi, S Fujita, et al. Pulsatile portal vein insulin delivery enhances hepatic insulin action and signaling. *Diabetes*, 61(9):2269–2279, 2012.
- [127] S Seino, T Shibasaki, and K Minami. Dynamics of insulin secretion and the clinical implications for obesity and diabetes. *The Journal of Clinical Investigation*, 121(6):2118, 2011.
- [128] DM Norris, P Yang, JR Krycer, DJ Fazakerley, DE James, and JG Burchfield. An improved Akt reporter reveals intra-and inter-cellular heterogeneity and oscillations in signal transduction. *Journal of Cell Science*, 130(16):2757–2766, 2017.
- [129] JP Keener and J Sneyd. *Mathematical Physiology: Cellular Physiology*. Springer Verlag, 2008.
- [130] NF Britton. *Essential Mathematical Biology*. Springer Verlag, 2003.
- [131] WE Boyce and RC DiPrima. *Elementary differential equations and boundary value problems*. Wiley New York, 8th edition, 2005.
- [132] Gilbert Strang. *Differential equations and linear algebra*. Wellesley-Cambridge Press, 2014.
- [133] Stephen A Wirkus and Randall J Swift. *A course in ordinary differential equations*. CRC Press, 2006.
- [134] X Tang, AM Powelka, NA Soriano, MP Czech, and A Guilherme. PTEN, but not SHIP2, suppresses insulin signaling through the phosphatidylinositol 3-kinase/Akt pathway in 3T3-L1 adipocytes. *Journal of Biological Chemistry*, 280(23):22523–22529, 2005.

- [135] J Avruch. Insulin signal transduction through protein kinase cascades. *Molecular and Cellular Biochemistry*, 182(1):31–48, 1998.
- [136] DJ Powell, E Hajdуч, G Kular, and HS Hundal. Ceramide disables 3-phosphoinositide binding to the pleckstrin homology domain of protein kinase B (PKB)/Akt by a PKC $\zeta$ -dependent mechanism. *Molecular and Cellular Biology*, 23(21):7794–7808, 2003.
- [137] ME Masip, J Huebinger, J Christmann, O Sabet, F Wehner, A Konitiotis, GR Fuhr, and PIH Bastiaens. Reversible cryo-arrest for imaging molecules in living cells at high spatial resolution. *Nature Methods*, 13(8):665, 2016.
- [138] R Heinrich and TA Rapoport. A linear steady-state treatment of enzymatic chains: general properties, control and effector strength. *European Journal of Biochemistry*, 42(1):89–95, 1974.
- [139] H Kacser and JA Burns. The control of flux. *Biochemical Society Transactions*, 23(2):341–366, 1995.
- [140] DA Fell. Metabolic control analysis: a survey of its theoretical and experimental development. *Biochemical Journal*, 286(2):313–330, 1992.
- [141] I Yudushkin. Getting the Akt together: Guiding intracellular Akt activity by PI3K. *Biomolecules*, 9(2):67, 2019.
- [142] M Ebner, I Lučić, TA Leonard, and I Yudushkin. PI (3,4,5)P<sub>3</sub> engagement restricts Akt activity to cellular membranes. *Molecular Cell*, 65(3):416–431, 2017.